Research Doctorate School in Biological and molecular Sciences

DOCTORATE THESIS

Student: **Alessio Giubellino**

e-mail: **giubella@mail.nih.gov**

Supervisor: **Prof. Generoso Bevilacqua**

e-mail: **generoso.bevilacqua@med.unipi.it**

Tutor: **Prof. Karel Pacak**

e-mail: **karel@mail.nih.gov**

Doctorate Program: **Molecular and Experimental Oncology**

Year: **2013**

TITLE OF THE PROJECT:

Molecular targets and targeted therapies in pheochromocytoma

Department/Laboratory/Institution: **Section on Medical Neuroendocrinology/NICHD/NIH**

ABSTRACT

Pheochromocytoma and paraganglioma are tumors of chromaffin cells occurring within the adrenal medulla or the sympathetic nervous system, respectively. About 15% of these tumors are malignant, especially in patients with mutations in the subunit B of the succinate dehydrogenase, who have a 40% probability of developing distant metastases. For these malignancies surgery is currently the treatment of choice, but, especially for advanced forms, treatment is unsatisfactory and prognosis is very poor. Thus, novel treatment options for these patients are urgently in need. Recent advances in our understanding of the molecular pathology of pheochromocytoma and paraganglioma have led to the identification of key oncogenic events. Several molecular pathways have been suggested to play a role in these tumors, including the RTKs/Ras/MAPK, PI3K/Akt/mTOR, HIF, HSP90 and mithocondrial proteins involved in energy-producing pathways. This increased knowledge can be matched by the increased number of novel compounds, including tyrosine kinase inhibitors and other novel targeted therapies already in clinical trial for other cancers, targeting signaling pathways important for tumor proliferation, survival and metastatic dissemination.

The overarching objective of this research project was to identify mechanism-based, molecularly targeted therapeutic approaches to modulate cancer cell growth and metastatic growth in pheochromocytoma, promoting the translational development of more effective therapeutic options for these tumors. The lack of sensitive animal models of pheochromocytoma has hindered the study of this tumor and *in vivo* evaluation of antitumor agents.To this end, two *in vivo* models for the evaluation of efficacy of several molecular targeted therapies were developed: an experimental metastasis model to

monitor tumor spreading and a subcutaneous model to monitor tumor growth and spontaneous metastasis. These models offer a platform for sensitive, non-invasive and real-time monitoring of pheochromocytoma primary growth and metastatic burden to follow the course of tumor progression and for testing relevant antitumor treatments in metastatic pheochromocytoma.

I then use *in vitro* experiments and the *in vivo* models above described to test the efficacy of selective ATP-competitive inhibitors targeting both mTORC1 and mTORC2 complexes, pointing out an important role for the mTOR signaling pathway in the development of pheochromocytoma.

Moreover, I investigated also the 90 kDa heat shock protein (Hsp90) as a potential therapeutic target for advanced pheochromocytoma, using both first and second generation Hsp90 inhibitors.

As an alternative approach to identify potential drugs that can more rapidly be implemented into clinical trials in patients with metastatic pheochromocytoma or paraganglioma, I used a drug repurposing/repositioning approach. With this strategy, several molecules with potential bioactivity in pheochromocytoma cells were identified, including an example of a combination with synergistic effect.

1. INTRODUCTION

1.1 The adrenal gland and paraganglia.

The adrenal glands (or suprarenal gland) are bilateral triangular organs located in the retroperitoneal space and lying on the superior pole of the kidney. The adrenal glands are major endocrine glands in mammals. They are mainly involved in the physiological response to stress by producing and secreting steroid hormones and catecholamines

Each adrenal grand is divided into two distinct areas: the outer cortex and the inner medulla. It is important to note that these two parts have a distinct embryological origin, structure and functions. Briefly, the adrenal cortex is further subdivided into three areas synthetizing and secreting several steroidal hormones. From the external surface these areas are: the zona glomerulosa (which produce the mineralcorticoid aldosterone), the zona fasciculata (which produce mainly the glucocorticoid cortisol) and the zona reticularis (which produce mainly the androgens, including testosterone).

The adrenal medulla is located in the center of the adrenal gland and represents only around 10% of the adrenal total weight. During embryogenesis, neuroblasts from the neural crest migrate to the medial side of the fetal adrenal cortex and, over time, these cells are mantled by the surrounding fetal cortex. These cells eventually differentiate into chromaffin cells (sometimes referred as pheochromocytes), so called because the granules inside the cells stains yellow-brown when exposed to chromium salts (*affin*ity to *chrom*ium): specifically chromium salts oxidize and polymerize cathecolamines which stain in the mentioned colors. Chromaffin cells are structurally similar to postsynaptic sympathetic neurons, and, similarly to the secretory hypothalamic neurons in the brain, release hormones directly into the systemic circulation. Outside the adrenal medulla, chromaffin cells can also be found in the sympathetic ganglia, paraganglia, in proximity

of the carotid body, the organ of Zuckerkandl (which contain the largest number of extraadrenal chromaffin cells in humans), and in small amount also in the wall of the bladder and the prostate. In margin, the enterochromaffin cells are distinct cells which only share a similar staining pattern but their function and embryological origin is different from the adrenal medulla chromaffin cells.

Chromaffin cells in the adrenal medulla make contact with presynaptic sympathetic ganglia of the sympathetic nervous system, representing collectively as the sympathoadrenal system. Chromaffin cells secretes three main types of cathecolamines: epinephrine (adrenaline), norepinephrine (noradrenaline) and dopamine.

1.2 Pheochromocytoma and paraganglioma

Pheochromocytoma is a rare catecholamine-producing neuroendocrine tumor derived from the chromaffin cells in the adrenal medulla [1] [2]. The embryological origin of these cells from the neural crest outlines the peculiar development and pathogenesis of these tumors. Catecholamine producing tumors arising from extra-adrenal cells are known as paragangliomas. These tumors share overlapping characteristics that span histopathology, epidemiology, and even molecular pathobiology, but also many differences in terms of their behavior, aggressiveness and metastatic potential, and they can be either sporadic or be present in multiple members of the same family [3] [4].

The study of familial syndromes of pheochromocytoma has been very important in understanding the pathogenic mechanisms involved in both familial as well as sporadic forms. Several susceptibility genes have been established as playing a central role in the

pathogenesis of both pheochromocytomas and paragangliomas [5] [6].. At the moment ten different genes have been implicated in the pathogenesis of these tumors: the von Hippel-Lindau (VHL) tumor suppressor gene, the Rearranged during transfection (RET) protooncogene, the neurofibromatosis type 1 (NF1) tumor suppressor gene, genes encoding for four subunit (A, B, C and D) of the succinate dehydrogenase (SDH) complex, a gene encoding for an enzyme responsible for flavination of the SDHA subunit (SDHAF2), and finally the genes TMEM127 and the MAX which have been recently described [7].. Genetic studies suggest that other genes may be involved in the pathogenesis of these tumors and investigations are under way to uncover novel mutations in "sporadic" cases. Extensive use of genetic analysis as common practice in the clinic, has significantly extended the number of patients identified to have genetic predisposition to pheochromocytoma and paraganglioma. Indeed, the old "rule of 10" to describe the percentage of patient with genetic disease is clearly outdated and now at least 25% of "sporadic" patients have been found to have genetic mutations in one of the genes mentioned above. The proteins encoded by these genes are involved in several cellular pathways. The detailed and thorough dissection of the molecular pathways will help to better understand the pathogenic mechanisms underlying the disease and to identify novel key molecules to be used for targeted molecular therapy, for diagnostic and prognostic purposes.

According to more recent publications, up to 30-32 % of these tumors are genetically inherited [8] and it is estimated that this number will rise in the future when new susceptibility genes will be discovered. Indeed, it is generally accepted that certain

susceptibility genes yet to be discovered may not 'at first look' seem to run in families due to their very low penetrance inspite of passing down several generations.

Hereditary pheochromocytomas and paragangliomas can be divided into two clusters based on transcription profile revealed by microarray analysis. One cluster is the tumors with VHL and SDHx mutant genes and the other cluster contains tumors with RET and NF1 mutant genes [9,10]. Sporadic tumors were surprisingly represented in both clusters. As newer genes were discovered further microarray studies tried to classify them into these two clusters and mutations in KIF1Bbeta, TMEM127 and MAX clustered with RET/NF1 and SDHAF2 and SDHA clustered with SDHx/VHL [11].

In the following discussion, we are briefly summarizing the current knowledge on the susceptibility genes in these two clusters.

1.3 Susceptibility genes and molecular pathways: the gateway to a better understanding of the pathophysiology of pheochromocytoma.

1.3.1 The VHL and SDH clusters

In the past a link between high altitude chronic hypoxia and an increased prevalence of hyperplasia of the carotid bodies as well as a higher prevalence of paragangliomas compared to those living at sea level has been observed. This association and the fact that the carotid body plays a central role in oxygen sensing made researchers believe that oxygen sensing might play a role in the tumorigenesis of paragangliomas [12]. The basis underlying this association seems to be confirmed with the pseudohypoxia hypothesis for tumorigenesis caused due to VHL and SDHx mutations. Mutations in these genes lead to accumulation and stablization of hypoxia inducible factor alpha. Hypoxia Inducible

Factor alpha (HIF) heterodimerizes with HIF beta and acts as an active transcription factor which induces a variety of genes involved in cellular and tissular adaptation to hypoxia (angiogenesis, metabolism and survival). The HIF alpha is hydroxylated by prolyl hydroxylases (more specifically EGLN1) under normoxic conditions into hydroxylated HIF alpha. This is recognized by the VHL protein and marked for degradation in the proteasome. If the VHL gene is mutated the protein is not formed and HIF alpha cannot be degraded and it accumulates. Succinate dehydrogenase enzymes convert succinate to fumarate and its mutation leads to accumulation of succinate. Succinate is a competitive inhibitor of the prolyl hydroxylase EGLN1 and leads to accumulation of stable HIF alpha. Therefore VHL and SDHx mutations both lead to induction of genes that would have also been induced via hypoxia and lead to tumor development by different mechanisms through the same pathway [11,13]. (Figure 1) A mutation in the prolyl hydroxylase domain 2 gene has recently been implicated in a case of recurrent paragangliomas and erythrocytosis. This mutation affects PHD2 function and stabilizes HIF-α proteins. Also loss of heterozygosity could be indicative that the *PHD2* could be a tumor-suppressor gene [14].

Patient with the von-Hippel Lindau disease, an autosomal dominant familial cancer, are prone to develop several types of tumors, including renal cell carcinoma and pheochromocytoma. Tumors of vascular origin are frequently a common clinical presentation in these patients. The VHL gene, located on the chromosome sub-band 3p25-26, encodes for the VHL protein, whose best characterized function is the ubiquitination and consequent degradation via the proteasome of the hypoxia inducible factor alpha (HIF-alpha) protein [15]. In patients with VHL disease, the loss of pVHL

function lead to lack of HIF-alpha ubiquitination and degradation and consequent upregulation of several hypoxia inducible genes.

The presence or absence of pheochromocytoma is one of the criteria to classify the VHL disease as a type 1 (absence) or type 2 (presence), with the subtype 2C classification reserved for families with pheochromocytoma only. Most of the VHL-related pheochromocytomas have a loss of the wild type allele as a second hit, according to the Knudson's two hit hypothesis of tumor suppressor genes.

Pheochromocytomas developing in VHL syndrome have several differences compared to the sporadic tumor, including the multifocal location and the earlier onset; more over they tend to have a noradrenergic phenotype [16].

More recently, pheochromocytoma susceptibility has been associated with mutations in the succinate dehydrogenase (SDH) gene. Succinate Dehydrogenase is both part of the Electron Transport Chain (ETC, complex II) and the Kreb's cycle, and its sub-units are encoded in the nucleus and imported to the mitochondria [17]. THE SDH gene encodes for four subunits: SDHA, SDHB, SDHC and SDHD. SDHA (flavinated by the SDHAF2 protein in the complex) and SDHB (iron-sulfur protein) hold catalytic function and are bound to the inner mitochondrial membrane by the SDHC and SDHD subunits. Mutations in these subunits cause the complete loss of enzymatic activity in the complex and lead to oncogenesis by upregulation of pro-angiogenic response genes [17]. In particular mutation in the SDHB subunit has been associated with a high likelihood of malignancy [18]. Interestingly, electron channeling through this complex does not result in H^+ gradient build up and its function is believed to primarily reduce the amount of

reactive oxygen species (ROS) that normally leaks from aerobic respiration. Pheochromocytomas represent excellent examples of the link between mitochondrial function and oncogenic proteins in the promotion of cancer development and the metabolic adaptation of tumor cells, combining increased glycolysis with a defective mitochondrial respiration.

The first association made between SDH and tumorigenesis was established by Baysal et al [19] when they investigated a hereditary paraganglioma. They were able to map a gene designated as *PGL1* in the chromosome band 11q23 and later confirmed to code for the subunit D of the SDH complex. Shortly after, mutations in genes that codes for sub-units B (*PGL4*) and C (*PGL3*) were identified as genes of susceptibility [20,21]. Missense, frameshift and nonsense mutations predisposing to pheochromocytoma have been identified in all the subunits of the SDH complex, including more recently in the SDHA subunit [22] and in the SDH5/SDHAF2 gene, identified in patients with head and neck paragangliomas [23].

Dopamine and norepinephrine or dopamine alone characterizes the biochemical phenotype in these patients [24].

1.3.2 The RET and NF1 cluster

This gene expression cluster is linked together by the activation of kinase signaling pathways driven by oncogenes. Activation of receptor tyrosine kinases (RTK) leads to downstream activation of several intracellular pathways through a series of consequent phosphorylation events. RET and NF1 mutations lead to activation of the RAS/RAF/MAPK and the PI3K/AKT/mTOR signaling pathways. TMEM127 mutant

tumors clusters with the RET/NF1 group and they enhance mTOR activity independent of the above two kinase pathways.

Microarray expression analysis of KIF1Bbeta mutant tumors also groups with RET/NF1 tumors though its potential role in kinase pathways is not yet known [11].

While the recently discovered MAX gene mutation, which leads to dysregulation of the MYC-MAX-MXD1 network, is grouped with this cluster for its connection with mTOR pathway [25].

The study of families with MEN2 A and B, which develop pheochromocytomas among other tumors, allowed the discovery of mutations in the RET (Rearranged during Transfection) protooncogene. The protooncogene RET is a tyrosine kinase receptor primarily expressed in neural crest cells (including parasympathetic and sympathetic ganglion cells) and urogenital cells [26]. The RET gene was originally found as a novel gene rearrangement within the NIH-3T3 fibroblast cell line following transfection with DNA from human lymphomas [27]. The name was subsequently used to designate the receptor tyrosine kinase within the fused oncogene. The RET gene resides in the pericentromeric region of the chromososome 10q11.2 and comprises 21 exons. [27,28]. The Ret protein is a transmembrane receptor with an extracellular ligand-binding portion containing four cadherin like repeats, a cysteine rich domain and a calcium-binding site. Interestingly, such organization makes RET a remote member of the cadherin cell adhesion protein superfamily [29]. These phospho-tyrosine residues are important docking sites for several intracellular adaptor proteins, making the RET receptor a versatile platform for signal transduction. Downstream targets include STAT3, Grb2, Grb7 and Grb10, Shc, PLC-gamma and Src, among others, allowing the activation of

major intracellular pathways, including the PI3K/AKT/mTOR, Ras/ERK and JNK pathways. Of note, Src is important for Ret signaling through focal adhesion kinase (FAK), which is an essential mediator of tumor cell migration and metastasis [30].
Gain-of-function point mutations in RET, causing ligand-independent activation of the gene product, is the initial oncogenic event in the hereditary cancer syndrome multiple endocrine neoplasia type 2 (MEN 2), which recognize three subtypes based on clinical presentation: 1) MEN 2A; 2) MEN 2B; and 3) familial medullary thyroid carcinoma (FMTC). Trisomy 10 with duplication of the mutant RET allele, loss of wild-type RET allele and tandem duplication with amplification of the mutant RET, are among the "second hit" mechanisms identified that favor tumor development in these patients [31].
Pheochromocytoma develops in about 50% of patients with MEN 2A and MEN 2B. There is a strong correlation between the position of the RET mutation and the clinical phenotype. For example, in MEN 2A pheochromocytomas occur more frequently in patients with RET mutations in codon 634 and less frequently when the mutation involves codons 618, 620 or 791 [32].
Loss-of-function mutations in the RET gene are responsible for a different congenital disorder, known as Hirschprung's disease (or aganglionic megacolon) in which normal enteric nerves are absent[33]. The occurrence of this disease reinforces the importance of RET in directing cells of the neural cell crest (which later become ganglionic cells) during development, and, as an important disease-causing gene.

Several groups have suggested that mutant RET in MEN 2B activates additional aberrant signaling pathways, which account for the more aggressive phenotype in patients with

this syndrome compared to patients affected by MEN 2A. Interestingly, also RET mutations in MEN 2A occur mainly in the extracellular domain cysteine residue, causing alterations in receptor dimerization, while MEN 2B RET mutation are predominantly located in the intracellular domain, resulting in activation of different signaling pathways and consequent expression of different target genes. Expression microarray analysis supports these conclusions [34]. Patients with MEN 2 syndrome have pheochromocytomas that secrete predominantly epinephrine [24].

The tumor suppressor gene Neurofibromatosis type 1 (NF 1) encodes for the protein neurofibromin, a GTPase-activating protein in the RAS signaling cascade and mTOR signaling pathway [35]. In patients with mutation in this gene, in conjunction with other tumors, pheochromocytoma is present in up to 5% of cases and it is frequently diagnosed later in life [36]. Neurofibromatosis is diagnosed clinically by a thorough physical examination or a positive family history so confirmation of diagnosis does not require genetic testing. Neurofibromatosis patients with pheochromocytomas produce both epinephrine and norepinephrine [24].

Studies on transgenic mice with NF1 mutations have clearly linked this gene with the development of pheochromocytoma. In addition, the only available mouse pheochromocytoma cells lines (the MPC cells and its derivative MTT cells) that we are using for pre-clinical experimentation were derived from this mouse model [37,38].

1.3.3 Other genes

Next generation sequencing technology and improvement in our understanding of the molecular basis of the disease, have allowed the discovery of newer pheochromocytoma susceptibility genes.

Screening more than one hundred samples from a large institutional collection of pheochromocytomas and paragangliomas, several germline mutation were identified in the TMEM127 gene [7], which encode for a transmembrane protein; although the function of TMEM 127 protein is not well characterized, a link with the mTOR pathway has been identified. Indeed, TMEM127 is involved in endosomal organelle dynamics, which may contribute to its modulation of mTOR kinase signaling [6]. Interestingly, tumor samples from patient with TMEM127 mutations have an increased activation of mTORC1[39]. Patients with TMEM127 mutation tend to have benign, bilateral adrenal pheochromocytomas; a clear association with other tumors still needs to be clarified.

Using exome sequencing, Comino-Mendez et al. [40] were able to identify MAX gene mutations in three independent familial cases of pheochromocytoma; the inactivating nature of the germline mutation points to a tumor suppression function for this gene. As mentioned before, the MAX (MYC-associated factor X) protein is a key component of the MYC-MAX-MXD1 cellular network, involved in several functions, including proliferation, differentiation and apoptosis. These tumors tend to be bilateral and are associated in 25% of cases with malignant behavior [41].

In summary, classification of pheochromocytoma into two clusters we described above is widely accepted to distinguish tumorigenesis amongst the multiple mutations observed. However, there is another proposed theory that different susceptibility genes converge into a single common pathway of tumorigenesis. According to this model the germline mutations in RET, VHL, NF1 and SDHx prevent apoptosis of the neuronal progenitor cells. Normally during embryogenesis as nerve growth factor becomes limiting, c-Jun becomes activated and induces the neuronal progenitor cells to undergo apoptosis [11].
The recognition that germline mutations in the genes described above are important in the pathogenesis and clinical presentation of patients with pheochromocytoma, provide a solid justification for genetic testing as an important part of patient management.
As new genes are identified as susceptibility genes for pheochromocytoma, this is going to be true even more so in the future. Clinical presentation, family history and histopathological and radiological characteristic of the tumor help guide the sequence in which genes must be tested.

1.4 Diagnosis

It can be difficult to decide which patients should be subjected to a work up for suspected pheochromocytoma, because is a rare disorder with a frequently aspecific clinical presentation [1]. A newer test measuring the urinary and plasma metanephrines has substituted the previously used urinary or plasma catecholamines measured to screen for pheochromocytomas. This is a better test because these metabolites of the catecholamines are released continuously from the tumor independent of the time of catecholamine

release. Thus plasma free metanephrines would offer better diagnostic sensitivity over other tests [42].

Increases in the plasma concentrations of normetanephrine and metanephrine four times above the upper reference limit are almost non-existing in patients without pheochromocytoma but occur in 70-80% of patients with the tumor [43]. In a recent study Eisenhofer et al concluded that plasma methoxytyramine (>0.2 nmol/L) is a novel biomarker for metastatic pheochromocytomas and paragangliomas. Such patients have increased likelihood of SDHB positivity, tumor size (>5 cm) and extraadrenal location of their tumor all predictors for higher likelihood of malignancy [44].

In patients with levels in the intermediate range that is above normal and below four times normal a clonidine suppression test is done to confirm the diagnosis.

Chromogranin A is an acidic protein that is stored with catecholamines in secretory granules and co released with them. It is not specific for pheochromocytomas but elevated levels are seen with many neuroendocrine tumors. Chromogranin A has a sensitivity of 83-89% for identifying pheochromocytomas and maybe elevated in both non-secretory and secretory tumors. High plasma levels indicate malignancy and correlate with tumor mass. Their levels may also be used to gauge tumor response and relapse [45].

Once the diagnosis of pheochromocytoma/paraganglioma is made with a positive biochemistry it is necessary to locate the tumor for surgical resection. Anatomical imaging is most widely used in the initial evaluation of patients as it is offers the advantages of low cost, almost universal availability, and less skill for use [5]. CT scan

can be used to localize adrenal tumors > 1 cm and extra adrenal tumors > 2 cm [46]. MRI with or without gadolinium enhancement is superior for the detection of extra-adrenal tumors. [47] Inspite of their excellent sensitivity, CT and MRI lack the specificity required to confirm a mass as a pheochromocytoma and thus functional imaging modalities are used which have a higher specificity for detection [5].

Whole body scanning using MIBG labeled with radioiodine (MIBG scintigraphy) has a higher specificity and helps to overcome the limitations of anatomical imaging [48]. MIBG scanning may be carried out with either ^{123}I or ^{131}I. MIBG scanning with ^{123}I offers a number of advantages over ^{131}I like much better sensitivity [49,50], additional utility for imaging by SPECT and shorter half-life hence higher doses can be used [50]. A recent study however found that low-dose diagnostic ^{123}I-MIBG whole-body scans at 6h and 24h detect less lesions compared to 3 days post treatment ^{131}I-MIBG whole-body scan in malignant pheochromocytoma and paraganglioma [51]. Positron Emission Tomography is another functional modality used due to its superior spatial resolution and low radiation exposure. ^{18}F-DA PET is more sensitive overall than ^{123}I-MIBG scintigraphy or somatostatin receptor scintigraphy (SRS) with ^{111}In-pentetreotide on a per patient basis. Hence it should be used in the evaluation of pheochromocytomas if available and if unavailable ^{123}I-MIBG scintigraphy should be used for nonmetastatic or adrenal pheochromocytomas and SRS should be used for metastatic pheochromocytomas [52]. Since pheochromocytomas and paragangliomas at different sites take up these biomarkers for imaging differently the sensitivity of various functional imaging studies varies for tumors according to site. Adrenal tumors should be imaged with either ^{123}I-MIBG scintigraphy, ^{18}F-DA PET or ^{18}F-DOPA PET to detect/exclude multifocal or

metastatic disease. Adrenal tumors associated with a VHL gene mutation are best imaged by ^{18}F-DA PET. In patients with extra-adrenal tumors imaging with MIBG is often not very accurate and imaging with ^{18}F-DA PET or ^{18}F-DOPA PET is a better approach. ^{18}F-DOPA PET is particularly useful to detect head and neck paragangliomas. In patients with metastatic pheochromocytomas and paragangliomas ^{123}I-MIBG scintigraphy has a limited role unless it is being used to determine whether or not the patient is eligible for ^{131}I-MIBG treatment. It is found that ^{18}FDG PET is superior in patients with metastatic SDHB paragangliomas and the ^{18}F-DOPA PET performs poorly. This radiopharmaceutical FDG is non-specific and taken up by rapidly growing tumors hence it can be used in patients with metastatic pheochromocytoma that is becoming undifferentiated to take up more specific agents. Provided that somatostatin receptors are not lost during dedifferentiation somatostatin analogues like ^{111}In-penetreotide, ^{68}Ga-DOTATOC and ^{68}Ga-DOTANOC maybe useful [5,53,54].

Genetic testing is important in patients who are <45 years, with multiple tumors, extra-adrenal tumors, family history, metastatic tumors and increased dopamine secretion. Decision for the sequence in which to test the genes is based on clinical presentation and investigations. About 40-50% patients with malignant pheochromocytoma will have mutations in SDHB (~35%), VHL (~5%) and SDHD (~1%) and hence should be offered testing for at least these 3 genes. The importance of genetic testing lies in that it helps predict prognosis for the patient, risk for the family and helps guide therapy [41].

In individuals who meet the criteria for genetic testing but for whom clinical indicators, biochemical indicators and imaging do not indicate which genes to test immunohistochemistry seems to offer an opportunity to narrow the mutations that should be tested for.

In an individual with SDHB positive immunohistochemistry staining one should test for VHL, RET or NF1 mutations. In those with negative staining implying absence of SDHB protein expression one should test for SDHB, SDHC or SDHD mutations. SDHB immunohistochemistry has a sensitivity of about 100% and a specificity of about 84% in a prospective series to detect the presence of an SDH mutation [55,56]. SDHA immmunohistochemistry has recently been shown to reveal the presence of SDHA mutations in about 3% of patients who are affected by apparently sporadic tumors [57].

There are no histological features that are certain for malignancy and the presence of lymph node involvement or distant metastases is the only widely accepted criteria for malignancy. About 10% of pheochromocytomas are malignant at the time of initial surgery or at follow up. The clinical value of the Pheochromocytoma of the Adrenal Gland Scaled Score (PASS score) based on invasion, diffuse growth, focal or confluent necrosis, high cellularity or tumor spindling has not been confirmed. Tumors that have increased likelihood of malignancy are usually larger in size, extra-adrenal, and secrete more dopamine. Also an index of tumor differentiation the epinephrine to epinephrine plus norepinephrine ratio, is lower in malignant than benign tumors [58,59].

1.5 Traditional therapeutic options

A multi-disciplinary, patient-centered approach is frequently required for an adequate management of patients with pheochromocytoma. This is accomplished byinvolving a number of specialists including an endocrinologist, a surgeon, an anesthesiologist and an oncologist at the very least along with ancillary staff.

The ultimate goal of therapy is tumor removal. In benign tumors this is more easily accomplished and once the tumor is removed the patient can have a normal symptom free life. However at the time of diagnosis it may be difficult to accurately distinguish patients who have benign tumors from patients with malignant tumors, so all patients need follow up to detect recurrence or malignancy.

Blood pressure control pre and intra-operatively to avert a hypertensive crisis is the cardinal medical management task. Postoperative hypotension maybe a risk and hence the patients need to be monitored closely as well. Most patients with hypertension are adequately controlled using the irreversible non-competitive alpha-blocker phenoxybenzamine. A portion of patients with clinical symptoms of beta-receptor stimulation (palpitations, anxiety, and chest pain) may need a beta-blockade (propranolol, atenolol or metoprolol). A beta-blocking agent should never be used in absence of an alpha-blocking agent as that could precipitate a hypertensive crisis [60]. Metyrosine a competitive inhibitor of tyrosine hydroxylase, the rate-limiting step in catecholamine synthesis decreases production of catecholamines thus making pre and intra operative blood pressure control easier [61].

Laparoscopic adrenalectomy is a safe and effective approach in most patients with a benign pheochromocytoma less than 6 cm and offers significant post-operative benefits.

Patients with large adrenal tumors (larger than 6 cm), evidence of venous involvement, or invasion into surrounding tissue should be approached cautiously [62,63]. Posterior retroperitoneoscopic adrenalectomy is now becoming the preferred approach for patients with PHEO [64]. It is a technique that is safely performed for a variety of adrenal lesions and is ideal for patients who have undergone earlier abdominal surgery, and is feasible in obese patients [65]. Patients with hereditary adrenal pheochromocytomas may undergo adrenal cortical sparing surgery, which is an alternative approach that aims to balance tumor removal with preservation of adrenocortical function [66]. The plasma or urinary metanephrine concentration should be checked 10 days after surgery, as catecholamine levels may remain high for the first week after tumor resection until all the extratumoral pools of catecholamines have emptied [58]. In malignant disease, surgical debulking of the recurrence or metastases is the primary management. In patients not amenable to surgery or in those that require additional therapy post surgery a number of palliative options are available, as discussed below.

^{131}I-MIBG therapy is indicated in patients with malignant inoperable ^{123}I-MIBG positive pheochromocytomas or paragangliomas. Its contraindications are mainly related to radiation safety and toxicity. Thyroid blockade with potassium iodide is necessary to protect the gland from radiation. The main side effects of this therapy are vomiting and rise in blood pressure (early side effects) and myelotoxicity and hypothyroidism inspite of blockage (late side effects). The routine initial dose in treatment of pheochromocytomas and paragangliomas is about 15-18.5 GBq (405-500 mCi). Doses greater than that show a significant increase in hematological toxicity without an additional improvement in response rate [67].

In rapidly progressing metastatic pheochromocytomas, the use of chemotherapy is the preferred treatment option. A combination of cyclophosphamide, vincristine and dacarbazine (CVD) have shown a 57% complete or partial radiologic response while 79% had some biochemical response [68]. The NIH updated this study with 4 more patients (total 18 patients) and followed them for 22 years. 55% patients had radiologic response to treatment and 72% had a biochemical response. This imply that CVD therapy is not indicated in every patient with metastatic disease, and should be used for patients with symptoms where tumor shrinkage might be beneficial and could lead to possible surgical resection. Based upon long-term follow-up, there is no statistically significant difference in overall survival between patients whose tumors responded to CVD compared to those whose tumors did not respond [69]. In another study done in 2011, around 33% of patients with metastatic pheochromocytoma/sympathetic paraganglioma experienced improvements in tumor size or hypertension (dose reduction/antihypertensive discontinuation) after chemotherapy. They also observed a trend toward longer survival in the responders than in the nonresponders to chemotherapy. Cyclophosphamide and dacarbazine combined with vincristine-based and/or doxorubicin-based chemotherapy was the regimen received by these patients [70]. CVD therapy can cause a hypertensive crisis due to catecholamine release during treatment and hence patients should be blocked beforehand [71].

Radiation therapy does not prevent local recurrence and cannot be used as a primary mode of therapy. This therapeutic option is mainly beneficial for relief from symptoms and pain associated with bone and lymph node metastasis [71]. Less commonly used option includes radiofrequency (RF) ablation (to control disease locally and alleviate

symptoms like pain and hypertension related to the tumor). Bone, chest wall, and retroperitoneal lesions are treated with either RF ablation or cryoablation, and liver tumors are treated with either RF ablation or ethanol ablation [72].

When recurrences are small with an accessible vascular supply surgical removal maybe preceded or replaced with therapeutic embolization. Preoperative embolization of the tumor can minimize blood loss and facilitate subsequent resection. Transcatheter arterial chemo-embolization (TACE) is particularly useful in hepatic metastases and can lead to significant reduction of the tumor mass (number and size of the lesions) in the liver without any major side effects. An increase in blood pressure after every TACE could be controlled by sufficient preadministration of an alpha-blocker [73]. Different approaches and embolizing agents has been described in the literature [74,75].

Another therapeutic approach is represented by Peptide Receptor Radionuclide Therapy. The somatostatin receptors are expressed in pheochromocytomas, particularly subtype 2A and 3 [76]. This therapy utilizes radiolabelled ^{111}In, ^{90}Y, or ^{177}Lu-labelled somatostatin analogues and is of use in patients with unresectable metastatic disease. Symptomatic improvement may occur with all radiolabelled somatostatin analogues though tumor size reduction is achieved with ^{90}Y and ^{177}Lu. High tumor uptake on somatostatin receptor scintigraphy and limited amount of liver metastases predict higher likelihood of tumor remission. Serious side-effects like myelodysplastic syndrome or renal failure are rare. The median duration of the therapy response for [^{90}Y-DOTA(0),Tyr(3)]octreotide is 30 months and for [^{177}Lu-DOTA(0),Tyr(3)]octreotate it is more than 36 months. This

treatment is being used for neuroendocrine tumors and is now gaining popularity for pheochromocytomas as well [77].

Overall, the long-term survival of patients after successful removal of a benign pheochromocytoma is basically the same as normal individuals adjusted for age due to advances in surgery and a multi-disciplinary approach in the management of these patients [78]. Patients should be followed up lifelong with annual check-ups of blood pressure measurement and urine or plasma metanephrine levels [58].

1.6 Emerging therapies

Especially for patients with malignant tumors. the therapeutic regimens above described have only limited efficacy and a great potential of significant toxicity and recurrence. Many of these treatments were introduced into clinical practice before the discovery of the genes and the molecular pathways responsible for onset of these tumors and exhibits nonselective cell toxicity.

A group of novel treatment agents, the so-called “targeted molecular therapies”, are emerging as a promising therapeutic option for several cancers [79]. At the moment, this promising cancer treatment option has been only marginally evaluated in pheochromocytoma. For example, the knowledge that chromaffin cell in tumors, especially the malignant forms, express high levels of vascular endothelial growth factor (VEGF) and other angiogenic factors, has prompted the use of inhibitor directed against these proteins and related pathways as a new treatment modality [80]. Sunitinib is a potent tyrosine kinase inhibitors targeting VEGF, platelet derived growth factor (PDGF),

RET, c-Kit and the FLT-3 receptors. Sunitinib has demonstrated promising results in a patient with advanced pheochromocytoma occurring within a VHL-syndrome [81], achieving radiologic partial remission and improved performance status after 6 months of therapy. In another study, thalidomide, which reduces VEGF levels, in combination with temozolomide, was tested in another patient with pheochromocytoma with partial radiologic response [82]. The limited number of patients involved in these clinical trials warrant only a cautious optimism, with the hope to include more patients in future studies. Other targeted therapies, including imatinib and everolimus, did not revealed positive results in a small subset of patients with pheochromocytoma [83,84]. A number of new therapeutic targets are being considered such as mTOR inhibitors, HIF inhibitors, Prolyl hydroxylase activators ERBB2 inhibitors and heat shock protein 90 inhibitors [71].

Altogether, these trials reveal that further studies are needed to evaluate this new class of medications as a possible treatment for malignant pheochromocytomas and paragangliomas.

2. MATERIAL AND METHODS

2.1 Cell line and reagents

The mouse pheochromocytoma cell lines MPC [85] and the metastatic MPC-derived MTT cell line [38] were maintained in Dulbecco's Modified Eagle Medium (DMEM) supplemented with 10% fetal bovine serum (FBS), 5% horse serum (Gibco, Invitrogen), and antibiotic/antimycotic. The highly metastatic MTT cells were generated by disaggregation and culture of tumor cells from a liver metastasis resected from mice inoculated with MPC cells, as described previously [38]. MTT-luc cells were generated by retroviral transduction of MTT cells with the firefly luciferase gene, as described previously [86]. The rat pheochromocytoma cell line PC12 [87] was maintained in Dulbecco's Modified Eagle Medium (DMEM) supplemented with 10% fetal bovine serum (FBS) and antibiotic/antimycotic. The mouse and rat pheochromocytoma cell lines were grown until 80% confluence, detached using 0.05% trypsin/EDTA, and resuspended in phosphate-buffered saline (PBS) at 5 x 10^5 cells/200 μl for injection. D-luciferin potassium salt (Caliper LifeSciences) was diluted in PBS at a concentration of 15mg/ml, filter-sterilized in a 0.22um filter, aliquot and stored and -20° C until use.

AZD8055 was provided by Astra-Zeneca (London, UK). Torin-1 was developed by the Dana-Farber Cancer Institute, Biological Chemistry and Molecular Pharmacology section, Harvard Medical School (Boston, MA). All of the compounds were dissolved in DMSO; stock solutions were stored at -20°C and thawed prior to use. Controls were treated with the highest concentration of DMSO in the panel.

The Hsp90 inhibitor 17-AAG was provided by the Cancer Therapy Evaluation Program at NCI-Frederick (Frederick, MD). The new generation Hsp90 inhibitor STA-9090 (Genatespib) was provided by Synta Pharmaceutical Corp. (Lexington, MA).

2.2 pLLuc construct and retroviral transduction

The EGFP gene in the retroviral vector pLEGFP-N1 (Clontech) was replaced with the firefly luciferase gene generated via PCR from the pGL3-Basic (Promega) vector and inserted between the BamH-1 and Not-1 sites resulting in the pLLuc retroviral vector. The retrovirus packaging cell line Amphopak-293 (Clontech) was transfected with the pLLuc retroviral vector to generage 293pLLuc cells. Selection with G418 enabled the generation of stably transfected 293pLLuc cells. Target cells were transduced with pLLuc by incubating them overnight with conditioned medium obtained from 293 pLLuc cells containing retroviral particles and filtered through a 0.45 mm filter to remove any cellular debris. Transduced cells were incubated with the filtered supernatant overnight and selected with G418 to generate stable cell lines expressing luciferase.

2.3 Animal experiment and BLI imaging

All animal studies were conducted in accordance to the principles and procedures outlined in the National Institutes of Health (NIH) Guide for the Care and Use of Animals and approved by the NIH Animal Care and Use Committee (ACUC).
Cells were growth until 80% confluence, then cells were detached using 0.05% Trypsin/EDTA, incubated for 3 minutes at 37° C and resuspended and counted to obtain the desired concentration. For the experiments involving the development of the animal

models, we obtained a concentration of 0.5 x 10^6 cell/200 µl before injection. Cells were injected tail vein or subcutaneously into female athymic nude mice (Taconic, Germantown, MD). Experimental groups consisted of 10 weeks old mice (n=6 for the experimental animal model experiments and for the spontaneous metastasis model) housed in a pathogen-free facility. The animals were imaged weekly by both Bioluminescence (BLI) and/or MRI imaging (described below). For BLI imaging, mice were anesthetized with isofluorane, injected with 0.1 mg/gr D-luciferin and imaged after 15 minutes as described below (MRI imaging) and then euthanized using CO2 inhalation and cervical dislocation. Several organs from the mice were dissected and preserved in 10% formalin.

For the experiment involving the use of the mTORC1/2 inhibitors (using the spontaneous metastasis model) 1.5 x 10^6 MTT-luc cells were injected subcutaneously in the right flank of female athymic nude mice (Taconic, Germantown, MD). The experimental group in this set of experiments consisted of 10 weeks old mice (n=7) housed in a pathogen-free facility. After 10 days, allowing for tumor cells to engraft, we started a treatment with 20 mg/kg of AZD8055 in one group of animals (n=7). Animals in control group (n=7) were treated with the same volume of vehicle instead, on a daily, seven days out of seven schedule. The animals were imaged weekly by Bioluminescence (BLI, described below).

For the experimets involving the testing of Hsp90 inhibitors: for the experimental metastasis model 0.5 x 10^5 MTT-luc cells were injected into the tail vein of female athymic mice (Taconic Farms). For the spontaneous metastasis model 1.5 x 10^6 MTT-luc cells were injected subcutaneously in the right flank of female athymic mice.

Experimental groups consisted of mice injected at 10 weeks (n=6 for 17-AAG; n=8 for ganetespib), housed in a pathogen-free facility. The animals were imaged weekly by bioluminescence imaging (BLI) as described below. For BLI imaging, mice were anesthetized with isoflurane, injected with 150mg/kg D-luciferin and imaged after 15 minutes as described below. For the experimental metastasis model (MTT-luc cell tail vein injection) we performed survival experiments; the endpoint criteria for euthanasia (performed by CO_2 inhalation and cervical dislocation) included a significantly hunched posture, significantly rough fur, a body condition score (BCS) of 1 (a BCS of 3 is ideal, with 2 representing a thin condition and 1 when the animal is emaciated), or a pain score (PS) of > 3 (a PS of 1 indicates no pain or distress; 2 indicates mild or transient pain or distress; and 3 and 4 indicate moderate to severe pain/distress, respectively). Conditions of the animals, including pain levels, were monitored daily. For the spontaneous metastasis model, on day 49, after *in vivo* bioluminescence measurements were taken, the animals were euthanized (using CO_2 inhalation and cervical dislocation), and both lungs and liver were excised and luciferase activity quantified. The organs from the mice were dissected and preserved in 10% formalin.

2.4 Hsp70 secretion

Secreted Hsp70 was measured in mouse plasma by enzyme-linked immunosorbent assay (ELISA; Assay Designs Inc.), following the manufacturer's protocol. Briefly, blood of tumor-bearing mice was collected before and 6 hours after intraperitoneal (i.p.) injection of 17-AAG as indicated. Plasma was separated by centrifugation (4°C, 14000 rpm, 10 minutes) and kept at -80°C until analysis.

2.5 Bioluminescence Imaging

All bioluminescent data were collected and analyzed with a Xenogen IVIS system (IVIS; Calipers, Perkin Elmer).

In vitro imaging, MTT-luc bioluminescent cells were serially diluted from 4000 to 8 cell in DMEM media in a 96 well plate, and D-luciferin at a concentration of 150 ug/ml was added directly to the media 10 minutes before imaging. Imaging was performed at 20 seconds/plate.

For *in vivo* imaging, luciferase activity was performed on anesthetized animals (1-2% isoflurane) 15 min following i.p. administration of 150mg/kg luciferin in phosphate-buffered saline. The mice were then placed inside a light-tight box under continous exposure to 1-2% isofluorane. The experiments were performed in the NIH Mouse Image Facility in accordance to ACUC regulations.

All imaging variables were equals and photographic and bioluminescent images at different time point were collected for each sample. The bioluminescence data are presented visually as a color overlay on the photographic image. Using the Living Image software (Caliper, Perkin Elmer), a region of interest (ROI) was drawn around tumor sites of interest and the total photons count or photons/s was quantified.

2.6 MRI

For MRI, anesthesia was induced in a chamber with 5% isoflurane in an 80%/20% medical air/oxygen mixture. The mouse was then transferred to a cradle with a built in mask and anesthesia was maintained at 30-45 breaths per minute with 1-2% isoflurane.

Temperature was maintained by blowing heated air through the bore of the scanner. (Bair-Hugger/Arizant, Eden Prarie, MN)

All scans were performed using a 7 Tesla Bruker Biospec system (Bruker-Biospin, Billerica, MA) and a 35mm linear bird cage coil. Each data set consisted of an initial locator scan, followed by a T_2-weighted scan, and a proton density weighted scan. To reduce motion artifacts, the acquisition was gated so that acquisition occurred between breaths (Small Animal Instruments, Inc. Stony Brook, NY).

T_2-weighted images consisted of twelve 1mm slices over a 6x3cm FOV acquired using a RARE (Rapid Acquisition Relaxation Enhanced) sequence. The image matrix was 256x256 and 4 echoes were acquired per excitation. The effective echo time was 20.6ms. Proton density weighted images consisted of twelve 1.5mm slices over a 3x3cm FOV acquired using a FLASH (Fast Low Angle Snapshot) sequence. The image matrix was 256x256, TE was 3ms, and the excitation flip angle was 30 degrees.

2.7 Real-time PCR

Real-time PCR was performed on a 7500 Real Time PCR System (Applied Biosystems) using detector Taqman, reporter FAM and quencher TAMRA for the genes and detector VIC for 18S rRNA. Primer sequences TaqMan® Gene Expression Assays were from Applied Biosystems as recommended for the genes. Primers were premixed to a concentration of 18 μM for each primer and 5 μM for the probe, which represented a 20X mix. Final reaction volume was 25 μl; amounts of templates for 18S rRNA and for other genes were 5 ng and 25 ng, respectively. PCR reaction was performed as follows: 50°C for 2 minutes, 95°C for 10 minutes, and 50 cycles of two-step PCR (95°C for 15 seconds

and 60°C for 1 minute). The results were analyzed by 7500 system software, version 1.3 (Applied Biosystems), calculated based on the delta-delta Ct method and then by Microsoft Excel. Each result was correlated to the housekeeping gene 18S rRNA.

2.8 Drug treatment and western blotting

MTT cells in logarithmic growth (~70% confluent) were treated with the indicated concentrations of rapamycin, AZD8055 or Torin-1 for 6 hours, or 17-AAG or ganetespib for 20 hours at 37^{o}C in 5% CO_2. Control cells were incubated with the vehicle for the same period of time. Cells were washed twice with cold PBS and lysed in TNESV lysis buffer (50 mM Tris-HCl pH 7.5, 2 mM EDTA, 100 mM NaCl, 1 mM sodium orthovanadate, 1% Nonidet P-40) or Cell lysis buffer (Cell Signaling) supplemented with Complete^{TM} (Roche) protease inhibitors cocktail). Protein lysates were denatured by boiling in 4X sodium dodecyl sulfate (SDS)-sample buffer for 5 minutes. Nuclear extracts were prepared as described by Isaacs et al. [88]. Proteins were separated by 4-20% gradient SDS-PAGE (Bio-Rad Laboratories) and transferred to a polyvinylidene fluoride (PVDF) membrane (Millipore).

For the experiment involving the use of the mTORC1/2 inhibitors, the membranes waere incubated with total-Akt, phospho-Akt (Ser473), phospho-S6 (Ser235/236), phospho-S6 (Ser240/244), phospho-eEF2k (Ser366), phospho-eIF4B (Ser422), and actin primary antibodies (Cell Signaling) overnight at 4°C which was followed by washing and incubation with the HRP- conjugated secondary antibody at RT for 1h. The blots were visualized using Amersham ECL Plus Western Blotting Reagents.

For the experiment involving the use of the Hsp90 inhibitos, PhosphoS473-Akt and Akt (Cell Signaling Technology), HIF-1α (Santa Cruz Biotechnology) and tubulin (BD Pharmingen, for loading control) were measured by immunoblotting. For poly(ADP-ribose) polymerase (PARP) cleavage, MTT cells were treated with the indicated concentrations of 17-AAG or ganetespib for 20 hours at 37°C and 5% CO_2. PARP (Cell Signaling Technology) and actin (Millipore, for loading control) were measured by immunoblotting.

For the experiment involving the use of drugs from the NPC library: for PARP cleavage, MTT cells were treated with the indicated dose and concentration of drug for 20 hrs at 37ºC and 5% CO_2. Cleaved and full-length PARP (rabbit anti-PARP antibody from Cell Signaling and HRP-conjugated anti-rabbit antibody from Jackson ImmunoResearch) and actin (mouse anti-actin antibody from Millipore and HRP-conjugated anti-mouse antibody from Jackson ImmunoResearch), for loading control, were measured by immunoblotting.

2.9 Cell proliferation assay

Cell proliferation was determined by 3-(4,5-dimethylthiazol-2-yl)-2,5-diphenyltetrazolium bromide assay. MTT cells (15×10^3) were incubated in 96-well plates for 24 hours in complete medium before the addition of the indicated concentrations of rapamycin, AZD8055, Torin1 or 17-AAG and ganetespib. A solution of 3-(4,5-dimethylthiazol-2-yl)-2,5-diphenyltetrazolium bromide (1 mg/ml; Sigma-Aldrich) was added and plates were incubated at 37°C for 3 hours before measuring

absorbance at 562 nm using a Wallac Victor 3 1420 Multilabel plate reader (Perkin Elmer).

2.10 Cell migration assay

Cell migration was measured using modified Boyden chambers / Transwell assay (BD Biosciences). MTT cells were seeded at 150,000 cells per chamber, and cell migration was stimulated for 24 hours with serum (10%) in the absence (control) or presence of the drugs (AZD8055 and Torin1; 17-AAG or ganetespib) using the indicated doses. After 24 hours cells were fixed and stained using the Diff-Quick assay (Dade Behring Inc.). Mean values from four fields (1 × 1.4 mm) were calculated for each of triplicate wells per condition. IC_{50} values were determined using Graph Pad Prism software (Graph Pad Software). Bright field images were digitally acquired using an Olympus photomicroscope and IPLab software (Scanalytics). Mean values from four fields (1 × 1.4 mm) were calculated for each of triplicate wells per condition. IC_{50} values were determined using GraphPad Prism software.

2.11 Ethics Statement

All animal studies were conducted in accordance with the principles and procedures outlined in the National Institutes of Health (NIH) Guide for the Care and Use of Animals and were approved by the Eunice Kennedy Shriver National Institute of Child Health and Human Development Animal Care and Use Committee,(Animal Study Proposal #12-028 and the PHS Assurance # A4149-01). Pheochromocytoma tumor tissue was obtained from patients visiting the Clinical Center (Institutional Review Board

(IRB) protocol # 00-CH-0093) at the National Institutes of Health (NIH), in accordance with the principles and procedures outlined in the NIH IRB Guidelines, and this was approved by the Institutional Review Board of Eunice Kennedy Shriver National Institute of Child Health and Human Development (NICHD) NIH. All patients signed an IRB approved consent that allowed for the collection of tissue samples

2.12 Human samples

Pheochromocytoma tumor tissue for the real time PCR and for drug testing was obtained from patients visiting our clinic (Institutional Review Board (IRB) protocol # 00-CH-0093); the study was approved by the IRB of the NICHD/NIH, and patients gave written informed consent. Table 1 and table 2 summarize patient clinical information. Guidelines for genetic testing was previously described [89]. Normal human adrenal medulla (n=4) was obtained form anonymous organ donors with absent adrenal tumor or dysfunction and collected within 2-5 hours after confirmed brain death at the Department of Urology, School of Medicine, Comenius University, Bratislava, Slovakia. Separation of cortex from adrenal medulla was ascertained as previously described [90].

2.13 Histopathology

In order to confirm the presence of pheochromocytoma tumor cells, we removed from the mice selected tissues and preserve them in 10% formalin immediately after *ex vivo* imaging. Tissues were paraffin embedded, sectioned and stained with hematoxylin and eosin, and analyzed by microscopy using a Leica microscope.

2.14 Tumor dissociation and tyrosine hydroxylase immunocytochemistry in primary cell culture

Pheochromocytoma tumor tissue obtained from two patients visiting our clinic (Institutional Review Board (IRB) protocol # 00-CH-0093) was minced to 2-3 mm pieces in a 100 mm Petri dish. The pieces were transferred to 15 ml Falcon tubes filled with culture medium containing collagenase B (1mg/ml; Roche Applied Science). The tissue pieces were incubated for 1 hour at 37°C, rocking the tube gently every 10 minutes. The pieces were allowed to settle, and the supernatant was aspirated and transferred to a new Falcon tube. The cell solution was centrifuged at 1,000 rpm/minute for 5 minutes. The pellets were resuspended in complete culture medium and the cells were seeded in 96-well plates coated with collagen IV (BD Biosciences). The following day, cells were washed with PBS and medium was added containing different concentrations of the drug (AZD8055 or 3uM Torin-1; ganetespib). The final concentration of DMSO did not exceed 0.03% including control wells. The cells were treated every other day for 10 days, with drug washout and readministration every two days. On day 10, the primary cultures were washed with PBS, incubated with H_2O_2 and blocked for 1 hour at room temperature. The cells were then incubated with primary anti-tyrosine hydroxylase (TH) antibody (Immunostar), diluted 1:500 in Signal Stain® Ab Diluent (Cell Signaling Technology), in humidifying chambers at 4°C overnight. TH is a marker of catecholamine-synthesizing ability, in order to discriminate tumor cells from non-neoplastic fibroblasts and other cell types in primary cultures [91]. The following day, cells were incubated with secondary anti-mouse-horseradish peroxidase (HRP)-conjugated antibody (Dako EnVision+ System- (HRP) Labeled Polymer; Dako) in

humidifying chambers at room temperature for 1 hour. The antigen-antibody interaction was visualized using Dako Liquid diaminobenzidine (DAB) + Substrate Chromogen System. The cells were counterstained with Mayer`s hematoxylin solution (Sigma-Aldrich) for 5 minutes and washed in dH_2O. Glycerol was added to prevent cells from drying and imaged immediately. TH-positive cells were counted and normalized to control (untreated) cultures.

2.15 Quantitative high-throughput proliferation assay summary and protocols for MTT cells

Cell viability after compound treatment was measured using a luciferase-coupled ATP quantitation assay (CellTiter-Glo, Promega) in MTT cells. The change of intracellular ATP content indicates the number of metabolically competent cells after compound treatment. MTT cells were harvested from T225 flasks and resuspended in DMEM medium with 5% FBS and 1% horse serum. Then 5µl of a suspension of 200,000 cells/ml was dispensed into each well of white, solid bottom, 1536-well tissue culture–treated plates using a Multidrop Combi dispenser. After overnight culture at 37°C with 5% CO_2, a total of 23 nl of compounds at 8 selected concentrations from the NPC or positive control (10mM stock of doxorubicin hydrochloride) in DMSO was transferred to each well of the assay plate using a pintool (Kalypsys, San Diego, CA), and the plates were further incubated at 37°C with 5% CO_2 for 24 or 48 hrs. After that, 4 µl of CellTilter-Glo^{TM} luminescent substrate mix (Promega) was added to each well (Supplementary Table X). The plate was incubated at room temperature for 15 minutes. The plates were

measured on a ViewLux plate reader (PerkinElmer) with a clear filter. The final concentration of the compounds in the 5 μl assay volume ranged from 0.5 nM to 46 μM.

2.16 NPC library screening

The NPC consists of 3,826 small molecule compounds, with 52% of the drugs approved for human or animal use by the FDA [92]. The remaining drugs are either approved for use internationally (i.e. in Europe, Canada, or Japan), or are compounds that have been tested in clinical trials. Additional detailed information on the drug library can be found at http://tripod.nih.gov/npc/.

The compounds from the NPC library were prepared as 15 interplate titrations, which were serially diluted 1:2.236 in dimethyl sulfoxide (DMSO) (Thermo Fisher Scientific, Waltham, MA) in 384-well plates. The stock concentrations of the test compounds ranged from 10 mM to 0.13 μM. The transfer of the diluted compounds from 384-well plates to 1536-well plates was performed using an Evolution P^3 system (PerkinElmer Life and Analytical Sciences, Waltham, MA). Each treatment plate included concurrent DMSO and positive control wells and concentration-response titrations of controls, all occupying columns 1 to 4. During screening, the compound plates were sealed and kept at room temperature, whereas other copies were maintained at −80°C for storage.

2.17 Data analysis

qHTS data analysis and curve fitting. To determine compound activity in the qHTS assay, the titration-response data for each sample were plotted and modeled by a four parameter logistic fit yielding IC_{50} and efficacy (maximal response) values. Raw plate reads for

each titration point were first normalized relative to positive control (doxorubicin hydrochloride, 100% inhibition) and DMSO-only wells (basal, 0%). Curve-fits were then classified by the criteria described [93]. Usually the qHTS screen yielded hits with a wide range of potencies and with substantial variation in the quality of the corresponding CRCs (efficacy and number of asymptotes), which included samples associated with shallow curves or single-point extrapolated concentration responses; these were assigned as low-confidence actives. In brief, Class 1.1 and 1.2 were the highest-confidence complete CRCs containing upper and lower asymptotes with efficacies ≥ 80% and < 80%, respectively. Class 2.1 and 2.2 were incomplete CRCs having only one asymptote with efficacy ≥ 80% and < 80%, respectively. Class 3 CRCs showed activity at only the highest concentration or were poorly fit. Class 4 CRCs were inactive, having a curve-fit of insufficient efficacy or lacking a fit altogether.

There were a total of 30 plates in the primary qHTS screen, which included 24 plates corresponding to the NPC library set and 6 DMSO plates. Compounds from the primary qHTS screen were classified into three categories according to the quality of curve fit and efficacy. Actives were compounds in curve class 1.1, 1.2, 2.1 and 2.2 curves with efficacy higher than 60%; inactives were compounds with class 4 curves; and inconclusive included all other compounds including those shallow curves and curves with single point activity.

2.18 Determination and quantification of viable cells by flow cytometry

PC12 cells were plated overnight and incubated with three different concentrations of the various drugs for 24 hrs. To determine apoptotic and viable cells, cells were washed with

PBS buffer (2mM EDTA, 0.05% BSA in PBS) and stained with 5 µl of 7-AAD (BioLegend) for 10 min. Cells were acquired by flow cytometry (MACSQuant Analyzer, Miltenyi Biotec) and 7-AAD-negative viable cells (%) were analyzed by FlowJo software (Tree Star).

2.19 Murine MTT cell microarray processing and analysis

Three separate MTT cell samples were prepared according to Affymetrix protocols (Affymetrix, Inc.). RNA quality and quantity was ensured using a Bioanalyzer (Agilent, Inc.) and NanoDrop (Thermo Scientific, Inc.) respectively. Per RNA labeling, 200 ng of total RNA was used in conjunction with the Affymetrix recommended protocol for GeneChip 1.0 ST chips.

The hybridization cocktail containing fragmented and labeled cDNAs was hybridized to the Affymetrix Mouse Genome ST 1.0 GeneChip. The chips were washed and stained by the Affymetrix Fluidics Station using the standard format and protocols as described by Affymetrix. The probe arrays were stained with streptavidin phycoerythrin solution (Molecular Probes, Carlsbad, CA) and enhanced using an antibody solution containing 0.5 mg/ml of biotinylated anti-streptavidin (Vector Laboratories, Burlingame, CA). An Affymetrix Gene Chip Scanner 3000 was used to scan the probe arrays. Gene expression intensities were calculated using Affymetrix AGCC software.

Partek Genomic Suite was used to RMA normalize (Robust Multichip Analysis), summarize, logtransform the data, and run ANOVA analysis and hierarchical clustering.

2.20 Microarray data analysis

RNA extraction from MTT cells was performed as previously described [90]. RNA quality and quantity were ensured using Bioanalyzer (Agilent Technologies, Inc., Santa Clara, CA, USA) and NanoDrop (Thermo Scientific, Wilmington, DE, USA) analysis, respectively. Samples in triplicate were processed following the recommended Affymetrix protocol. Fragmented and labeled cDNA was hybridized onto Mouse GeneChip 1.0ST chip arrays (Affymetrix, Santa Clara, CA, USA). Staining of biotinylated cDNA and scanning of arrays were performed according to the manufacturer's recommendations. These data are available at the GEO database. Raw CEL-files were imported into R statistical package [94] (http://www.bioconductor.org) to perform probe set summarization, background subtraction, and quantile normalization using the RMA method. Gene-wise *Z*-score normalization across all samples was applied to adjust for technical variation [95]. The replicate correlation was measured to be >0.98, and an average of replicates was used for further analysis.

A subset of patient data that was previously published [96] (GSE 39716) containing *SDHB* mutation samples was used for comparison with MTT cell line expression. Gene targets for the drugs tested on MTT cell lines were compiled from databases (NPC, Drug Bank and Therapeutic Target Database), and a total of 2129 genes were mapped to 22 drugs. Datasets from mouse cell lines and SDHB samples were independently scaled to Z-scores before merging them. The merged data was subset by the common genes from drug targets, with a total of 1753 genes in common.

Genes corresponding to < 2-fold change between the MTT cell line and SDHB PHEO datasets were considered for further analysis. This selection criterion resulted in a list of

1440 genes with an overall correlation of 0.86. To evaluate the similarity of drug targets between MTT vs. SDHB samples, a Pearson correlation coefficient was computed between a set of target genes from each drug with an overall average correlation of 0.8.

2.21 Network construction, visualization and analysis

Two metabolic models corresponding to different levels of information were constructed. One is a general model that contains the 22 tested drugs and their curated target genes (Figure 4). The second network derives from the first one, which is based on the top 20 hub nodes. Network assembling, visualization and determination of statistical parameters were performed using Cytoscape v2.8.3 [97]. For functional and topological analysis, Reactome FI [98] and cytoHubba, plugins for Cytoscape were used. The Reactome FI plugin was designed to find network patterns related to cancer and other types of disease. This plugin accesses the Reactome FI network, a highly reliable, manually curated pathway-based protein functional interaction network covering close to 50% of human proteins, and allows construction of a FI subnetwork based on a set of genes. The cytoHubba plugin allows analysis of the topology of interaction networks and identification of essential nodes (hub nodes) that may serve as candidates of drug targets for developing novel therapies. The subnetwork of these essential nodes may help us get a more precise insight into the functions and how they collaborate together. As a measure of node importance, eccentricity scores were computed. The eccentricity is a node centrality index. The eccentricity of a node v is calculated by computing the shortest path between the node v and all other nodes in the graph, then choosing the “longest” shortest path (let (v, K) be a path, where K is the most distant node from v). Once this path with

length dist(v, K) is identified, its reciprocal is calculated (1/dist(v,K)). By doing that, an eccentricity with higher value assumes a positive meaning in terms of node proximity.

2.22 Drug synergism analysis

For the synergism study we used the CalcuSyn Windows software for dose-effect analysis and synergism/antagonism quantification, following the manufacturer's instructions. Drug synergism was determined from median effect analysis equations developed by Chou-Talalay [99,100]. Cell proliferation data (MTT assay) were analyzed using CalcuSyn software (Biosoft UK). Combination Index (CI) indicates *additivity* when CI = 0.8-1.2; synergism when CI < 0.8; and antagonism when CI < 1.2. The DRI shows the potential dose reduction of each single drug in synergistic combination at a given effect level achieved by combining these drugs.

2.23 Statistical analysis

Tumor volume and mean bioluminescence was determined for each experiment together with the standard errors of the mean. To illustrate the relationship between bioluminescent signal, tumor volume and cell number a regression plot was used. Statistical analyses were performed using Graph Pad Prism software, including unpaired t test and non-parametric Mann-Whitney test (Graph Pad Software).

3. RESULTS

3.1 CHARACTERIZATION OF TWO MOUSE MODELS OF METASTATIC PHEOCHROMOCYTOMA USING BIOLUMINESCENCE IMAGING.

3.1.1 Generation of stably transduced luciferase expressing MTT cells.

The generation of aggressive, rapidly growing mouse pheochromocytoma cell line MTT from liver metastasis of MPC cells has been previously described [38,85]. For retroviral delivery and expression of luciferase in MTT cells, I first generated the construct pLLuc via replacement of EGFP with a luciferase gene between the BamH-1 and Not-1 sites of the retroviral vector pLEGFP. This construct employs the human cytomegalovirus (CMV) immediate early promoter to drive firefly luciferase expression while the expression of the neomycin resistance gene is driven by a separate constitutively active viral promoter contained within the 5' LTR. After transfection with the pLLuc and selection with G418 of the packaging cell line Amphopak-293, filtered conditioned medium from the stably transfected 293-LLuc cells containing retroviral particles was used to transduce MTT cells. The infected MTT cells were then selected with G418 for four weeks to obtain stably transduced MTT-Luc cells. Quantitation of firefly luciferase expression in MTT-Luc cells was done by directly adding a luciferin substrate into the culture medium of plated cells. Luminescence was imaged to obtain photon/s per cell 15 minutes after addition of the substrate. As shown in Figure 1 (panel A), serial dilutions of these cells showed a proportional decrease in mean photon emission, with an average of 200 photons/s per cell, indicating a stable and sustained intensity of the bioluminescence signal. These new cell line were names "MTT-luc".

Analysis of covariation between number of cells plated and light intensity (total photon flux) showed a highly significant correlation ($R^2 = 0.995$) as illustrated in Figure 1B.

3.1.2 Detection and non-invasive BLI monitoring of MTT-luc cell in an experimental metastasis model.

I then used a tail vein (experimental metastasis) injection of MTT-luc cells to evaluate the sensitivity of BLI to detect experimental metastasis after systemic circulation of the tumor cells. Mice were imaged immediately after injection to verify the success of the procedure and subsequently imaged over time by BLI over a 7-weeks period. BLI Images of a representative nude mouse is shown in Figure 2A (upper sequence). In parallel animals were subjected to serial MRI. Shown in Figure 2A (lower sequence) are MRI images of the same mouse over the same time period.

The results show that tumor signals increased significantly over the seven weeks of the study with exponential growth seen especially localized in the upper abdominal cavity. As expected, localized bioluminescent signals indicating metastasis began to appear in the area of the liver and were detectable at an early stage of development, starting at the second week post-injection. By the third week, several areas of tumor growth were evident by both BLI and MRI. Total photon flux from tumors seen in BLI was found to correlate well with the number of lesions observed by MRI (Figure 2B). An analysis of covariation between number of metastatic lesion as counted on the MRI image and bioluminescent light intensity (total photon flux) shows a highly significant correlation ($R^2 = 0.992$) as illustrated in Figure 2C. By the 4^{th} week the tumor masses were clearly identifiable by MRI. Figure 2D illustrates the progression of tumor size over time from

the 4th week represented as a sphere from averaged tumor diameters calculated by MRI analysis. The survival curve representation for this model is shown in Figure 2E.

At necropsy, several organs were excised, imaged *ex vivo* and preserved for histological evaluation. *Ex vivo* bioluminescence confirmed the presence of MTT-luc metastasis in the liver and in several other organs, including lungs, spleen, ovaries, kidney and brain (Figure 2F and Table 1). The total photons/sec of the organs were quantified for each animals (n = 6) and mean values are displayed in Figure 2F.

Table 1. Comparison of number of metastatic lesions in the two animal models (metastatic-take).

	Experimental metastasis model (tail vein injection)	**Spontaneous metastasis model (subcutaneous injection)**
Liver	6/6 (100 %)	6/6 (100 %)
Lungs	6/6 (100 %)	6/6 (100 %)
Brain	4/6 (66 %)	5/6 (83 %)
Spleen	6/6 (100 %)	2/6 (33 %)
Ovary	4/6 (66 %)	4/6 (66 %)
Kidney	1/6 (16%)	3/6 (50 %)

3.1.3 Tumorigenicity and spontaneous metastasis of subcutaneously implanted MTT-luc cells.

To assess the tumorigenicity and tumor growth modality of the MTT-luc cells in immunocompromised animals, I injected 1x10^6 cells s.c. into the left flank of 6 week old nude mice. The use of luciferase-reporter cells allowed for the immediate detection of tumor cells at the time of injection and enabled the detection of cells implanted at various sites. The growth of the MTT-luc tumors in the nude mice was monitored over time *in vivo* by bioluminescent imaging. Images at key time points from a representative animal are shown in Figure 3A, illustrating the progressive increase in the bioluminescence signal over time. Mean photons emitted from the tumors over time and tumor volume in figure 3C as assessed by caliper dimensions when the tumors became measurable (by week 4) are illustrated in Figure 3B. Notably, the tumor cells were visible by bioluminescence imaging much earlier than the tumor became measurable or palpable. Analysis of covariation between BMI light intensity (total photon flux) and measured tumor volume showed a high degree of correlation ($R^2 = 0.99$) as shown in Figure 3C. Only a few aggressive cell lines have been reported to spontaneously metastasize from subcutaneous implantation in the literature. For this reason, at the end of the 7-week experiment I wanted to verify if any metastatic MTT-luc tumor cells waere detectable by bioluminescence analysis in several organs. Fifteen minutes after luciferin injections, the mice were euthanized and several internal organs, including liver, lungs, spleen, ovaries and brain, were analyzed for bioluminescence signals (Figure 3D and Table 1 above). Indeed, I was able to detect MTT-luc cells in several of these organs. The lungs, which

represented the organ most consistently seeded by subcutaneously implanted MTT-luc cells, are also a favored site of metastasis of human pheochromocytomas [101].

3.1.4 Bioluminescence signals correlate with metastatic lesions identified by histopathology.

To confirm the presence of metastatic tumor cells in the main organs targeted in the two metastatic models we described, I performed histopathological examination of formalin-fixed tissues collected after *ex vivo* imaging. For the experimental metastasis model in which tumor cells were injected in the mouse tail vein, the most intense and reproducible signals were derived from the livers; indeed, histopathological analyis of livers from these animals revealed macro and micro metastasis (Figure 2G, left panel).

In the second models (subcutaneous injection of tumor cells), histopathological analyis confirmed the presence of micrometastasis in the lungs (Figure 3E, right panel), consistent with the *ex vivo* bioluminescence signal.

3.2 COMBINED INHIBITION OF MTORC1 AND MTORC2 SIGNALING PATHWAYS FOR THE TREATMENT OF PHEOCHROMOCYTOMA.

3.2.1 mTOR, Raptor and Rictor Are Over-expressed in Subsets of Pheochromocytomas

First, I wanted to verify the expression of mTOR, Raptor and Rictor in several tumors from our collection of PHEO/PGL from patients with different genetic backgrounds. Expression analysis was performed with 20 tumor samples from patients with VHL, SDH-B, SDH-B metastases (SDH-B Meta), SDH-D adrenal, SDH-D head and neck PGL mutations, and 4 normal adrenal medulla (NAM). Table 2 summarizes the clinical information of the patients used for these studies. Expression of the three genes in these groups was analyzed by real-time PCR (Figure 4). As shown in Figure 4, patients with SDH-B and VHL mutations showed a significant increase (compared to normal adrenal medulla) in mTOR expression when compared with the other samples analyzed in this panel. Interestingly, both SDH-B and metastatic SDH-B pheochromocytoma showed a significant increase in expression of mTOR compared to normal adrenal medulla ($p < 0.05$). Analysis of both Raptor and Rictor expression demonstrated a significant increase in SDH-B pheochromocytoma tissue when compared to patients in other groups as well as the normal adrenal medulla.

Table 2: Patients information relative to the samples used for the gene expression study.

	SEX	AGE	TYPE	LOCATION	GENETIC BACKGROUND	BIOCHEMISTRY
Pt-1	M	26	Met	retroperitoneal	SDHB	NE, NMN
Pt-2	F	36	Met	peri illiac	SDHB	NE
Pt-3	M	31	P	left peri-aortic mass	SDHB	DA
Pt-4	M	53	Mlt	nasopharingeal	SDHB	NE, DA
Pt-5	F	9	Mlt	left illiac bifurcation	SDHB	Epi, NE, DA
Pt-6	M	31	Mlt	left adrenal	SDHD	NE, DA
Pt-7	M	62	P	left adrenal	SDHD	
Pt-8	F	37	P	adrenal	SDHD	
Pt-9	F	26	Mlt	right carotid body	SDHD_HNP	NE
Pt-10	M	67	Bi	carotid body	SDHD_HNP	
Pt-11	F	47	Mlt	carotid body	SDHD_HNP	
Pt-12	F	64	P	right glomus jugulare tumor	SDHD_HNP	
Pt-13	M	33	Bi and Mlt	bilateral adrenal	VHL	
Pt-14	F	42	Bi	right adrenal	VHL	
Pt-15	M	25	P	right adrenal	VHL	
Pt-16	M	7	P	left adrenal	VHL	NE, Epi,
Pt-17	M	45	Met	liver	SDHB met	NE, NMN, DA
Pt-18	M	39	Met	right lung	SDHB met	NE
Pt-19	M	48	Met	liver	SDHB met	NE, DA
Pt-20	F	37	Met	parietal bone mass	SDHB met	Epi, NE

Mlt – multiple; P – primary; Met – metastatic; Bi – bilateral; NE – norepinephrine; NMN – normetanephrine; DA – dopamine; Epi – epinephrine; HNP – head and neck paragangliomas.

3.2.2 mTORC1/2 Inhibitors Inhibit Pheochromocytoma Cell Proliferation and Migration

Based on the importance of the mTOR pathway in pheochromocytomas and paragangliomas, I tested mTOR inhibitors in a proliferation assay using the metastatic MPC-derived MTT cell line [38]. As shown in Figure 2, the original mTOR inhibitor rapamycin was able to inhibit MTT cell proliferation with an IC50 of 756 nM (Figure 4D). In comparison, the novel mTORC1/2 inhibitors AZD-8055 and Torin-1 were able to significantly inhibit cellular proliferation in a dose-dependent manner in MTT cells over a range of concentrations (1nM to 1μM) with an IC_{50} of 96 nM (Figure 4D) and 207 nM (Figure 4D), respectively. These data show that rapamycin induces only partial growth inhibition, while the dual inhibitors have a much greater suppression of proliferation.

The effect of mTORC1/2 inhibitors treatment on cell migration was tested in the metastatic pheochromocytoma cell line MTT; I found that AZD8055 reduced serum-stimulated migration (Figure 4E and 4F), with an IC_{50} of 260 nM. Torin-1 was also able to significantly inhibit MTT cell migration, with an IC_{50} of 400 nM (Figure 4E and 4F). Interestingly, MTT cells tended to become confluent in clusters, reminiscent of the "zellballen" nested arrangement characteristic of pheochromocytoma histopathology. As shown in the micrograph images in Figure 4E, inhibition with either mTOR inhibitor reduced the formation of such clusters.

3.2.3 AZD8055 and Torin-1 Treatment Affects mTOR Downstream Signaling

As a part of the assessment of mTORC1/2 inhibitor activity in pheochromocytoma cells, MTT cells were exposed to different concentrations of rapamycin, AZD8055 and Torin-1

for 6 hours to assess downstream markers of mTOR kinase activity. Both AZD8055 and Torin-1 decreased phosphorylation of S6 ribosomal protein on Ser235/236 and Ser240/244, as well as phosphorylation of eIF4B on Ser422. Unlike the allosteric mTOR inhibitor rapamycin, the dual inhibitors were also able to significantly decrease phosphorylation of Akt on Ser473. Moreover, lower concentrations of AZD8055 and Torin-1 were necessary to obtain the same degree of biomarker modulation compared to rapamycin (Figure 5).

3.2.4 AZD8055 Reduces Pheochromocytoma Tumor and Metastatic Burden *in vivo*

The antitumor effect of AZD8055 was assessed *in vivo* in a recently-developed spontaneous metastasis model of pheochromocytoma [86]. From week 3 through week 7, a significant reduction of tumor burden was observed in the AZD8055-treated animals (n=7) compared to vehicle-treated animals (n=7; Figure 6A). As previously described [86] in the MTT pheochromocytoma model, the two main organs where spontaneous metastases develop are the lungs and liver. On day 49, after *in vivo* bioluminescence measurements had been taken, the animals were sacrificed and both lungs and livers were excised and luciferase activity was measured by Xenogen imaging. A trend of reduced metastatic burden was observed in lungs (Figure 6B) and livers (Figure 6C) of the treated animals compared with the control group, although only differences in lung metastasis were statistically significant using non-parametric statistics in the time-frame of our experiment.

3.2.5 AZD8055 and Torin-1 inhibits proliferation of primary cells from patients with Pheochromocytoma

The growth inhibitory effect of AZD8055 and Torin-1 was evaluated in human primary cell derived from donated tumor tissue collected from patients suffering from pheochromocytoma, including one SDHB tumor. Immunohistochemical staining for tyrosine hydroxylase (TH), the rate-limiting step in the biosynthesis of catecholamines, was used as a marker of pheochromocytoma cells to discriminate them from other cell types that are inevitably present in primary cultures. As shown in Figure 6, AZD8055 (Figure 6E) as well as Torin-1 (Figure 6F) decreased the number of TH-positive cells to 50% of control cells, confirming their cytotoxic effect also on human pheochromocytoma cells. Table 3 summarizes the clinical information on the patients used for these studies.

Table 3: Patient information of the samples used for primary cell cultures and treatments.

	SEX	AGE	TYPE	LOCATION	GENETIC BACKGROUND	BIOCHEMISTRY	inhibition at 1 uM AZD8055 (%)	inhibition at 3 uM AZD8055 (%)
Pt1	F	44	P	right adrenal	sporadic	NE, DA, NMN	27.1	48.5 (Torin-1: 48.2)
Pt2	F	28	P	right adrenal	SDHB	NE, DA, NMN, CgA	22.6	68.9
Pt3	F	47	P	right carotid body	sporadic	CgA	23.2	-
Pt4	M	5	P	left adrenal	VHL	MN, NMN	17.1	51.9 (Torin-1: 52.4)

Included are the percent inhibition with 1μM and 3μM AZD8055, and 3μM Torin-1. P – primary; NE – norepinephrine; NMN – normetanephrine; DA – dopamine; CgA - chromogranin A; MN –metanephrine.

3.3 TARGETING HEAT SHOCK PROTEIN 90 FOR THE TREATMENT OF MALIGNANT PHEOCHROMOCYTOMA.

3.3.1 17-AAG and ganetespib inhibit pheochromocytoma cell proliferation and migration.

17-AAG significantly inhibited cellular proliferation in a dose-dependent manner in all the available pheochromocytoma cell lines, namely MPC (Figure 7A), MTT (Figure 7C) and PC12 (Figure 7E) cells over a range of concentrations (1 nM to 1 μM) with an IC_{50} of 235 nM, 286 nM and 181 nM, respectively. Ganetespib also caused significant inhibition of proliferation of the three pheochromocytoma cell lines and was more potent than 17-AAG, with IC_{50} values of 50 nM, 18 nM, and 28 nM in MPC (Figure 7B), MTT (Figure 7D), and PC12 cells (Figure 7F).

We tested the effect of Hsp90 inhibitor treatment on cell migration in the metastatic pheochromocytoma cell line MTT and found that 17-AAG reduced serum-stimulated migration (Figure 7I and 7J), with an IC_{50} of 144 nM. Ganetespib was also able to significantly inhibit MTT migration, with an IC_{50} of 44 nM. Interestingly MTT cells tend to become confluent in clusters, reminiscent of the "zellballen" nested arrangement characteristic of pheochromocytoma histopathology. As shown in the micrograph images of Figure 7 (G and H), inhibition with either Hsp90 inhibitor markedly reduced the formation of such clusters.

3.3.2 17-AAG and ganetespib treatment affects Hsp90 client proteins in MTT cells.

To better understand the mechanisms of cytotoxicity and growth inhibition by Hsp90 inhibitors, I treated MTT cells with different concentrations of 17-AAG (Figure 8A) or ganetespib (Figure 8B) for 20 hours. After treatment the levels of two established Hsp90 clients, HIF-1α and phospho-S473-Akt, were measured by western blotting. As can be seen in Figure 8, 17-AAG reduced the amount of both proteins in MTT cells. Ganetespib demonstrated a similar effect. In addition, I analyzed cleaved PARP by western blot after treatment with 17-AAG (Figure 8C) and ganetespib (Figure 8D) in MTT cells. Cleaved PARP increased in a dose-dependent manner, indicating that both Hsp90 inhibitors induced apoptosis in MTT cells.

3.3.3 Pheochromocytoma metastasis is inhibited by 17-AAG and ganetespib

To evaluate the effect of 17-AAG *in vivo* I employed a tail vein model of metastasis with MTT cells stably expressing the luciferase gene (MTT-luc cells). Mice were imaged immediately after injection to verify the success of the procedure (week 0, data not shown) and subsequently imaged weekly for five weeks. Tumor signals increased significantly over the six weeks of the study with exponential growth especially localized in the upper abdominal cavity (Figure 9A). Eight days after tumor cell inoculation the animals were divided in two groups: one group (17-AAG, n=6) received 60 mg/kg three times a week (i.p.); a second group (control, n=6) received vehicle alone (DMSO) on the same schedule. 17-AAG significantly reduced the metastatic tumor burden (Figure 9A and C) and prolonged survival (Figure 9D, $p<0.0001$) when compared with the control

group, with a median survival of 34 days for the control group and 51.5 days in the 17-AAG treated group.

To confirm the engagement of Hsp90 by 17-AAG *in vivo*, we measured the level of Hsp70 in plasma pre- and 6 hours post-treatment with 17-AAG. It has been reported that 17-AAG induces the synthesis of Hsp70 [102,103] and that increases in intracellular and plasma Hsp70 can be used as a pharmacodynamic marker of Hsp90 inhibitor response [104,105]. Thus, we measured Hsp70 levels in plasma as a biomarker for drug activity. As expected, treatment with 17-AAG increased plasma Hsp70 levels (Figure 9B), indicative of Hsp90 inhibition *in vivo*.

Using a spontaneous metastasis model of pheochromocytoma [86], I injected 1.5 x 10^6 MTT-luc cells in the subcutaneous tissue of athymic mice. After 10 days, allowing for tumor cells to engraft, I started treatment with 20 mg/kg ganetespib, in the treated group of animals (n=8) and the same volume of vehicle in the control group of animals (n=8), on a daily x5, five days out of seven schedule. I then followed the growth of the subcutaneous tumor by bioluminescence detection, weekly, weeks 3 thorough 7, which demonstrated a significant reduction of tumor burden over time (Figure 10A). As previously described [86] in the MTT pheochromocytoma model, the two main organs where spontaneous metastases develop are the lungs and livers. On day 49, after *in vivo* bioluminescence measurements were taken the animals were sacrificed and lungs and liver were excised and luciferase activity was measured by Xenogen imaging (Figure 10C and D). Metastatic burden was dramatically reduced in lungs and livers of the treated animals compared with the vehicle control group. Primary subcutaneous tumors from each of the animals were excised and are shown in Figure 5 (Figure 10B).

3.3.4 Inhibition of human pheochromocytoma cells *in vitro*

All efforts to establish cell lines from primary human pheochromocytomas and paragangliomas have been unsuccessful. Typically, tumor cells from surgical specimens can survive up to three weeks but then senesce and die [106]. To test the effect of ganetespib on human primary cell cultures, we used primary cells derived from tumor tissue collected from pheochromocytoma patients who were surgical candidates on NIH clinical protocol 00-CH-0093.

Immunohistochemical staining for TH, the rate-limiting enzyme in the biosynthesis of catecholamines, was used as a marker of pheochromocytoma cells to discriminate tumor from cells of the tumor microenvironment. As shown in Figure 10E, treatment with ganetespib for 10 days, with drug washout and readministration every two days resulted in a dose-dependent decrease in pheochromocytoma cell number.

3.4 DRUG REPOSITIONING HIGH-THROUGPUT SCREENING FOR THE IDENTIFICATION OF NEW THERAPEUTIC OPTIONS FOR METASTATIC PHEOCHROMOCYTOMA AND PARAGANGLIOMA.

3.4.1 High-throughput screening (HTS) of the NPC Library

I screened the NIH Chemical Genomic Center Pharmaceutical Collection of clinically approved drugs, which contains 1,760 US FDA approved drugs, 785 drugs approved by other countries, 1,225 compounds in clinical trials and 56 bioactive molecules, employing a model of metastatic PHEO (by using MTT mouse PHEO cells), the most common tumor of the adrenal medulla.

The assay, in a 1536 HTS plate format, measured cell viability by determining metabolically active cells (viable cells) in culture using a luciferase, ATP-dependent readout (as described in Material and Methods), at two different time points of compound incubation (24 hrs and 48 hrs). A number of compounds showed significant cell killing, with potency below 10 μM (at 48 hrs, when the compounds showed to be more potent and efficacious). Compounds were tested at 8 doses using a quantitative HTS (qHTS) approach [93].

The qHTS identified 76 high-confidence active compounds with curve class (CRC) 1.1, 1.2, 2.1 and 2.2 [93], with the maximal inhibition over 60%, 3481 inactive and 269 inconclusive compounds with lower confidence CRC or showing low efficacy in the MTT cell line. Of the 76 high-confidence actives, 40 had efficacy higher than 60% and potency below 10 μM, which corresponded to a 1% hit rate from the qHTS screening.

Five compounds showed significant cell killing effect with potency less than or equal to 1 μM: the protein synthesis inhibitor and antileukemic (induces apoptosis) drug homoharringtonine (IC_{50} = 0.24 μM); the tubulin inhibitors colchicine (IC_{50} = 0.47 μM), nocodazole (IC_{50} = 0.53 μM) and fenbendazole (IC_{50} = 1 μM); and the proteasome inhibitor bortezomib/velcade (IC_{50} = 0.59 μM). Then I performed an enrichment analysis into therapeutic categories of the compounds obtained from the primary screening. I identified that the top 5 enriched drug categories active in MTT cells were antiseptic, antimalarial, antineoplastic, estrogen and anthelmintic agents (Figure 11). However, these categories also represented the ones with fewer compounds, so, relatively, the two major categories with the most hits were represented by antineoplastic and antiseptic drugs. Top-ranked hits (50 compounds) based on the CRC, efficacy and potency are reported in Table 4.

Table 4. Top-ranked compounds (hits) with high confidence antiproliferative activity in MTT PHEO cells. The table illustrates the drug name, efficacy, IC_{50} (in μM) and curve class.

Sample Name	Curve Class	IC_{50} (μM)	Efficacy (%)
Colchicine[1] (Colcrys™)	-1.1	0.47	-85
Dipyrithione (Crimanex™)	-1.1	1.50	-81
Zinc pyrithione	-1.1	2.11	-91
1-Hydroxypyridine-2-thione zinc salt	-1.1	2.11	-96
Mersalyl sodium	-1.1	2.66	-92
Auranofin (Ridaura™)	-1.1	2.66	-87
Thimerosal[4]	-1.1	2.99	-87
Deslorelin acetate (Suprelorin™)	-1.1	2.99	-89
Paclitaxel[1] (Abraxane™, Onxol™)	-1.2	0.04	-51
5-Aza-2'-deoxycytidine, Decitabine[2] (Dacogen™)	-1.2	0.07	-52
Homoharringtonine	-1.2	0.24	-74
Trimetrexate glucuronate[5] (Neutrexin™)	-1.2	0.38	-51
Rubitecan[2] (Orathecin™)	-1.2	0.42	-55
Nocodazole[1]	-1.2	0.53	-60
Fenbendazole[1] (Panacur™)	-1.2	1.01	-61
Artemisinimum	-1.2	1.33	-60

Carmofur (Mifurol™)	-1.2	1.88	-57
Suberoylanilide hydroxamic acid[2] (SAHA) (Zolinza™)	-1.2	2.37	-59
Tenovin-1	-1.2	2.66	-56
Carubicinum[2]	-1.2	2.99	-59
Captan[4]	-1.2	2.99	-66
Lissamine green B	-1.2	6.68	-54
Mycophenolic acid (CellCept™, Myfortic™)	-2.1	1.14	-97
Tyrothricin[4]	-2.1	1.50	-84
Mycophenolate mofetil	-2.1	1.68	-92
Brilliant Green[4]	-2.1	1.68	-108
Rotenone[5]	-2.1	2.66	-124
Lestaurtinib	-2.1	2.66	-83
Ciclopirox ethanolamine	-2.1	4.53	-85
RTA 402	-2.1	6.68	-108
Sanguinarine	-2.1	8.41	-88
Proflavine hemisulfate[2]	-2.1	8.41	-92
Parthenolide	-2.1	8.41	-104
Bortezomib[5] (Velcade™)	-2.2	0.60	-75
Albendazole[1] (Albenza™)	-2.2	0.72	-58
Sobuzoxane[2] (Perazolin™)	-2.2	0.84	-56
Azacitidine[2] (Vidaza™)	-2.2	1.33	-71
Tiquizium bromide	-2.2	1.88	-52

Flavopiridol hydrochloride hydrate	-2.2	1.88	-71
Ancitabina	-2.2	2.37	-68
Ethaverine hydrochloride	-2.2	3.60	-60
2,2',4'-Trichloroacetophenone	-2.2	3.76	-71
Berberine chloride	-2.2	4.22	-54
17-Allylamino-geldanamycin (17-AAG)	-2.2	4.22	-81
Proguanil hydrochloride[5]	-2.2	4.53	-60
Topotecan hydrochloride[2] (Hycamtin)	-2.2	4.73	-90
Phenelzine sulfate	-2.2	5.08	-53
Oxapium iodide	-2.2	6.68	-60
Methyl violet[4]	-2.2	7.50	-70
Malachite Green Oxalate	-2.2	8.41	-61

Legend: [1]Anti-tubulin agents; [2]Drugs targeting DNA and nucleotide analogues; [3]proteasome inhibitors; [4]antimicrobial agents; [5]antimetabolite.

3.4.2 Secondary screening of selected drugs

The top 50 drugs considered active compounds based on the primary screening were grouped and mostly classified in 5 main functional categories: 1) antitubulin agents; 2) drugs targeting DNA and nucleotide analogues; 3) proteasome inhibitors; 4) antimicrobial agents; 5) antimetabolite. I found that antitubulin agents, which have a prominent class effect on protein polymerization and mitotic spindle organization, were the drug category with the most entries in the top compounds in the high-confidence list (five entries, which included colchicine, paclitaxel, and several –azoles drugs). Another class effect was represented by topoisomerase inhibitors (including carubicinum, rubitecan, sobuzoxane and topotecan), which have a prominent effect on DNA replication and telomerase maintenance.

A representative selection of compounds from the categories described above were selected for further investigation and validated in additional assays to confirm the activity of the hits from the HTS screen. For the secondary assays, I took advantage of a traditional proliferation assay, namely the colorimetric MTT assay, and a flow cytometric analysis for viable cells after drug treatment. I used three different PHEO cell lines, namely PC12, MPC and MTT cells (see Material and Methods for a complete description). All the compounds tested produced dose-response curves in all three cell lines, and were potent compounds having IC_{50} values in the low nanomolar range (Figure 12 A-I).

To further validate the activity of the selected compounds, I performed a flow cytometry cell viability assay using 7-AAD after overnight treatment with the selected compounds (Figure 12J). In addition, a Western blot assay was used for detection of PARP cleavage (Figure 12K) in MTT cells after 20 hr treatment. The results from both assays from two different cell lines confirmed the activity of several antitubulin agents, including colchicine, taxol and nocodazole. Other compounds with dose-related activity included the HDAC inhibitor suberoylanilide hydroxamic acid (SAHA), the tyrosine kinase inhibitor lestaurtinib (which is an inhibitor of FLT3, JAK2, TrkA, TrkB and TrkC) and the topoisomerase inhibitor rubitecan. Furthermore, the Hsp90 inhibitor 17-AAG showed activity, confirming previously published results [107].

3.4.3 Microarray data analysis and metabolic model.

Because the primary and secondary screening was performed in murine cell lines (due to the unavailability of human PHEO cell lines), a strategy using microarray data from murine and human samples was used to further select a clinically relevant set of drugs from our data that could be potentially developed in human clinical trials. I first compiled a list of genes directly targeted by the top drugs discovered by the primary screening using the NPC library databank. Compounds for which information on specific targets was not available were excluded from the analysis. Based on the list of genes compiled, I selected a subset of microarray data from a new murine MTT cell microarray and a published human SDHB microarray. In particular, I focused on the human microarray of patients with SDHB disease, as these patients are the ones that can benefit the most from the discovery of novel therapies. To extrapolate the murine screening data for clinical

relevance, for each drug I measured the Pearson correlation coefficient between the target genes and the expression profiles from these two microarray data sets (Figure 13A). This analysis allowed us to bridge and relate the data from the murine screening with the data from an available human PHEO expression profile [96].

Two metabolic models were constructed with compounds and targets that have been compiled from the data set. The first model was constructed as a complete hypothetical network for visualization of the network assembly of 22 compounds tested on the MTT cell line. It contained 2153 nodes and 3091 edges (Figure 13B). All targets of a given drug were connected to all other drugs, generating a network from which maximum connected nodes can be visualized. Using eccentricity scores, a list of the top 20 targets was identified (Table 5) that were predicted to be biologically relevant. Functional enrichment analysis using Reactome Functional Interaction (FI) identified 406 gene ontology (GO) biological categories ($p < 0.05$). Interestingly, the HDAC inhibitor SAHA (vorinostat) was one of the compounds with the highest correlation (Figure 13A) between MTT cells and human PHEO/PGL samples based on the gene profile. The second network was constructed using targets associated with GO categories (DNA replication and histone deacetylation) corresponding to two of the top hub nodes: topoisomerase and histone deacetylase, respectively. This subnetwork (Supplementary Figure 13C and D) contained 55 nodes and 99 edges and included 5 of the 22 drug targets. Based on eccentricity analysis, carubicinum, rubitecan and colchicine (Table 6) were found to have a greater influence on the subnetwork.

Table 5.

Rank	Name	Score
1	TP53	0.24919
1	PARP1	0.24919
1	HDAC2	0.24919
1	SUMO1	0.24919
1	APAF1	0.24919
1	TOP2A	0.24919
1	CDKN1A	0.24919
1	CASP9	0.24919
1	CDK1	0.24919
1	MAPK8	0.24919
1	HDAC1	0.24919
1	MAPT	0.24919
1	POLR2A	0.24919
1	FGF1	0.24919
1	CASP3	0.24919
1	RAD51	0.24919
1	EGFR	0.24919
1	BIRC5	0.24919
1	MDM2	0.24919
1	MAPK1	0.24919

Table 6.

Rank	Name	Score
1	Carubicinum	0.33333
1	Rubitecan	0.33333
1	Colchicine	0.33333
4	LIG4	0.25
4	17-Allylamino-geldanamycin	0.25
4	KRT7	0.25
4	TOP1	0.25
4	HDAC9	0.25
4	SSRP1	0.25
4	CHEK1	0.25
4	RAD9A	0.25
4	CDC25C	0.25
4	HMGB2	0.25
4	HDAC2	0.25
4	HDAC6	0.25
4	RMI1	0.25
4	Flavopiridol hydrochloride hydrate	0.25
4	EGF	0.25
4	TYMS	0.25
4	RFC4	0.25

3.4.4 An example of drug combination with synergism analysis

The compiled list of drugs derived from the screening represented a useful selection of compounds with the potential to work effectively in the treatment of metastatic PHEO/PGL, either as single drugs or in combination. Moreover, the combined analysis of the drug screening and the microarray data sets suggested possible drug combinations that are supported by sporadic, but useful, reports in the literature on similar drugs or drug categories in the treatment of metastatic PHEO/PGL patients.

The subnetwork represented in Figure 13C and D constitutes a potential source of relevant drug combinations because of the potential biological relationship between any of two nodes in the network. As an example, I selected for study the combination of the HDAC1/2 inhibitor SAHA and a structural analogue of carubicinum, namely epirubicin, which is a more clinically relevant compound based on the reported use in therapeutic combination for PHEO [108] and for other tumors [109]. I combined epirubicin with SAHA at a constant ratio (1:200) in doses approximately equal to their IC_{50} and also in concentrations equally distributed above and below the relative IC_{50}s. For this reason I first determined the relative IC_{50} for each single compound: 1 uM for SAHA and 5 nM for epirubicin (Figures 14A and B). As shown in Table 7 and Figure 14C (median-effect index) and D (algebraic estimate of the combination index), this combination produced a synergistic effect at all concentrations tested. The benefits of combining these two drugs were seen in the dose reduction index (DRI), as described in Materials and Methods. Reducing the concentration of a single drug when given in combination may lead to a reduction of the side effects of each drug. This strategy represents a promising approach to test potentially clinically useful combinations, using a combination of traditional qHTS

screening testing with innovative microarray analysis.

Table 7. Combination of SAHA and epirubicin in MTT cells. CI = Combination index. DRI = Dose reduction index.

IC_{50} folds	EPI/SAHA [µM]	Fraction Affected	CI	Effect	DRI EPI/SAHA
4x	20/4000	0.808566317	0.719	Synergistic	8.227/1.674
2x	10/2000	0.740589432	0.537	Synergistic	8.593/2.378
1x	5/1000	0.588437471	0.568	Synergistic	5.459/2.6
0.5	2.5/500	0.446667935	0.553	Synergistic	4.23/3.156
0.25	1.25/250	0.328056979	0.518	Synergistic	3.675/4.069

4. DISCUSSION AND CONCLUSIONS

The treatment of rare tumors represents a major challenge in oncology. In particular, neuroendocrine tumors, such as pheochromocytomas and paragangliomas, are rare tumors for which there are very limited therapeutic options [1,71]. Malignant pheochromocytomas have been historically very difficult to treat, as traditional chemotherapy has been mostly unsuccessful and data from clinical trials are difficult to interpret due to the low prevalence of the disease and the inability to recruit in the same trial an adequate number of patients [110].

However, the study of the molecular determinants of pheochromocytoma tumorigenesis has suggested a handful of potential targets to explore with novel targeted therapies, which have already demonstrated successful treatment for other forms of cancer [111]. Currently, there is increasing interest in the pheochromocytoma research community to seek novel targeted therapies which have predominantly a cytostatic effect by interfering with a specific molecular target needed for carcinogenesis and sustained tumor growth [110,112,113].

We used the following cell lines, which represent the only available permanent PHEO cell lines available to the scientific community and include a range of models of PHEO. The rat PHEO cell line PC12, developed in 1976, has a MAX gene deletion that has been recently discovered in a human PHEO kindred [40]. The mouse MPC cell line, derived from *NF1* knock-out mice, represents a well differentiated model, with a behavior very similar to most slow-growing PHEO/PGL; interestingly, recent evidence points to NF1 loss of function as a frequent occurrence in sporadic PHEO [114]. Finally, the MTT cell

line, which is rapidly growing and derived from the liver metastases of MPC cells, is a model related to some more aggressive human PHEO/PGL, with accelerated metastatic behavior [38].

Bioluminescence has been used for the detection of primary tumor growth and tumor metastasis in animal models of several tumors, but, to our knowledge, this is the first report on the use of bioluminescence in animal models of pheochromocytoma. The use of this technology allow for the non-invasive and real-time assessment of tumor burden in the same group of animals over time [115]. This type of model is particularly well suited for the evaluation of efficacy of novel therapy and it has been developed with the intent to create a platform for the pre-clinical evaluation of new targeted therapy for pheochromocytoma.

Previous studies in our group have established a metastatic model of pheochromocytoma by mouse passages of the murine pheochromocytoma cell line MPC [38]. Through disaggregation and culturing of liver tumor metastasis, we established the MTT cell line, which display a reproducible metastatic phenotype when injected intravenously. In order to follow the localization of these cells in the intact animal longitudinally, we generated a bioluminescent MTT cell line and compared the bioluminescent signal with serial MRI imaging.

In our study we demonstrated a strong correlation between the detection of photons and the radiologic examination. BLI offers several advantages over more traditional radiologic techniques, such as MRI and CT scanning, which require long scan times and expensive instrumentation. Bioluminescence offers a signal with practically no

background, as other source of significant bioluminescence are absent in mammals, and the light generated easily penetrate mammalian tissues and can be detected by sensitive charge-coupled device (CCD) cameras and quantified more precisely by the conversion of the luminescence signal into a digital value. This is in contrast with the use of fluorescent tags, that require an excitation signal (which penetrate tissue layers with difficulty), and are limited by the presence of tissue autofluorescence and photobleaching. Moreover, the luciferase gene can be stably integrated into the chromosomes of target cells, and so carry over subsequent cell divisions and not lost over time.

Luciferase-transfected cells can be easily monitored in virtually any location in the body, including sanctuary sites, where only a few cells are sufficient to generate a detectable signal that would be undetectable by MRI or CT scanning; thus, it is by far the most sensitive of the noninvasive technique. Consequently, among the several imaging techniques available for *in vivo* studies, bioluminescence is the more sensitive to detect minimal residual disease, which is one of the more daunting and elusive entities in clinical oncology.

Moreover, BLI can represent quantitatively the amount of viable tumor cells in the body, allowing comparison not only within the same experiment but also across several experiments. The ability to non-invasively track the growth of tumors and metastasis *in vivo* also permit a better understanding of the mechanism of cancer development and intervention. Several investigations in other type of cancers have already demonstrated the power of BLI in longitudinal therapy intervention studies for the follow-up of tumor growth after treatment with experimental drugs [116]. In these

types of studies the BLI signal in the animal injected with tumor cells is determined prior to intervention with the drug of interest to establish a reference/starting measurement. Subsequent scanning are then normalized relative to the reference signal in the same animal and differences are calculated between the control group (receiving vehicle alone) versus the group receiving the tested drug.

We have also established a spontaneous metastasis model of pheochromocytoma, in which cells from a subcutaneous implant send micrometastases to the lungs. These models are rare in the literature, and represent a unique opportunity to explore steps of the metastatic cascade that are not testable in an experimental metastasis model [117]. Indeed, spontaneous metastasis spread following a natural mechanism of invasion of the surrounding tissue, and allow the examination of all steps of the metastatic cascade. This model could in particular be more clinically relevant, when testing for drugs that target more advanced disease stages. For example other groups using a spontaneous metastasis model of the breast cancer cell line MDA-MB-435 [118] was able to demonstrate the responsiveness of metastasis to therapies that were initially found to be ineffective in the treatment of the primary tumor. On the same line other groups have successfully used these animal models for testing novel molecular targeted therapies [119].

Beside the study of intact animals along the course of the study, *ex vivo* analysis at the end of the experiments allows for additional important information to be collected from the same animal. Namely, *ex vivo* bioluminescence can help to identify very small metastatic lesions that are not easily detectable by *in vivo* imaging, more accurately assessing metastatic burden. For example, while it was relatively easy to detect signals from the abdominal cavity, brain lesions were undetectable by both MRI imaging and *in*

vivo BLI. In contrast, *ex vivo* BLI was able to promptly detect a small number of tumor cells that crossed the blood-brain barrier causing micrometastatic brain disease.
A technical point of interest was that we were able to use G418 to exert selective pressure on transduced MTT cells. This was somewhat unexpected because the primary tumor from which MPC and MTT are derived arose in a *Nf1* knockout mouse generated by insertion of a neomycin resistance gene in reverse orientation into the *Nf1* gene [120] and the original MPC line was intrinsically G418-resistant (JF Powers, unpublished). The apparent loss of intrinsic resistance might have resulted from somatic recombination, a possibility that itself has implications for design of targeted cancer therapy.

In summary, the experiments on the animal models demonstrate the ability of bioluminescent imaging to follow the progression of pheochromocytoma cells in live animals in order to study the course of tumor progression and to test clinically relevant antitumor treatments in in a mouse model of metastatic pheochromocytoma. The sites of metastasis in this model are also favored for metastases of human pheochromocytomas [101]. No comparable human cell-based model currently exists.

A significant number of pheochromocytomas is associated with familial etiology, and can be included in familial syndromes such as von Hippel-Lindau (VHL), multiple endocrine neoplasia type 2 (MEN2), neurofibromatosis type 1 (NF1) and SDH mutation-related tumors (4). VHL and SDH-related tumors in these cases seem to share the same tumorigenic pseudohypoxia/angiogenesis pathways. There are currently no human cell lines available for these tumors, hindering the testing of novel drugs *in vitro*.

Molecular profiling studies have identified ten germline mutations that cause hereditary pheochromocytoma and paragangliomas [121,122]. It has been suggested that these mutations can be divided into distinct molecular pathways causing errors in the HIF hypoxia-driven pathway (*VHL*, *SDHB* and *SDHD*) and errors in RNA synthesis and metabolism (*RET*, *NF1*, *MAX*, and *TMEM127*), while *KIF1BBeta* is thought to impact both pathways [123,124]. VHL targets HIF to the proteasome under normoxic conditions and loss of VHL results in HIF overexpression and angiogenesis [123]. *SDHB* and *SDHD* mutations result in accumulation of succinate, which inhibits HIF prolyl hydroxylation, and in the absence of prolyl-hydroxylated HIF VHL cannot recognize HIF and target it for degradation, and thus HIF is overexpressed via a different but complementary mechanism from VHL mutation [125].

Hereditary pheochromocytomas and paragangliomas can be divided into two clusters based on the transcription profile revealed by microarray analysis. Cluster 1 includes the tumors with VHL and SDHx mutant genes, cluster 2 involves tumors with mutations in RET and NF1 genes [9,10]. Sporadic tumors were surprisingly represented in both clusters [126]. As further genes were discovered, additional microarray studies were performed in order to classify them into these two clusters. Mutations in KIF1Bb, TMEM127 and MAX genes were clustered with RET/NF1 [11]. RET and NF1 mutations lead to activation of the RAS/RAF/MAPK and the PI3K/Akt/mTOR signaling pathways. TMEM127 mutant tumors cluster with the RET/NF1 group and they enhance mTOR activity independent of the above two kinase pathways. Microarray expression analysis of KIF1Bb mutant tumors also groups them with tumors associated with RET/NF1

mutations, though a potential role of the mutation in kinase pathways is not yet known [11]. On the other hand, a recently discovered MAX gene mutation, which leads to dysregulation of the MYC-MAX-MXD1 network, is grouped with this cluster for its connection with mTOR pathway [25]. Conversely, SDHAF2 and SDHA mutations, recently described, can be clustered with SDHx/VHL [11].

Identification of a unifying player in tumor cells with deregulated energy metabolism and altered redox balance is required in order to elucidate molecular mechanisms associated with these discrepancies. Several pieces of experimental evidence indicate a potential role for the PI3K/Akt/mTOR pathway. Recently identified mutations in the TMEM127 gene have confirmed the importance of this pathway in the pathogenesis of pheochromocytoma [127] and further stress the importance of studying the molecular pathways downstream of susceptibility genes in expanding our understanding of the disease [1,6]. Elevated levels of the phosphorylated form of S6K1 were observed in both cluster 1 and cluster 2 tumor samples with more significant increases in cluster 2 tumors. Such results further support an important role for the mTOR pathway in PHEO/PGL [128].

The work presented has shown that the dual mTORC1 and mTORC2 inhibitors AZD8055 and Torin-1 were able to block proliferation in our mouse pheochromocytoma cell line, and were more effective than the pure mTORC1 inhibitor rapamycin. The Western blotting studies confirmed inhibition of the targets downstream to mTOR, but additionally the dual inhibitors decrease Akt phosphorylation. We have previously

demonstrated increased levels of activated Akt in a model of pheochromocytoma induced by ectopic expression of ErbB-2 [129], in conjunction with reduction of the PTEN protein, consistent with other experimental work [130]. These experimental studies reinforce the importance of the pathway.

The dual inhibitors also blocked cell migration. These results translated to the *in vivo* situation in our transplanted athymic mice. Finally, we were able to use small number of human tumors to show cell loss induced by the inhibitors. Thus, it would appear that the dual TORC1/2 inhibitors may offer a novel and effective therapy for phaeochromocytomas and paragangliomas with invasive and/or malignant characteristics, and it is worth considering their use in the clinical situation.

Of note, all efforts to establish cell lines from human pheochromocytomas and paragangliomas have been unsuccessful because the cells survive but do not proliferate *in vitro* [106]. For this reason we used first passage primary cell cultures from patients with pheochromocytoma to access the effect of AZD8055 on human samples. Tyrosine hydroxylase (TH), a marker of catecholamine producing cells, was used to distinguish pheochromocytoma cells from non-neoplastic fibroblast and other cell types in the primary cell culture.

Our results suggest that dual inhibition of mTORC1 and mTORC2 [131] is a potential novel therapeutic approach for patients with pheochromocytoma and may overcome the problem encountered with the use of mTORC1 inhibitors alone [84,132]. Future efforts

will be directed towards using these compounds in combinations with other chemotherapeutic drugs or novel targeted therapies.

Progress in the treatment of malignant pheochromocytomas has been limited, in part because of the rarity of this malignancy, the lack of sensitivity to cytotoxic therapy, and the anecdotal nature of responses to therapy reported in small case studies or very limited numbers of patients in larger clinical trials [1,71]. The genetic characterization of pheochromocytoma has indicated that targeting angiogenesis with small molecule or monoclonal antibody antiangiogenics may present a rational therapeutic strategy for metastatic pheochromocytoma patients [128]. The molecular characterization of hereditary pheochromocytoma is also supported by data indicating that VEGF is overexpressed in the majority of paragangliomas and pheochromocytomas. Moreover, pheochromocytomas and paragangliomas are often hypervascular, both radiographically and at resection [133,134], and VEGF expression and increased microvessel density are associated with an aggressive phenotype [135,136]. Interestingly, in a study of familial and sporadic pheochromocytomas and paragangliomas VEGF, hypoxia-inducible factor-1α and hypoxia-inducible factor-2 α (HIF-1α and HIF-2α) were prominently expressed in both tumor cells and in endothelial cells lining tumor blood vessels, and VEGF and HIF-1α and HIF-2α were more highly expressed in familial versus sporadic tumors. These data, together with transcriptional profiling analyses [137], are consistent with a pseudohypoxic angiogenic drive in the pathogenesis and progression of malignant pheochromocytoma and paraganglioma (Favier J et al Endocr Pathol 2012).

Our data showing downregulation of HIF-1α protein by Hsp90 inhibition, together with the Hsp90 inhibitor-induced cytotoxicity demonstrated here, are consistent with hypoxia as a critical adaptive response promoting survival in these tumors. In this context, Hsp90, a central player in several oncogenic signaling pathways that promote angiogenesis, tumor cell survival in low-oxygen conditions and unlimited growth, is a rational target for pheochromocytoma. Moreover, the development of inhibitors of this protein in pheochromocytoma is further supported by the knowledge that Hsp90 is overexpressed in malignant pheochromocytoma when compared with benign disease [1,71,138].

Hsp90 chaperones hundreds of intracellular proteins [139-141] (http://www.picard.ch/downloads/Hsp90interactors.pdf) and regulates the activity of a broad range of signal transduction pathways. Among these proteins are important elements of survival signaling networks including the PI3K/Akt pathway. In our study we have demonstrated the activity of the Hsp90 inhibitors 17-AAG and ganetespib in reducing expression of Hsp90-dependent phospho-Akt [142,143]. It is thus of interest that levels of phospho-Akt are reported to be increased in pheochromocytoma compared to normal adrenal tissue [129].

Clinical experience has demonstrated that targeted therapies can elicit the formation of secondary mutations in target molecules, leading to formation of drug resistance [144]. The critical role of Hsp90 in the maintenance of several oncogenic drivers, represents an additional rationale for the use of Hsp90 inhibitors to eradicate cancer cells that have developed resistance to other targeted therapies.

Moreover, the capacity of Hsp90 inhibitors, such as 17-AAG and ganetespib, to interfere with several survival and resistance signaling pathways make them attractive drugs for combination therapy. Indeed, the inhibition by these drugs of multiple oncogenic signaling cascades [145] can overcome pathway redundancy and sensitize cancer cells to other chemotherapeutic compounds [146,147].

Examination of the effect of treatment with 17-AAG in intact animals showed an increase in Hsp70 blood levels, demonstrating that the dose used in our experiment achieves biologically active plasma concentrations and affects its target. This is in agreement with other studies [104,105]. Rajan et al. [148] have shown a statistically significant correlation of Hsp70 protein levels in peripheral blood mononuclear cells with pharmacokinetic parameters. While Hsp70 up-regulation is a clear indication of biological activity, its usefulness as a clinical biomarker for Hsp90 inhibitor therapy remains to be explored. Hsp70 is thought to promote survival of normal and tumor cells in response to cellular insults, and this prosurvival activity may contribute to therapy resistance (Wissing, Li et al. 1992). Future therapy involving Hsp90 inhibitors will be likely in combination with other therapeutics, and Hsp70 induction will provide guidance for dose selection.

The metastatic mouse model using highly metastatic MTT cells that was recently developed as described above can be used for testing drugs for advanced metastatic disease [86]. Although other animal models of pheochromocytoma have been described (and recently reviewed by Korpershoek et al. [149]), only three have been reported to have pheochromocytoma metastasis in lungs and pelvic nerve. However our model has the advantage of reproducibly obtaining metastases in 100% of animals, and offers the

advantage of monitoring tumor burden and tumor metastasis over time via non-invasive bioluminescence imaging [86]. Targeted anticancer drugs that have excellent activity *in vitro* and in subcutaneous models of *in vivo* tumor growth are rarely analyzed for activity in metastatic models, and can have markedly more limited activity or even growth-promoting activity in the metastatic milieu. The failure to test targeted therapy in orthotopic or metastatic models, as well as immunocompetent models, may contribute to late stage failure in drug development. Although the *in vivo* model used here is not in an immunocompetent host, it is a model of metastatic disease with measurable tumor growth in lung and liver, which along with bone and lymph nodes represent two of the four sites most observed in human disease. In this context, the first generation Hsp90 inhibitors have been shown to be very active against subcutaneous xenografts but to increase growth of prostatic and breast carcinoma cells in bone. In contrast, the second-generation inhibitor SNX-5422 had activity against both subcutaneous and bone tumor. Here we have used two different Hsp90 inhibitors, 17-AAG and ganetespib for *in vivo* studies, and demonstrated dramatic antitumor activity against both subcutaneous and metastatic tumor growth.

In our experiments using primary human cell cultures, we observed a dose-dependent reduction in tumor cells after treatment with ganetespib, further emphasizing the efficacy of this compound on pheochromocytoma tumor cells. In conclusion, our study supports the inclusion of pheochromocytoma and paraganglioma in the list of indications that can potentially benefit from Hsp90-directed therapy.

From an industry perspective, drug development programs for rare ("orphan") diseases such as PHEO/PGL (approximately 1,000 new cases are diagnosed in the US each year) are less appealing because of the low return on investment. Thus, alternative approaches must be sought to discover novel therapeutic options for these tumors. One potential strategy is to "recycle" drugs that have been approved for use in the treatment of other diseases, a strategy known as drug repurposing or repositioning [150-152]. Drugs that received regulatory approval have already proven to be safe and effective for a particular disease. In addition, historical information regarding their pharmacokinetics, pharmacodynamics and long-term side effects in a large population is available, which makes repurposing for other diseases less time-consuming and expedites their introduction into clinical trials that are very much needed. Of particular concern are patients carrying mutations in the SDHB gene, as these patients are more prone than other patients to develop more aggressive and metastatic disease [153,154].

HTS of chemical libraries is a powerful generator of potentially clinically useful compounds to treat metastatic PHEO/PGL. This approach is novel for the field of PHEO/PGL, which is now experiencing a renaissance of interest in drug discovery, in particular in the evaluation of novel targeted therapies, especially following the discovery of several novel gene mutations (and consequently several intracellular signaling pathways with potential cellular targets) predisposing to the disease [155].

Compared with other cancer types, one of the major challenges in the development of novel therapeutics for metastatic PHEO/PGL is the absence of *bona fide* human cell lines

for cell-based preliminary testing; viable and functionally active primary cells can be obtained from donated tumor tissue but unfortunately do not proliferate [106]. For this reason we used an alternative approach to extract clinically useful information by crossing and combining data from our primary qHTS drug screening with information available about the expression profiles of a murine and a human microarray data set. Of note, however, the cell lines we used in our assays represented viable models of PHEO. For example, the recent discovery of mutations in the MAX gene (which is part of the Myc-Max-Mxd1 network) [40] highlights the value of the rat PHEO cell line PC12, which lacks a functional MAX gene, as previously described [85,156]. Also NF1 loss of function, found in the MPC cell line used in our assays, has been recently identified as a frequent occurrence in sporadic PHEO [114].

Using meta-analysis information from molecular targets of the top drugs identified by our screening with gene expression data from human and murine microarrays, we identified potential drugs to be used as single drugs or in combination.

There are multiple advantages of screening small molecule libraries of clinically approved compounds by repurposing strategies, including the possibility of introducing these drugs more rapidly into clinical trials because those drugs have already been used in humans for the treatment of other diseases, including other types of cancer. Drugs that received regulatory approval have already proven to be safe and effective for a particular disease, and we have historical information regarding the long-term side effects of the drug in a large population, which makes repurposing them for other diseases less time-

consuming. Moreover this approach overcomes several of the economic and technical bottlenecks that are inherent to the drug discovery process [157]. Furthermore, the repurposing of drugs for new indications, including rare diseases such as PHEO/PGL, is gaining momentum in several areas of medicine, as the cost of developing novel chemical entities is becoming extremely expensive and time-consuming, often with a questionable outcome for the patients [150,158].

Our primary qHTS screening has identified several compounds with potential activity on PHEO/PGL. The repertoire of compounds identified is a potential source available to the PHEO/PGL community for further testing, either as single drugs or in combination, either with other drugs in our list or with other drugs that have shown activity on PHEO. Of particular interest, the antitubulin drugs seem to emerge from our screening as a group of drug with a prominent "class effect" on PHEO, with potent activity in the low nanomolar range. This suggests that these compounds may have activity as single agents in the treatment of metastatic PHEO and possibly PGL.

The secondary screening confirmed activity of several compounds, including the antitubulin agents, the HDAC inhibitor SAHA and the topoisomerase inhibitor rubitecan. Subsequent analysis combining the results from the screening with data from expression microarray assays resulted in the selection of two drugs for combination testing.

The drug combination we chose as an example of using data from the human microarray crossed with the cellular network of gene targets of the drug identified by the screening

find validation also in the literature. Interestingly, SAHA has been described as a drug that induces SDHB protein stabilization and the entry of this protein (although mutated but still functional) into the mitochondria [159]. HDAC inhibitors were also found to be excellent drugs to increase the uptake of MIBG into PHEO cells [160]. Moreover, the anthracycline drug epirubicin has been already used with success in a drug combination study for the treatment of malignant PHEO [108]. The combination of topoisomerase and HDAC inhibitors has been explored also in other cancer types. Recently, Gray et al. [109] described this combination in small cell lung cancer, and other reports validate this therapeutic approach. The optimal dosing and timing of administration is still an open debate in the literature, and future experiments will need to address this problem in the setting of PHEO. Interestingly, another topoisomerase II inhibitor, doxorubicin, that was used as a control in the qHTS screening and in the MTT assays, showed good activity in inhibiting the proliferation of PHEO cell lines. In addition, HDAC inhibitors may influence the level of acetylation of other non-histone effector molecules, including Hsp90 and NF-kB, two other important molecular targets in PHEO.

Of note, our screening was able to identify compounds that we have already explored for the potential treatment of PHEO, and so they acted as internal controls of the validity of our approach. For example, one of the drugs in the top 50 active compound list was the Hsp90 inhibitor 17-AAG, which we investigated in further detail in another study [107]. Two other compounds, RTA 402 and parthenolide, have NF-kB as a molecular target, in agreement with our recent study on the role of its inhibition as a potential therapeutic approach [161]. Interestingly, we also found that several compounds from our screening

are in the same class/category of compounds in the mainstay chemotherapy treatment (CVD combination), such as microtubule inhibitors, which represent a prominent category in our results.

Another prominent category from our screening was represented by drugs targeting DNA. Recent evidence points to a role of DNA methylation in the pathogenesis of SDH mutant PHEOs [162], opening the opportunity to use drugs such as the DNA methyltransferase inhibitor decitabine (5-aza-2'deoxycytabine), which was one of the hits in our screening.

In conclusion, we have presented here the adoption of an integrated approach to discover potentially clinically useful compounds for the treatment of metastatic PHEO/PGL, and we hope that this strategy will help to move forward the field of drug development for other orphan diseases.

ACKNOWLEDGMENTS

I want to thank Prof. Bevilacqua and Prof. Pacak for their mentorship and my family for their continuous support.

Bibliography

1. Pacak K (2011) Phaeochromocytoma: a catecholamine and oxidative stress disorder. Endocr Regul 45: 65-90.
2. Manger WM (2006) An overview of pheochromocytoma: history, current concepts, vagaries, and diagnostic challenges. Ann N Y Acad Sci 1073: 1-20.
3. Adler JT, Meyer-Rochow GY, Chen H, Benn DE, Robinson BG, et al. (2008) Pheochromocytoma: current approaches and future directions. Oncologist 13: 779-793.
4. Amar L, Servais A, Gimenez-Roqueplo AP, Zinzindohoue F, Chatellier G, et al. (2005) Year of diagnosis, features at presentation, and risk of recurrence in patients with pheochromocytoma or secreting paraganglioma. J Clin Endocrinol Metab 90: 2110-2116.
5. Kantorovich V, Pacak K (2010) Pheochromocytoma and paraganglioma. Prog Brain Res 182: 343-373.
6. Qin Y, Buddavarapu K, Dahia PL (2009) Pheochromocytomas: from genetic diversity to new paradigms. Horm Metab Res 41: 664-671.
7. Qin Y, Yao L, King EE, Buddavarapu K, Lenci RE, et al. (2010) Germline mutations in TMEM127 confer susceptibility to pheochromocytoma. Nat Genet 42: 229-233.
8. Petri BJ, van Eijck CH, de Herder WW, Wagner A, de Krijger RR (2009) Phaeochromocytomas and sympathetic paragangliomas. Br J Surg 96: 1381-1392.
9. Favier J, Briere JJ, Burnichon N, Riviere J, Vescovo L, et al. (2009) The Warburg effect is genetically determined in inherited pheochromocytomas. PLoS One 4: e7094.
10. Waldmann J, Fendrich V, Holler J, Buchholz M, Heinmoller E, et al. (2010) Microarray analysis reveals differential expression of benign and malignant pheochromocytoma. Endocr Relat Cancer 17: 743-756.
11. Welander J, Soderkvist P, Gimm O (2011) Genetics and clinical characteristics of hereditary pheochromocytomas and paragangliomas. Endocr Relat Cancer 18: R253-276.
12. Hensen EF, Bayley JP (2011) Recent advances in the genetics of SDH-related paraganglioma and pheochromocytoma. Fam Cancer 10: 355-363.
13. Favier J, Gimenez-Roqueplo AP (2010) Pheochromocytomas: the (pseudo)-hypoxia hypothesis. Best Pract Res Clin Endocrinol Metab 24: 957-968.
14. Ladroue C, Carcenac R, Leporrier M, Gad S, Le Hello C, et al. (2008) PHD2 mutation and congenital erythrocytosis with paraganglioma. N Engl J Med 359: 2685-2692.
15. Kaelin WG, Jr. (2002) Molecular basis of the VHL hereditary cancer syndrome. Nat Rev Cancer 2: 673-682.
16. Eisenhofer G (2001) The role of neuronal and extraneuronal plasma membrane transporters in the inactivation of peripheral catecholamines. Pharmacol Ther 91: 35-62.
17. Kantorovich V, King KS, Pacak K (2010) SDH-related pheochromocytoma and paraganglioma. Best Pract Res Clin Endocrinol Metab 24: 415-424.

18. Timmers HJ, Kozupa A, Eisenhofer G, Raygada M, Adams KT, et al. (2007) Clinical presentations, biochemical phenotypes, and genotype-phenotype correlations in patients with succinate dehydrogenase subunit B-associated pheochromocytomas and paragangliomas. J Clin Endocrinol Metab 92: 779-786.
19. Baysal BE, Ferrell RE, Willett-Brozick JE, Lawrence EC, Myssiorek D, et al. (2000) Mutations in SDHD, a mitochondrial complex II gene, in hereditary paraganglioma. Science 287: 848-851.
20. Niemann S, Muller U (2000) Mutations in SDHC cause autosomal dominant paraganglioma, type 3. Nat Genet 26: 268-270.
21. Astuti D, Latif F, Dallol A, Dahia PL, Douglas F, et al. (2001) Gene mutations in the succinate dehydrogenase subunit SDHB cause susceptibility to familial pheochromocytoma and to familial paraganglioma. Am J Hum Genet 69: 49-54.
22. Burnichon N, Briere JJ, Libe R, Vescovo L, Riviere J, et al. (2010) SDHA is a tumor suppressor gene causing paraganglioma. Hum Mol Genet 19: 3011-3020.
23. Hao HX, Khalimonchuk O, Schraders M, Dephoure N, Bayley JP, et al. (2009) SDH5, a gene required for flavination of succinate dehydrogenase, is mutated in paraganglioma. Science 325: 1139-1142.
24. Karasek D, Frysak Z, Pacak K (2010) Genetic testing for pheochromocytoma. Curr Hypertens Rep 12: 456-464.
25. Jafri M, Maher ER (2012) GENETICS IN ENDOCRINOLOGY: The genetics of phaeochromocytoma: using clinical features to guide genetic testing. Eur J Endocrinol 166: 151-158.
26. Pachnis V, Mankoo B, Costantini F (1993) Expression of the c-ret proto-oncogene during mouse embryogenesis. Development 119: 1005-1017.
27. Takahashi M, Ritz J, Cooper GM (1985) Activation of a novel human transforming gene, ret, by DNA rearrangement. Cell 42: 581-588.
28. Hahn M, Bishop J (2001) Expression pattern of Drosophila ret suggests a common ancestral origin between the metamorphosis precursors in insect endoderm and the vertebrate enteric neurons. Proc Natl Acad Sci U S A 98: 1053-1058.
29. Anders J, Kjar S, Ibanez CF (2001) Molecular modeling of the extracellular domain of the RET receptor tyrosine kinase reveals multiple cadherin-like domains and a calcium-binding site. J Biol Chem 276: 35808-35817.
30. Panta GR, Nwariaku F, Kim LT (2004) RET signals through focal adhesion kinase in medullary thyroid cancer cells. Surgery 136: 1212-1217.
31. Huang SC, Torres-Cruz J, Pack SD, Koch CA, Vortmeyer AO, et al. (2003) Amplification and overexpression of mutant RET in multiple endocrine neoplasia type 2-associated medullary thyroid carcinoma. J Clin Endocrinol Metab 88: 459-463.
32. Yip L, Cote GJ, Shapiro SE, Ayers GD, Herzog CE, et al. (2003) Multiple endocrine neoplasia type 2: evaluation of the genotype-phenotype relationship. Arch Surg 138: 409-416; discussion 416.

33. Pusch CM, Sasiadek MM, Blin N (2002) Hirschsprung, RET-SOX and beyond: the challenge of examining non-mendelian traits (Review). Int J Mol Med 10: 367-370.
34. Jain S, Watson MA, DeBenedetti MK, Hiraki Y, Moley JF, et al. (2004) Expression profiles provide insights into early malignant potential and skeletal abnormalities in multiple endocrine neoplasia type 2B syndrome tumors. Cancer Res 64: 3907-3913.
35. Jouhilahti EM, Peltonen S, Heape AM, Peltonen J (2011) The pathoetiology of neurofibromatosis 1. Am J Pathol 178: 1932-1939.
36. Bausch B, Borozdin W, Mautner VF, Hoffmann MM, Boehm D, et al. (2007) Germline NF1 mutational spectra and loss-of-heterozygosity analyses in patients with pheochromocytoma and neurofibromatosis type 1. J Clin Endocrinol Metab 92: 2784-2792.
37. Powers JF, Schelling K, Brachold JM, Tsokas P, Schayek H, et al. (2002) High-level expression of receptor tyrosine kinase Ret and responsiveness to Ret-activating ligands in pheochromocytoma cell lines from neurofibromatosis knockout mice. Mol Cell Neurosci 20: 382-389.
38. Martiniova L, Lai EW, Elkahloun AG, Abu-Asab M, Wickremasinghe A, et al. (2009) Characterization of an animal model of aggressive metastatic pheochromocytoma linked to a specific gene signature. Clin Exp Metastasis 26: 239-250.
39. Burnichon N, Lepoutre-Lussey C, Laffaire J, Gadessaud N, Molinie V, et al. (2011) A novel TMEM127 mutation in a patient with familial bilateral pheochromocytoma. Eur J Endocrinol 164: 141-145.
40. Comino-Mendez I, Gracia-Aznarez FJ, Schiavi F, Landa I, Leandro-Garcia LJ, et al. (2011) Exome sequencing identifies MAX mutations as a cause of hereditary pheochromocytoma. Nat Genet 43: 663-667.
41. Jafri M, Maher E (2011) REVIEW TOPIC: GENETICS IN ENDOCRINOLOGY The genetics of phaeochromocytoma - using clinical features to guidegenetic testing. Eur J Endocrinol.
42. Eisenhofer G, Keiser H, Friberg P, Mezey E, Huynh TT, et al. (1998) Plasma metanephrines are markers of pheochromocytoma produced by catechol-O-methyltransferase within tumors. J Clin Endocrinol Metab 83: 2175-2185.
43. Lenders JW, Pacak K, Eisenhofer G (2002) New advances in the biochemical diagnosis of pheochromocytoma: moving beyond catecholamines. Ann N Y Acad Sci 970: 29-40.
44. Eisenhofer G, Lenders JW, Siegert G, Bornstein SR, Friberg P, et al. (2011) Plasma methoxytyramine: A novel biomarker of metastatic pheochromocytoma and paraganglioma in relation to established risk factors of tumour size, location and SDHB mutation status. Eur J Cancer.
45. Andersen KF, Altaf R, Krarup-Hansen A, Kromann-Andersen B, Horn T, et al. (2011) Malignant pheochromocytomas and paragangliomas - the importance of a multidisciplinary approach. Cancer Treat Rev 37: 111-119.
46. Maurea S, Cuocolo A, Reynolds JC, Neumann RD, Salvatore M (1996) Diagnostic imaging in patients with paragangliomas. Computed tomography, magnetic resonance and MIBG scintigraphy comparison. Q J Nucl Med 40: 365-371.

47. Schmedtje JF, Jr., Sax S, Pool JL, Goldfarb RA, Nelson EB (1987) Localization of ectopic pheochromocytomas by magnetic resonance imaging. Am J Med 83: 770-772.
48. Pacak K, Eisenhofer G, Ahlman H, Bornstein SR, Gimenez-Roqueplo AP, et al. (2007) Pheochromocytoma: recommendations for clinical practice from the First International Symposium. October 2005. Nat Clin Pract Endocrinol Metab 3: 92-102.
49. Nakatani T, Hayama T, Uchida J, Nakamura K, Takemoto Y, et al. (2002) Diagnostic localization of extra-adrenal pheochromocytoma: comparison of (123)I-MIBG imaging and (131)I-MIBG imaging. Oncol Rep 9: 1225-1227.
50. Shapiro B, Gross MD, Shulkin B (2001) Radioisotope diagnosis and therapy of malignant pheochromocytoma. Trends Endocrinol Metab 12: 469-475.
51. Kayano D, Taki J, Fukuoka M, Wakabayashi H, Inaki A, et al. (2011) Low-dose (123)I-metaiodobenzylguanidine diagnostic scan is inferior to (131)I-metaiodobenzylguanidine posttreatment scan in detection of malignant pheochromocytoma and paraganglioma. Nucl Med Commun 32: 941-946.
52. Ilias I, Chen CC, Carrasquillo JA, Whatley M, Ling A, et al. (2008) Comparison of 6-18F-fluorodopamine PET with 123I-metaiodobenzylguanidine and 111in-pentetreotide scintigraphy in localization of nonmetastatic and metastatic pheochromocytoma. J Nucl Med 49: 1613-1619.
53. Havekes B, King K, Lai EW, Romijn JA, Corssmit EP, et al. (2010) New imaging approaches to phaeochromocytomas and paragangliomas. Clin Endocrinol (Oxf) 72: 137-145.
54. Ilias I, Pacak K (2004) Current approaches and recommended algorithm for the diagnostic localization of pheochromocytoma. J Clin Endocrinol Metab 89: 479-491.
55. Gill AJ, Benn DE, Chou A, Clarkson A, Muljono A, et al. (2010) Immunohistochemistry for SDHB triages genetic testing of SDHB, SDHC, and SDHD in paraganglioma-pheochromocytoma syndromes. Hum Pathol 41: 805-814.
56. van Nederveen FH, Gaal J, Favier J, Korpershoek E, Oldenburg RA, et al. (2009) An immunohistochemical procedure to detect patients with paraganglioma and phaeochromocytoma with germline SDHB, SDHC, or SDHD gene mutations: a retrospective and prospective analysis. Lancet Oncol 10: 764-771.
57. Korpershoek E, Favier J, Gaal J, Burnichon N, van Gessel B, et al. (2011) SDHA immunohistochemistry detects germline SDHA gene mutations in apparently sporadic paragangliomas and pheochromocytomas. J Clin Endocrinol Metab 96: E1472-1476.
58. Plouin PF, Amar L, Lepoutre C (2010) Phaeochromocytomas and functional paragangliomas: clinical management. Best Pract Res Clin Endocrinol Metab 24: 933-941.
59. Thompson LD (2002) Pheochromocytoma of the Adrenal gland Scaled Score (PASS) to separate benign from malignant neoplasms: a clinicopathologic and immunophenotypic study of 100 cases. Am J Surg Pathol 26: 551-566.

60. Eisenhofer G, Rivers G, Rosas AL, Quezado Z, Manger WM, et al. (2007) Adverse drug reactions in patients with phaeochromocytoma: incidence, prevention and management. Drug Saf 30: 1031-1062.
61. Sjoerdsma A, Engelman K, Spector S, Udenfriend S (1965) Inhibition of catecholamine synthesis in man with alpha-methyl-tyrosine, an inhibitor of tyrosine hydroxylase. Lancet 2: 1092-1094.
62. Vargas HI, Kavoussi LR, Bartlett DL, Wagner JR, Venzon DJ, et al. (1997) Laparoscopic adrenalectomy: a new standard of care. Urology 49: 673-678.
63. Winfield HN, Hamilton BD, Bravo EL, Novick AC (1998) Laparoscopic adrenalectomy: the preferred choice? A comparison to open adrenalectomy. J Urol 160: 325-329.
64. Dickson PV, Alex GC, Grubbs EG, Ayala-Ramirez M, Jimenez C, et al. (2011) Posterior retroperitoneoscopic adrenalectomy is a safe and effective alternative to transabdominal laparoscopic adrenalectomy for pheochromocytoma. Surgery 150: 452-458.
65. Dickson PV, Jimenez C, Chisholm GB, Kennamer DL, Ng C, et al. (2011) Posterior retroperitoneoscopic adrenalectomy: a contemporary American experience. J Am Coll Surg 212: 659-665; discussion 665-657.
66. Diner EK, Franks ME, Behari A, Linehan WM, Walther MM (2005) Partial adrenalectomy: the National Cancer Institute experience. Urology 66: 19-23.
67. Voo S, Bucerius J, Mottaghy FM (2011) I-131-MIBG therapies. Methods 55: 238-245.
68. Averbuch SD, Steakley CS, Young RC, Gelmann EP, Goldstein DS, et al. (1988) Malignant pheochromocytoma: effective treatment with a combination of cyclophosphamide, vincristine, and dacarbazine. Ann Intern Med 109: 267-273.
69. Huang H, Abraham J, Hung E, Averbuch S, Merino M, et al. (2008) Treatment of malignant pheochromocytoma/paraganglioma with cyclophosphamide, vincristine, and dacarbazine: recommendation from a 22-year follow-up of 18 patients. Cancer 113: 2020-2028.
70. Ayala-Ramirez M, Feng L, Habra MA, Rich T, Dickson PV, et al. (2011) Clinical benefits of systemic chemotherapy for patients with metastatic pheochromocytomas or sympathetic extra-adrenal paragangliomas: Insights from the largest single-institutional experience. Cancer.
71. Grogan RH, Mitmaker EJ, Duh QY (2011) Changing paradigms in the treatment of malignant pheochromocytoma. Cancer Control 18: 104-112.
72. McBride JF, Atwell TD, Charboneau WJ, Young WF, Jr., Wass TC, et al. (2011) Minimally invasive treatment of metastatic pheochromocytoma and paraganglioma: efficacy and safety of radiofrequency ablation and cryoablation therapy. J Vasc Interv Radiol 22: 1263-1270.
73. Watanabe D, Tanabe A, Naruse M, Tsuiki M, Torii N, et al. (2006) Transcatheter arterial embolization for the treatment of liver metastases in a patient with malignant pheochromocytoma. Endocr J 53: 59-66.
74. Hidaka S, Hiraoka A, Ochi H, Uehara T, Ninomiya T, et al. (2010) Malignant pheochromocytoma with liver metastasis treated by transcatheter arterial chemo-embolization (TACE). Intern Med 49: 645-651.

75. Kumar P, Bryant T, Breen D, Stedman B, Hacking N (2011) Transarterial embolization and doxorubicin eluting beads-transarterial chemoembolization (DEB-TACE) of malignant extra-adrenal pheochromocytoma. Cardiovasc Intervent Radiol 34: 1325-1329.
76. Mundschenk J, Unger N, Schulz S, Hollt V, Steinke R, et al. (2003) Somatostatin receptor subtypes in human pheochromocytoma: subcellular expression pattern and functional relevance for octreotide scintigraphy. J Clin Endocrinol Metab 88: 5150-5157.
77. Van Essen M, Krenning EP, De Jong M, Valkema R, Kwekkeboom DJ (2007) Peptide Receptor Radionuclide Therapy with radiolabelled somatostatin analogues in patients with somatostatin receptor positive tumours. Acta Oncol 46: 723-734.
78. Stenstrom G, Ernest I, Tisell LE (1988) Long-term results in 64 patients operated upon for pheochromocytoma. Acta Med Scand 223: 345-352.
79. McClellan M, Benner J, Schilsky R, Epstein D, Woosley R, et al. (2011) An accelerated pathway for targeted cancer therapies. Nat Rev Drug Discov 10: 79-80.
80. Joshua AM, Ezzat S, Asa SL, Evans A, Broom R, et al. (2009) Rationale and evidence for sunitinib in the treatment of malignant paraganglioma/pheochromocytoma. J Clin Endocrinol Metab 94: 5-9.
81. Jimenez C, Cabanillas ME, Santarpia L, Jonasch E, Kyle KL, et al. (2009) Use of the tyrosine kinase inhibitor sunitinib in a patient with von Hippel-Lindau disease: targeting angiogenic factors in pheochromocytoma and other von Hippel-Lindau disease-related tumors. J Clin Endocrinol Metab 94: 386-391.
82. Kulke MH, Stuart K, Enzinger PC, Ryan DP, Clark JW, et al. (2006) Phase II study of temozolomide and thalidomide in patients with metastatic neuroendocrine tumors. J Clin Oncol 24: 401-406.
83. Gross DJ, Munter G, Bitan M, Siegal T, Gabizon A, et al. (2006) The role of imatinib mesylate (Glivec) for treatment of patients with malignant endocrine tumors positive for c-kit or PDGF-R. Endocr Relat Cancer 13: 535-540.
84. Druce MR, Kaltsas GA, Fraenkel M, Gross DJ, Grossman AB (2009) Novel and evolving therapies in the treatment of malignant phaeochromocytoma: experience with the mTOR inhibitor everolimus (RAD001). Horm Metab Res 41: 697-702.
85. Powers JF, Evinger MJ, Tsokas P, Bedri S, Alroy J, et al. (2000) Pheochromocytoma cell lines from heterozygous neurofibromatosis knockout mice. Cell Tissue Res 302: 309-320.
86. Giubellino A, Woldemichael GM, Sourbier C, Lizak MJ, Powers JF, et al. (2012) Characterization of two mouse models of metastatic pheochromocytoma using bioluminescence imaging. Cancer Lett 316: 46-52.
87. Greene LA, Tischler AS (1976) Establishment of a noradrenergic clonal line of rat adrenal pheochromocytoma cells which respond to nerve growth factor. Proc Natl Acad Sci U S A 73: 2424-2428.

88. Isaacs JS, Jung YJ, Mimnaugh EG, Martinez A, Cuttitta F, et al. (2002) Hsp90 regulates a von Hippel Lindau-independent hypoxia-inducible factor-1 alpha-degradative pathway. J Biol Chem 277: 29936-29944.
89. Erlic Z, Rybicki L, Peczkowska M, Golcher H, Kann PH, et al. (2009) Clinical predictors and algorithm for the genetic diagnosis of pheochromocytoma patients. Clin Cancer Res 15: 6378-6385.
90. Fliedner SM, Breza J, Kvetnansky R, Powers JF, Tischler AS, et al. (2010) Tyrosine hydroxylase, chromogranin A, and steroidogenic acute regulator as markers for successful separation of human adrenal medulla. Cell Tissue Res 340: 607-612.
91. Tischler AS, Ruzicka LA, Riseberg JC (1992) Immunocytochemical analysis of chromaffin cell proliferation in vitro. J Histochem Cytochem 40: 1043-1045.
92. Huang R, Southall N, Wang Y, Yasgar A, Shinn P, et al. (2011) The NCGC pharmaceutical collection: a comprehensive resource of clinically approved drugs enabling repurposing and chemical genomics. Sci Transl Med 3: 80ps16.
93. Inglese J, Auld DS, Jadhav A, Johnson RL, Simeonov A, et al. (2006) Quantitative high-throughput screening: a titration-based approach that efficiently identifies biological activities in large chemical libraries. Proc Natl Acad Sci U S A 103: 11473-11478.
94. Team RDC (2010) R: A Language and Environment for Statistical Computing.
95. Schuetz CS, Bonin M, Clare SE, Nieselt K, Sotlar K, et al. (2006) Progression-specific genes identified by expression profiling of matched ductal carcinomas in situ and invasive breast tumors, combining laser capture microdissection and oligonucleotide microarray analysis. Cancer Res 66: 5278-5286.
96. Shankavaram U, Fliedner SM, Elkahloun AG, Barb JJ, Munson PJ, et al. (2013) Genotype and tumor locus determine expression profile of pseudohypoxic pheochromocytomas and paragangliomas. Neoplasia 15: 435-447.
97. Shannon P, Markiel A, Ozier O, Baliga NS, Wang JT, et al. (2003) Cytoscape: a software environment for integrated models of biomolecular interaction networks. Genome Res 13: 2498-2504.
98. Wu G, Feng X, Stein L (2010) A human functional protein interaction network and its application to cancer data analysis. Genome Biol 11: R53.
99. Chou TC, Talalay P (1984) Quantitative analysis of dose-effect relationships: the combined effects of multiple drugs or enzyme inhibitors. Adv Enzyme Regul 22: 27-55.
100. Chou TC (2006) Theoretical basis, experimental design, and computerized simulation of synergism and antagonism in drug combination studies. Pharmacol Rev 58: 621-681.
101. Amar L, Baudin E, Burnichon N, Peyrard S, Silvera S, et al. (2007) Succinate dehydrogenase B gene mutations predict survival in patients with malignant pheochromocytomas or paragangliomas. J Clin Endocrinol Metab 92: 3822-3828.

102. Zou J, Guo Y, Guettouche T, Smith DF, Voellmy R (1998) Repression of heat shock transcription factor HSF1 activation by HSP90 (HSP90 complex) that forms a stress-sensitive complex with HSF1. Cell 94: 471-480.
103. Jhaveri K, Taldone T, Modi S, Chiosis G (2012) Advances in the clinical development of heat shock protein 90 (Hsp90) inhibitors in cancers. Biochim Biophys Acta 1823: 742-755.
104. Zhang H, Chung D, Yang YC, Neely L, Tsurumoto S, et al. (2006) Identification of new biomarkers for clinical trials of Hsp90 inhibitors. Mol Cancer Ther 5: 1256-1264.
105. Modi S, Stopeck AT, Gordon MS, Mendelson D, Solit DB, et al. (2007) Combination of trastuzumab and tanespimycin (17-AAG, KOS-953) is safe and active in trastuzumab-refractory HER-2 overexpressing breast cancer: a phase I dose-escalation study. J Clin Oncol 25: 5410-5417.
106. Tischler AS, Powers JF, Alroy J (2004) Animal models of pheochromocytoma. Histol Histopathol 19: 883-895.
107. Giubellino A, Sourbier C, Lee MJ, Scroggins B, Bullova P, et al. (2013) Targeting heat shock protein 90 for the treatment of malignant pheochromocytoma. PLoS One 8: e56083.
108. Nakane M, Takahashi S, Sekine I, Fukui I, Koizumi M, et al. (2003) Successful treatment of malignant pheochromocytoma with combination chemotherapy containing anthracycline. Ann Oncol 14: 1449-1451.
109. Gray J, Cubitt CL, Zhang S, Chiappori A (2012) Combination of HDAC and topoisomerase inhibitors in small cell lung cancer. Cancer Biol Ther 13: 614-622.
110. Santarpia L, Habra MA, Jimenez C (2009) Malignant pheochromocytomas and paragangliomas: molecular signaling pathways and emerging therapies. Horm Metab Res 41: 680-686.
111. Schilsky RL (2010) Personalized medicine in oncology: the future is now. Nat Rev Drug Discov 9: 363-366.
112. Ye L, Santarpia L, Gagel RF (2010) The evolving field of tyrosine kinase inhibitors in the treatment of endocrine tumors. Endocr Rev 31: 578-599.
113. Nolting S, Grossman AB (2012) Signaling pathways in pheochromocytomas and paragangliomas: prospects for future therapies. Endocr Pathol 23: 21-33.
114. Burnichon N, Buffet A, Parfait B, Letouze E, Laurendeau I, et al. (2012) Somatic NF1 inactivation is a frequent event in sporadic pheochromocytoma. Hum Mol Genet 21: 5397-5405.
115. Klerk CP, Overmeer RM, Niers TM, Versteeg HH, Richel DJ, et al. (2007) Validity of bioluminescence measurements for noninvasive in vivo imaging of tumor load in small animals. Biotechniques 43: 7-13, 30.
116. Hong H, Yang Y, Zhang Y, Cai W (2010) Non-invasive cell tracking in cancer and cancer therapy. Curr Top Med Chem 10: 1237-1248.
117. Khanna C, Hunter K (2005) Modeling metastasis in vivo. Carcinogenesis 26: 513-523.
118. Vantyghem SA, Wilson SM, Postenka CO, Al-Katib W, Tuck AB, et al. (2005) Dietary genistein reduces metastasis in a postsurgical orthotopic breast cancer model. Cancer Res 65: 3396-3403.

119. Francia G, Cruz-Munoz W, Man S, Xu P, Kerbel RS (2011) Mouse models of advanced spontaneous metastasis for experimental therapeutics. Nat Rev Cancer 11: 135-141.
120. Jacks T, Shih TS, Schmitt EM, Bronson RT, Bernards A, et al. (1994) Tumour predisposition in mice heterozygous for a targeted mutation in Nf1. Nat Genet 7: 353-361.
121. Cascon A, Tennant DA (2012) From transcriptional profiling to tumor biology in pheochromocytoma and paraganglioma. Endocr Pathol 23: 15-20.
122. Buffet A, Venisse A, Nau V, Roncellin I, Boccio V, et al. (2012) A decade (2001-2010) of genetic testing for pheochromocytoma and paraganglioma. Horm Metab Res 44: 359-366.
123. Kaelin WG, Jr. (2008) The von Hippel-Lindau tumour suppressor protein: O2 sensing and cancer. Nat Rev Cancer 8: 865-873.
124. Schlisio S, Kenchappa RS, Vredeveld LC, George RE, Stewart R, et al. (2008) The kinesin KIF1Bbeta acts downstream from EglN3 to induce apoptosis and is a potential 1p36 tumor suppressor. Genes Dev 22: 884-893.
125. Gimenez-Roqueplo AP, Dahia PL, Robledo M (2012) An update on the genetics of paraganglioma, pheochromocytoma, and associated hereditary syndromes. Horm Metab Res 44: 328-333.
126. Dahia PL, Ross KN, Wright ME, Hayashida CY, Santagata S, et al. (2005) A HIF1alpha regulatory loop links hypoxia and mitochondrial signals in pheochromocytomas. PLoS Genet 1: 72-80.
127. Jiang S, Dahia PL (2011) Minireview: the busy road to pheochromocytomas and paragangliomas has a new member, TMEM127. Endocrinology 152: 2133-2140.
128. Favier J, Igaz P, Burnichon N, Amar L, Libe R, et al. (2012) Rationale for anti-angiogenic therapy in pheochromocytoma and paraganglioma. Endocr Pathol 23: 34-42.
129. Lai EW, Rodriguez OC, Aventian M, Cromelin C, Fricke ST, et al. (2007) ErbB-2 induces bilateral adrenal pheochromocytoma formation in mice. Cell Cycle 6: 1946-1950.
130. Di Cristofano A, De Acetis M, Koff A, Cordon-Cardo C, Pandolfi PP (2001) Pten and p27KIP1 cooperate in prostate cancer tumor suppression in the mouse. Nat Genet 27: 222-224.
131. Sparks CA, Guertin DA (2010) Targeting mTOR: prospects for mTOR complex 2 inhibitors in cancer therapy. Oncogene 29: 3733-3744.
132. Chrisoulidou A, Kaltsas G, Ilias I, Grossman AB (2007) The diagnosis and management of malignant phaeochromocytoma and paraganglioma. Endocr Relat Cancer 14: 569-585.
133. Jyung RW, LeClair EE, Bernat RA, Kang TS, Ung F, et al. (2000) Expression of angiogenic growth factors in paragangliomas. Laryngoscope 110: 161-167.
134. Brieger J, Bedavanija A, Gosepath J, Maurer J, Mann WJ (2005) Vascular endothelial growth factor expression, vascularization and proliferation in paragangliomas. ORL J Otorhinolaryngol Relat Spec 67: 119-124.

135. Favier J, Plouin PF, Corvol P, Gasc JM (2002) Angiogenesis and vascular architecture in pheochromocytomas: distinctive traits in malignant tumors. Am J Pathol 161: 1235-1246.
136. Rooijens PP, de Krijger RR, Bonjer HJ, van der Ham F, Nigg AL, et al. (2004) The significance of angiogenesis in malignant pheochromocytomas. Endocr Pathol 15: 39-45.
137. Lopez-Jimenez E, Gomez-Lopez G, Leandro-Garcia LJ, Munoz I, Schiavi F, et al. (2010) Research resource: Transcriptional profiling reveals different pseudohypoxic signatures in SDHB and VHL-related pheochromocytomas. Mol Endocrinol 24: 2382-2391.
138. Boltze C, Mundschenk J, Unger N, Schneider-Stock R, Peters B, et al. (2003) Expression profile of the telomeric complex discriminates between benign and malignant pheochromocytoma. J Clin Endocrinol Metab 88: 4280-4286.
139. Dezwaan DC, Freeman BC (2008) HSP90: the Rosetta stone for cellular protein dynamics? Cell Cycle 7: 1006-1012.
140. Neckers L, Tsutsumi S, Mollapour M (2009) Visualizing the twists and turns of a molecular chaperone. Nat Struct Mol Biol 16: 235-236.
141. Neckers L, Mollapour M, Tsutsumi S (2009) The complex dance of the molecular chaperone Hsp90. Trends Biochem Sci 34: 223-226.
142. Schulte TW, Blagosklonny MV, Ingui C, Neckers L (1995) Disruption of the Raf-1-Hsp90 molecular complex results in destabilization of Raf-1 and loss of Raf-1-Ras association. J Biol Chem 270: 24585-24588.
143. Basso AD, Solit DB, Chiosis G, Giri B, Tsichlis P, et al. (2002) Akt forms an intracellular complex with heat shock protein 90 (Hsp90) and Cdc37 and is destabilized by inhibitors of Hsp90 function. J Biol Chem 277: 39858-39866.
144. Engelman JA, Settleman J (2008) Acquired resistance to tyrosine kinase inhibitors during cancer therapy. Curr Opin Genet Dev 18: 73-79.
145. Bishop SC, Burlison JA, Blagg BS (2007) Hsp90: a novel target for the disruption of multiple signaling cascades. Curr Cancer Drug Targets 7: 369-388.
146. Xu W, Neckers L (2007) Targeting the molecular chaperone heat shock protein 90 provides a multifaceted effect on diverse cell signaling pathways of cancer cells. Clin Cancer Res 13: 1625-1629.
147. Banerji U (2009) Heat shock protein 90 as a drug target: some like it hot. Clin Cancer Res 15: 9-14.
148. Rajan A, Kelly RJ, Trepel JB, Kim YS, Alarcon SV, et al. (2011) A phase I study of PF-04929113 (SNX-5422), an orally bioavailable heat shock protein 90 inhibitor, in patients with refractory solid tumor malignancies and lymphomas. Clin Cancer Res 17: 6831-6839.
149. Korpershoek E, Pacak K, Martiniova L (2012) Murine models and cell lines for the investigation of pheochromocytoma: applications for future therapies? Endocr Pathol 23: 43-54.
150. Weir SJ, DeGennaro LJ, Austin CP (2012) Repurposing approved and abandoned drugs for the treatment and prevention of cancer through public-private partnership. Cancer Res 72: 1055-1058.

151. Duenas-Gonzalez A, Garcia-Lopez P, Herrera LA, Medina-Franco JL, Gonzalez-Fierro A, et al. (2008) The prince and the pauper. A tale of anticancer targeted agents. Mol Cancer 7: 82.
152. Collins FS (2011) Mining for therapeutic gold. Nat Rev Drug Discov 10: 397.
153. King KS, Prodanov T, Kantorovich V, Fojo T, Hewitt JK, et al. (2011) Metastatic pheochromocytoma/paraganglioma related to primary tumor development in childhood or adolescence: significant link to SDHB mutations. J Clin Oncol 29: 4137-4142.
154. Ayala-Ramirez M, Feng L, Johnson MM, Ejaz S, Habra MA, et al. (2011) Clinical risk factors for malignancy and overall survival in patients with pheochromocytomas and sympathetic paragangliomas: primary tumor size and primary tumor location as prognostic indicators. J Clin Endocrinol Metab 96: 717-725.
155. Vicha A, Musil Z, Pacak K (2013) Genetics of pheochromocytoma and paraganglioma syndromes: new advances and future treatment options. Curr Opin Endocrinol Diabetes Obes 20: 186-191.
156. Hopewell R, Ziff EB (1995) The nerve growth factor-responsive PC12 cell line does not express the Myc dimerization partner Max. Mol Cell Biol 15: 3470-3478.
157. DiMasi JA, Hansen RW, Grabowski HG (2003) The price of innovation: new estimates of drug development costs. J Health Econ 22: 151-185.
158. Sardana D, Zhu C, Zhang M, Gudivada RC, Yang L, et al. (2011) Drug repositioning for orphan diseases. Brief Bioinform 12: 346-356.
159. Yang C, Matro JC, Huntoon KM, Ye DY, Huynh TT, et al. (2012) Missense mutations in the human SDHB gene increase protein degradation without altering intrinsic enzymatic function. FASEB J 26: 4506-4516.
160. Martiniova L, Perera SM, Brouwers FM, Alesci S, Abu-Asab M, et al. (2011) Increased uptake of [(1)(2)(3)I]meta-iodobenzylguanidine, [(1)F]fluorodopamine, and [(3)H]norepinephrine in mouse pheochromocytoma cells and tumors after treatment with the histone deacetylase inhibitors. Endocr Relat Cancer 18: 143-157.
161. Pacak K, Sirova M, Giubellino A, Lencesova L, Csaderova L, et al. (2012) NF-kappaB inhibition significantly upregulates the norepinephrine transporter system, causes apoptosis in pheochromocytoma cell lines and prevents metastasis in an animal model. Int J Cancer.
162. Killian JK, Kim SY, Miettinen M, Smith C, Merino M, et al. (2013) Succinate dehydrogenase mutation underlies global epigenomic divergence in gastrointestinal stromal tumor. Cancer Discov.

Figure 1

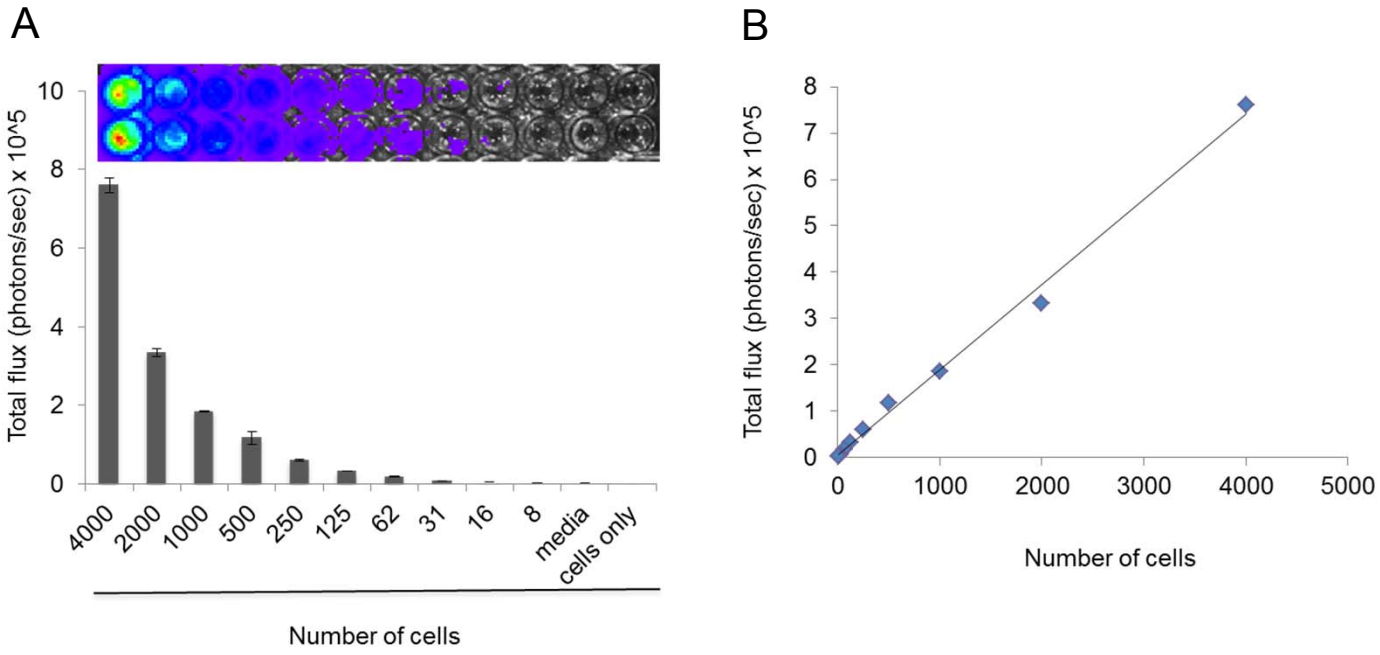
A
B
Total flux (photons/sec) x 10^5
10
8
6
4
2
0
4000
2000
1000
500
250
125
62
31
16
8
media
cells only
Number of cells
Total flux (photons/sec) x 10^5
8
7
6
5
4
3
2
1
0
0
1000
2000
3000
4000
5000
Number of cells

Figure 2

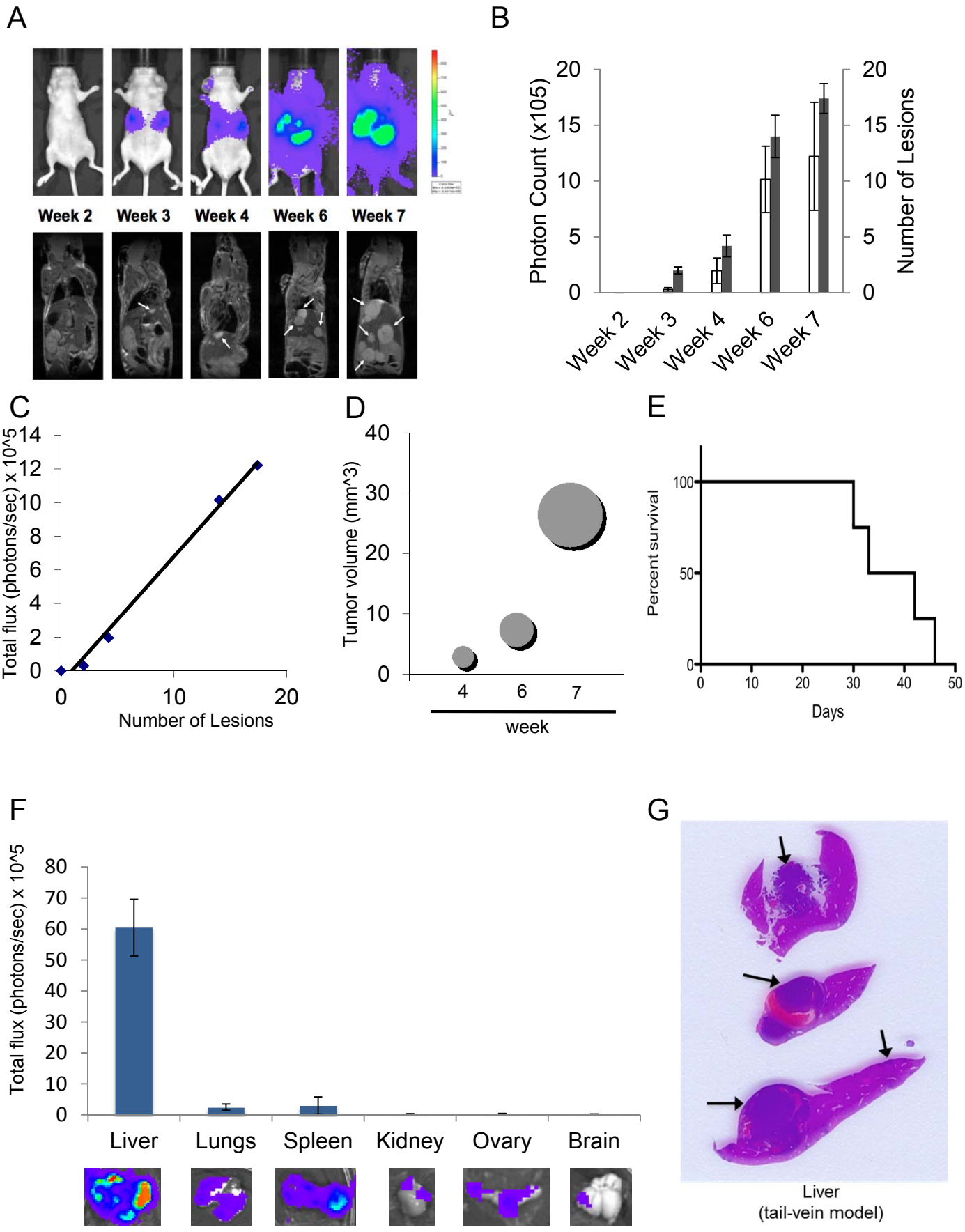
A
Week 2
Week 3
Week 4
Week 6
Week 7
B
Photon Count (x105)
Number of Lesions
0
5
10
15
20
Week 2
Week 3
Week 4
Week 6
Week 7
C
Total flux (photons/sec) x 10^5
0
2
4
6
8
10
12
14
0
10
20
Number of Lesions
D
Tumor volume (mm^3)
0
10
20
30
40
4
6
7
week
E
Percent survival
0
50
100
0
10
20
30
40
50
Days
F
Total flux (photons/sec) x 10^5
0
10
20
30
40
50
60
70
80
Liver
Lungs
Spleen
Kidney
Ovary
Brain
G
Liver
(tail-vein model)

Figure 3

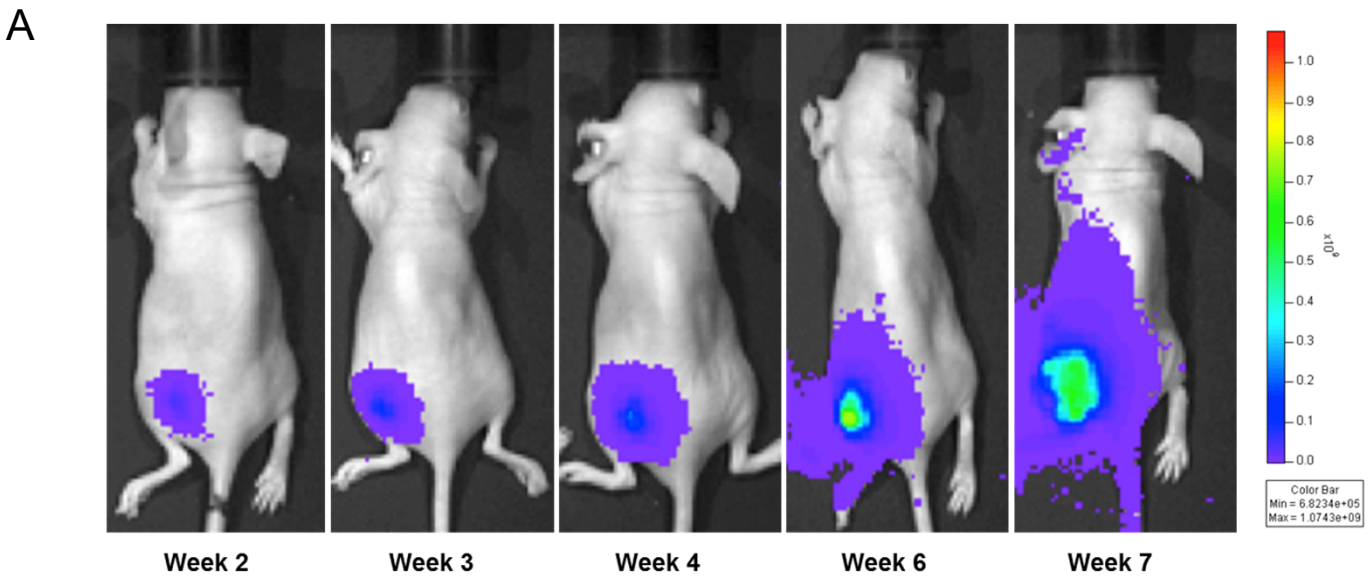

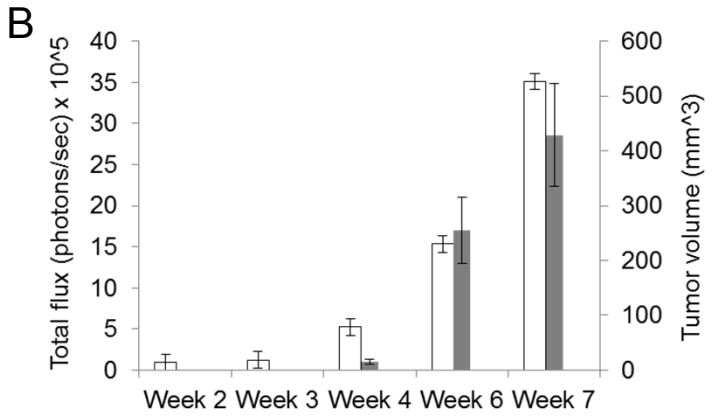

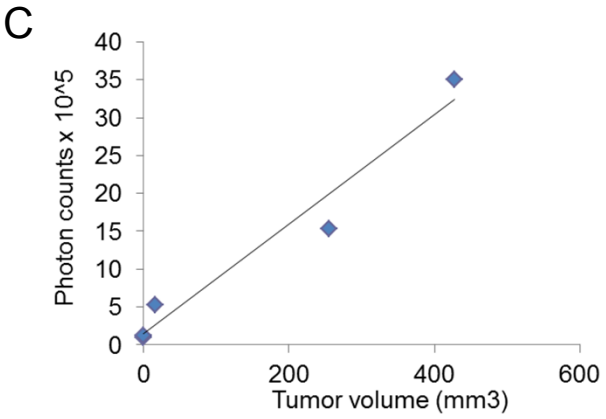

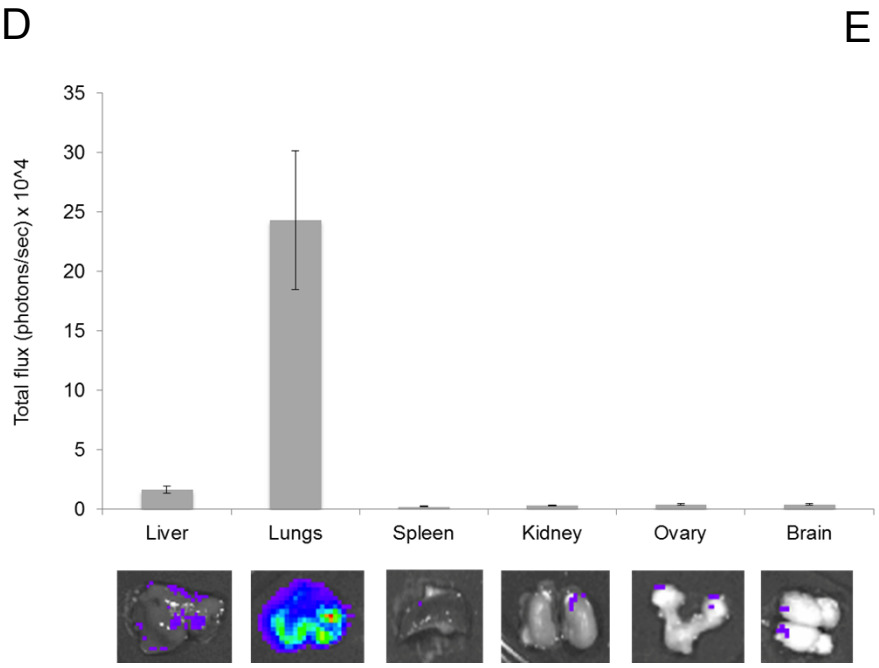

Lungs
(subcutaneous model)

Figure 4

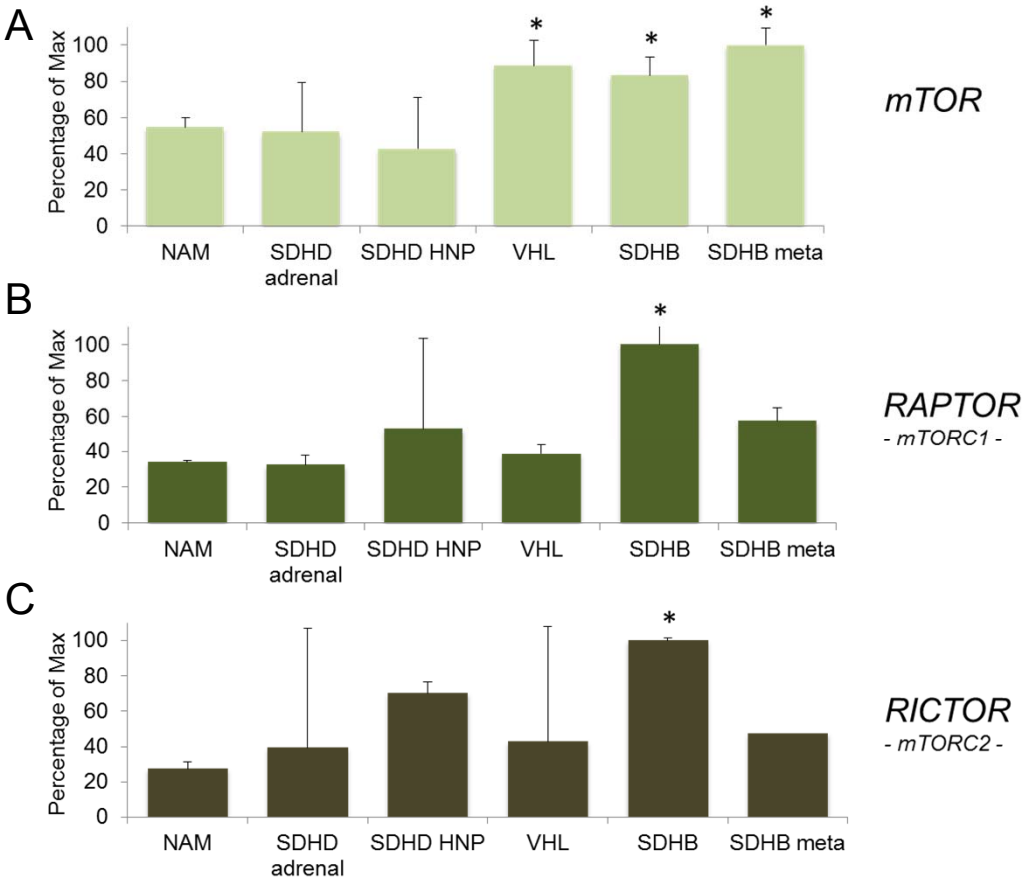
A
Percentage of Max
100
80
60
40
20
0
NAM
SDHD adrenal
SDHD HNP
VHL
SDHB
SDHB meta
*
mTOR
B
RAPTOR
- mTORC1 -
C
RICTOR
- mTORC2 -

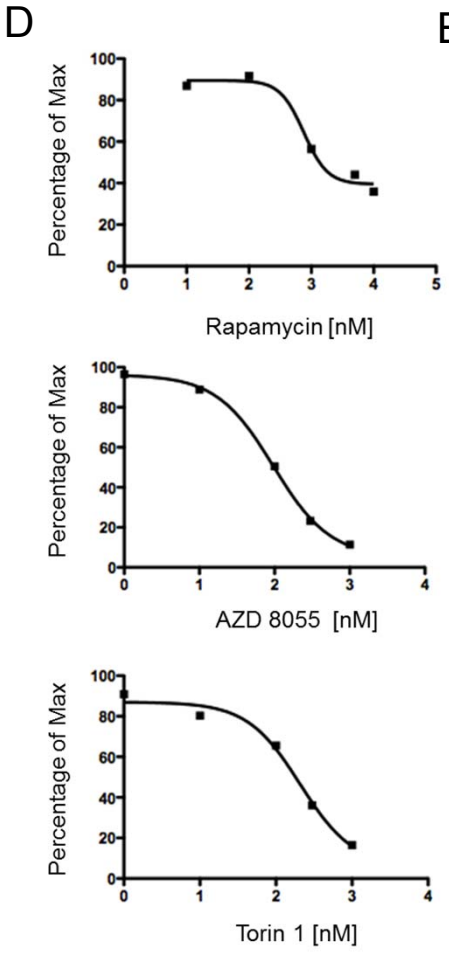
D
Percentage of Max
Rapamycin [nM]
AZD 8055 [nM]
Torin 1 [nM]

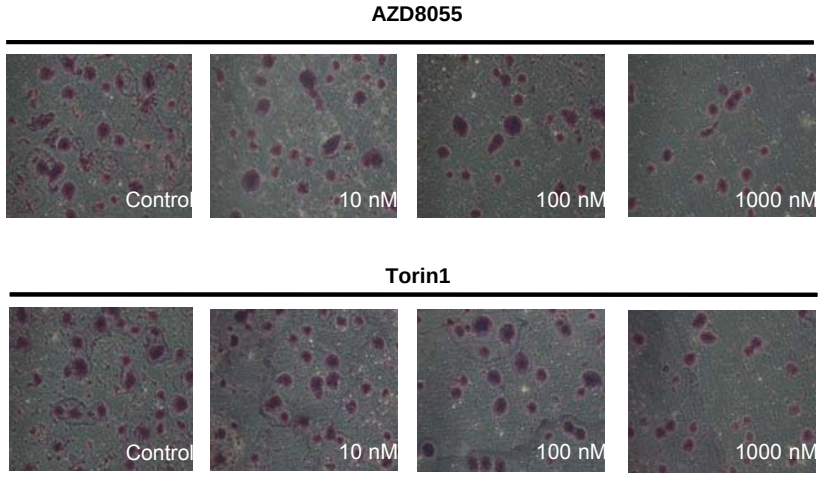
E
AZD8055
Control
10 nM
100 nM
1000 nM
Torin1

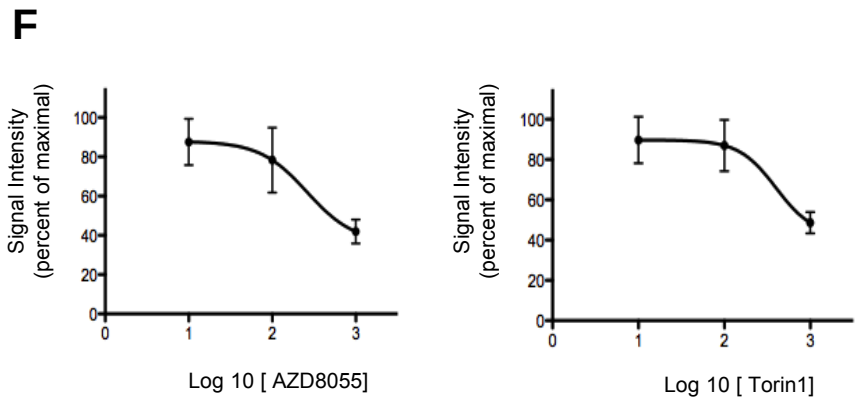
F
Signal Intensity (percent of maximal)
Log 10 [AZD8055]
Log 10 [Torin1]

Figure 5

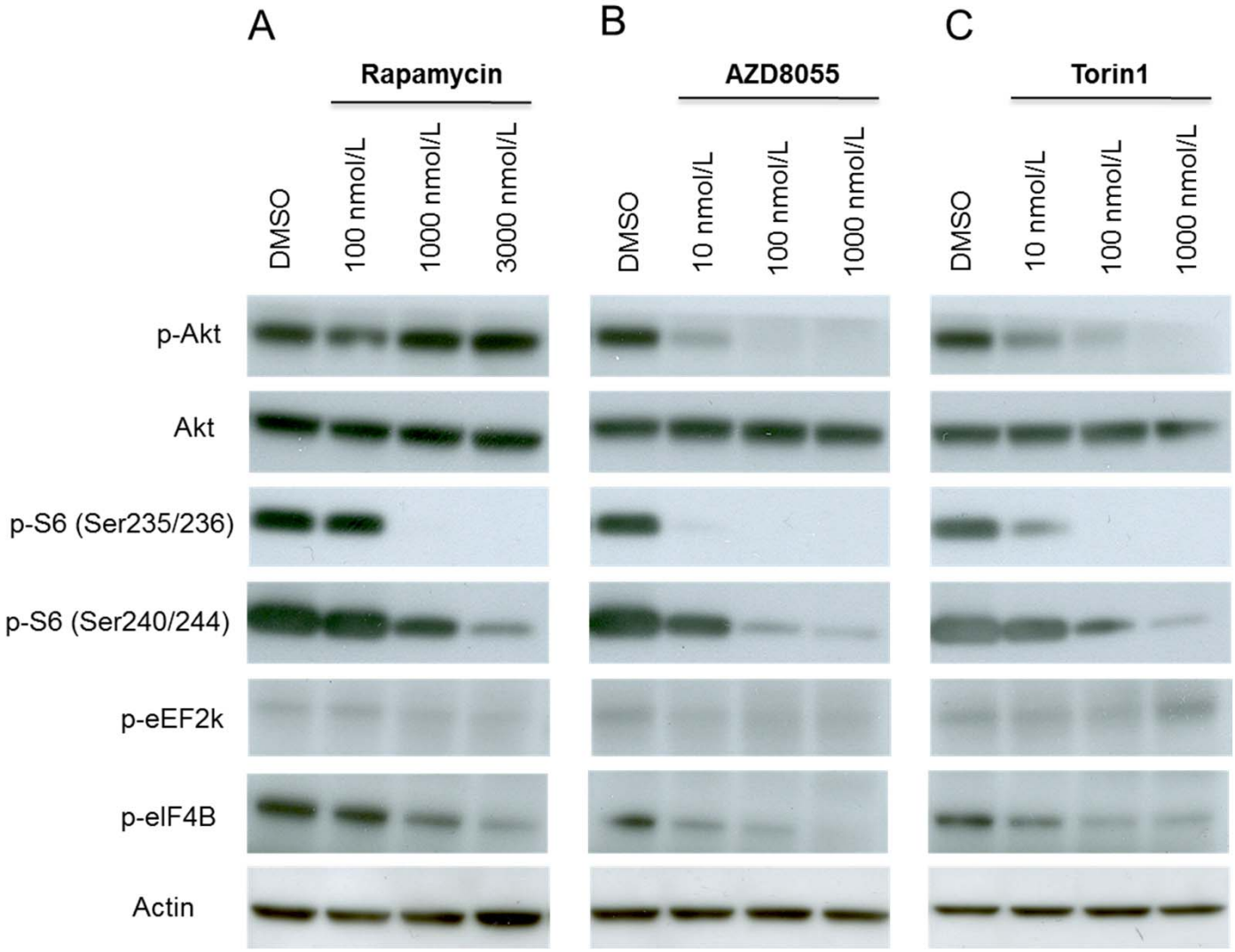
A
Rapamycin
DMSO
100 nmol/L
1000 nmol/L
3000 nmol/L
B
AZD8055
DMSO
10 nmol/L
100 nmol/L
1000 nmol/L
C
Torin1
DMSO
10 nmol/L
100 nmol/L
1000 nmol/L
p-Akt
Akt
p-S6 (Ser235/236)
p-S6 (Ser240/244)
p-eEF2k
p-eIF4B
Actin

Figure 6

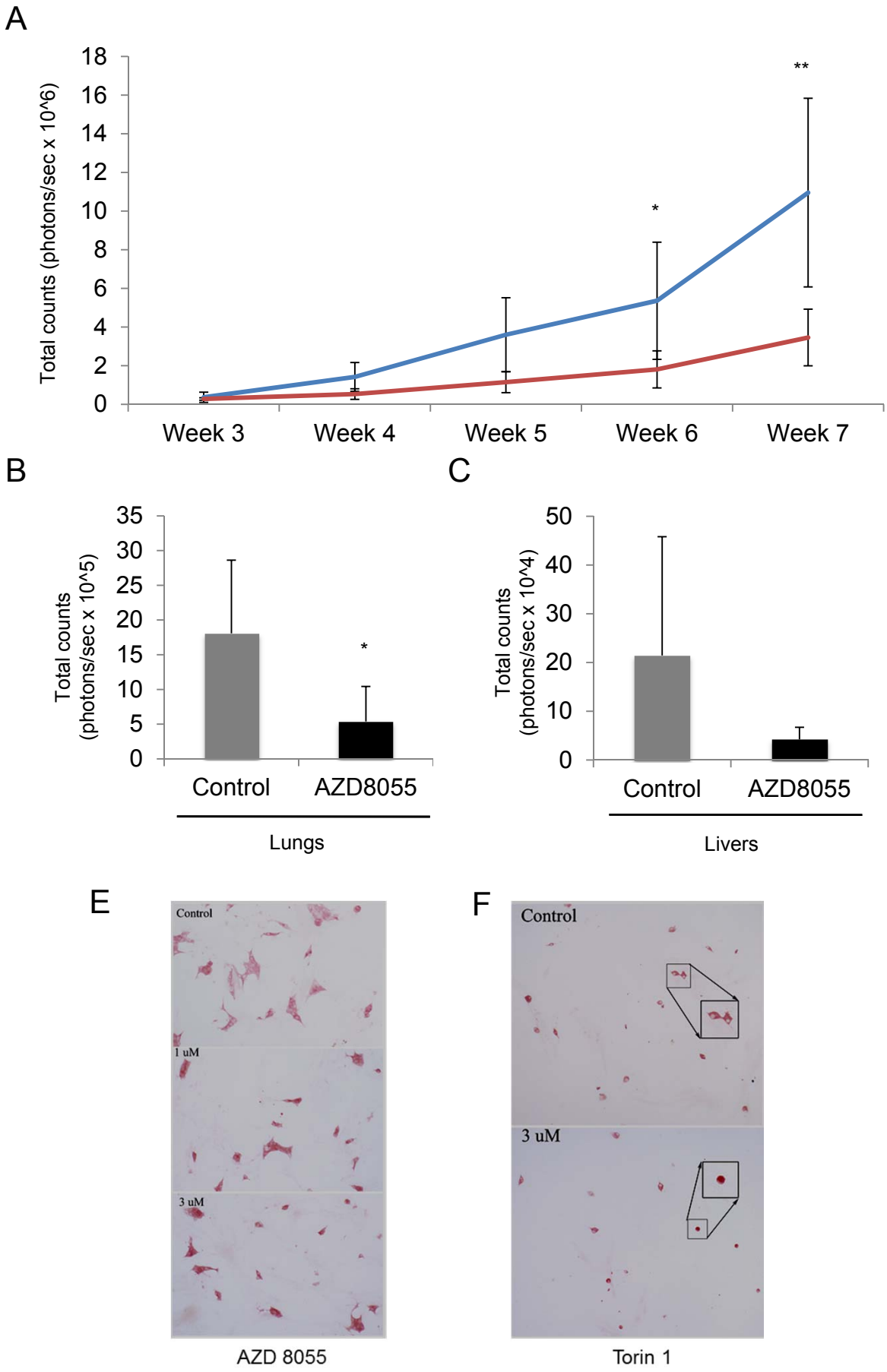
A
Total counts (photons/sec x 10^6)
18
16
14
12
10
8
6
4
2
0
Week 3
Week 4
Week 5
Week 6
Week 7
*
**
B
Total counts (photons/sec x 10^5)
35
30
25
20
15
10
5
0
*
Control
AZD8055
Lungs
C
Total counts (photons/sec x 10^4)
50
40
30
20
10
0
Control
AZD8055
Livers
E
Control
1 uM
3 uM
AZD 8055
F
Control
3 uM
Torin 1

Figure 7

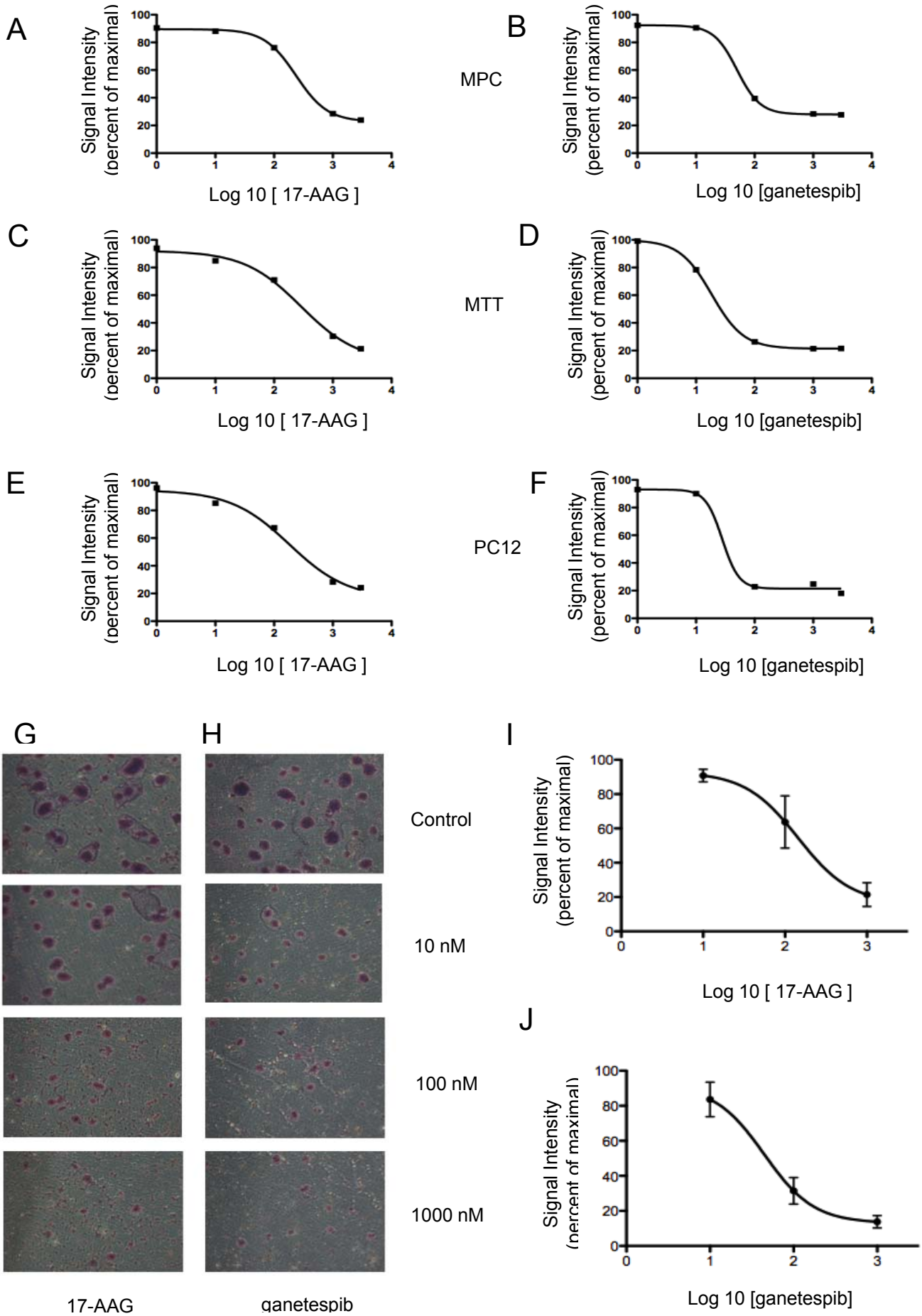
A
B
MPC
C
D
MTT
E
F
PC12
Signal Intensity (percent of maximal)
Log 10 [17-AAG]
Log 10 [ganetespib]
G
H
I
J
Control
10 nM
100 nM
1000 nM
17-AAG
ganetespib

Figure 8

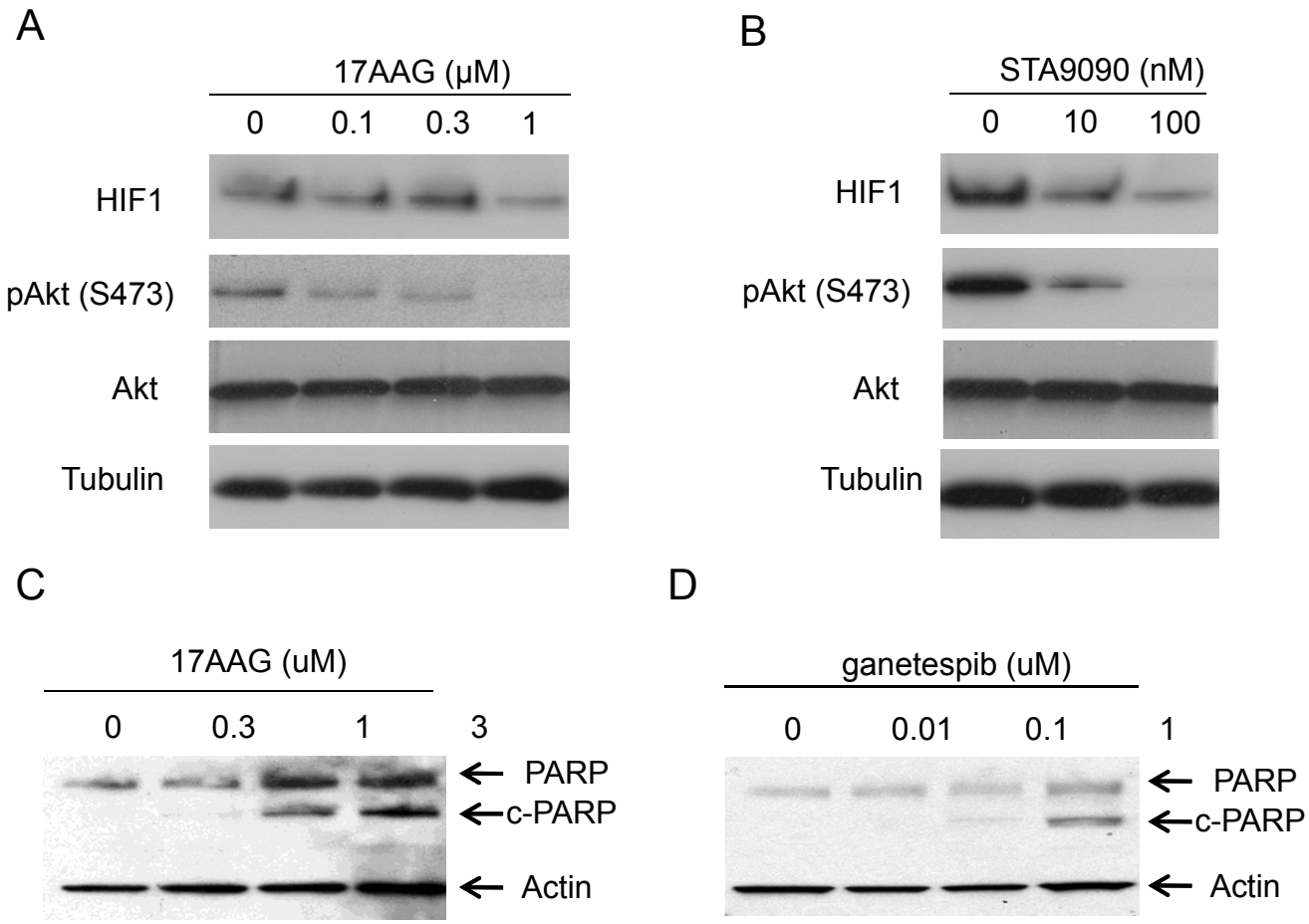
A
17AAG (μM)
0
0.1
0.3
1
HIF1
pAkt (S473)
Akt
Tubulin
B
STA9090 (nM)
0
10
100
HIF1
pAkt (S473)
Akt
Tubulin
C
17AAG (uM)
0
0.3
1
3
PARP
c-PARP
Actin
D
ganetespib (uM)
0
0.01
0.1
1
PARP
c-PARP
Actin

Figure 9

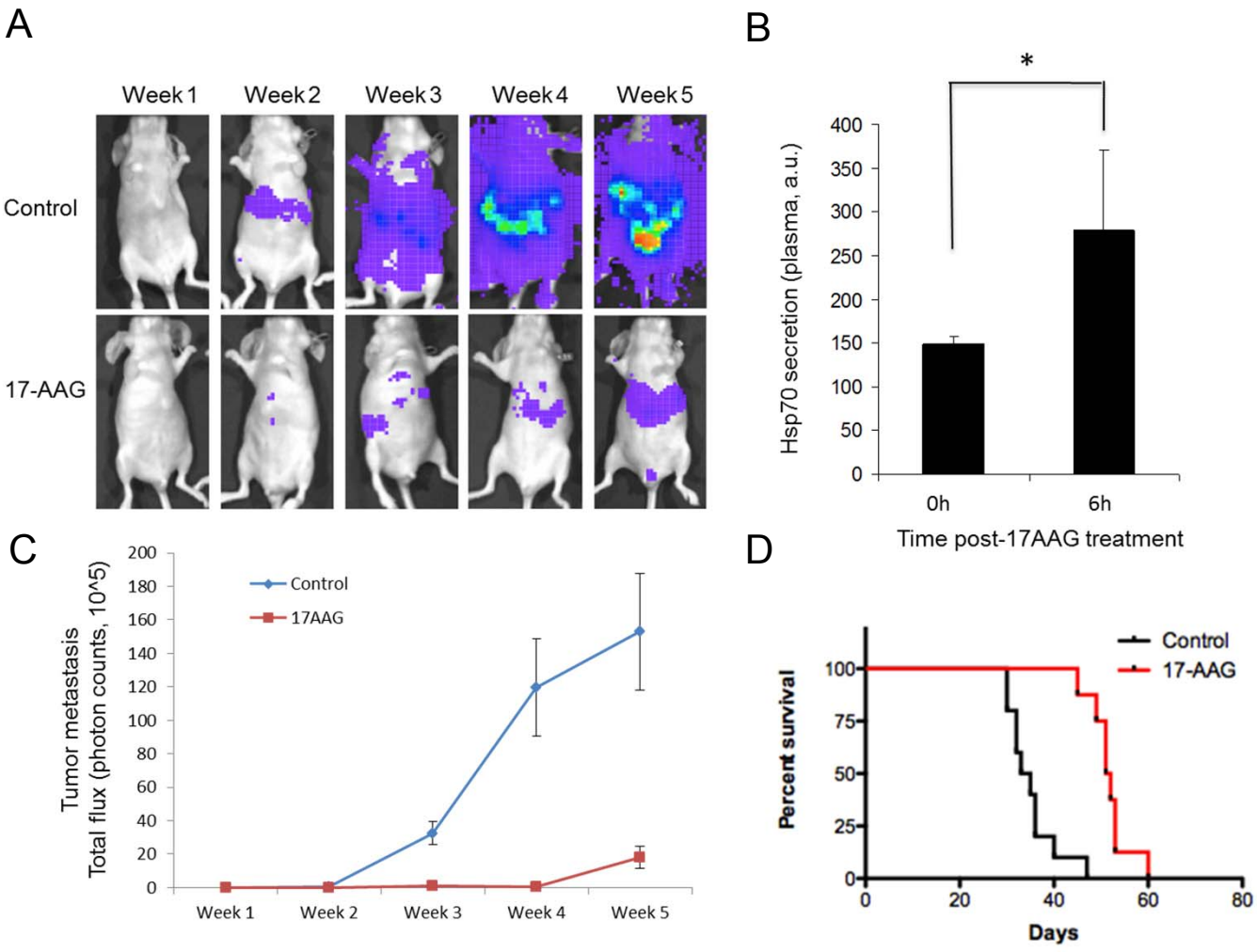
A
Week 1
Week 2
Week 3
Week 4
Week 5
Control
17-AAG
B
*
Hsp70 secretion (plasma, a.u.)
400
350
300
250
200
150
100
50
0
0h
6h
Time post-17AAG treatment
C
Tumor metastasis
Total flux (photon counts, 10^5)
200
180
160
140
120
100
80
60
40
20
0
Control
17AAG
Week 1
Week 2
Week 3
Week 4
Week 5
D
Percent survival
100
75
50
25
0
0
20
40
60
80
Days
Control
17-AAG

Figure 10

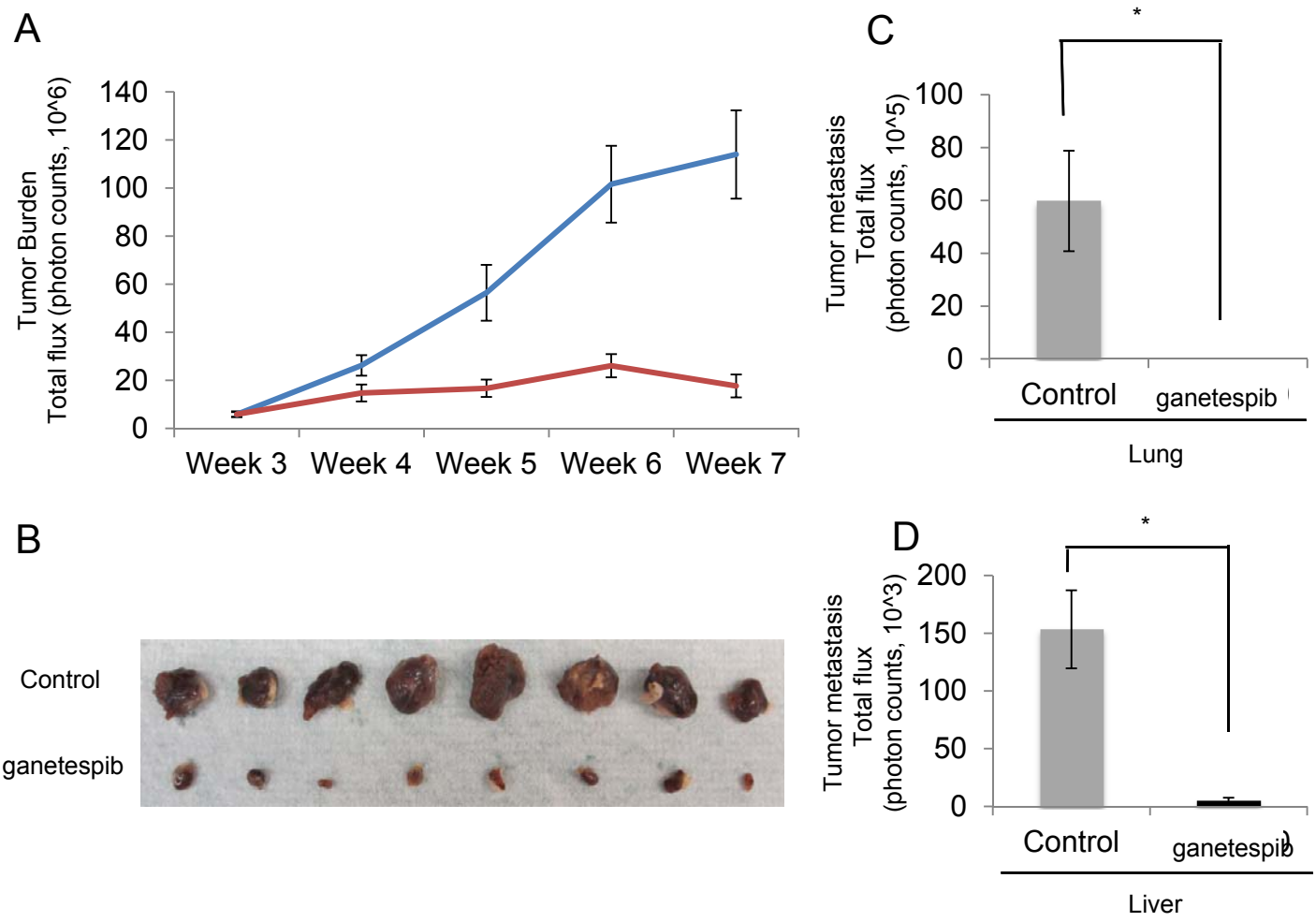
A
Tumor Burden
Total flux (photon counts, 10^6)
140
120
100
80
60
40
20
0
Week 3
Week 4
Week 5
Week 6
Week 7
C
*
Tumor metastasis
Total flux
(photon counts, 10^5)
100
80
60
40
20
0
Control
ganetespib
Lung
B
Control
ganetespib
D
*
Tumor metastasis
Total flux
(photon counts, 10^3)
200
150
100
50
0
Control
ganetespib
Liver

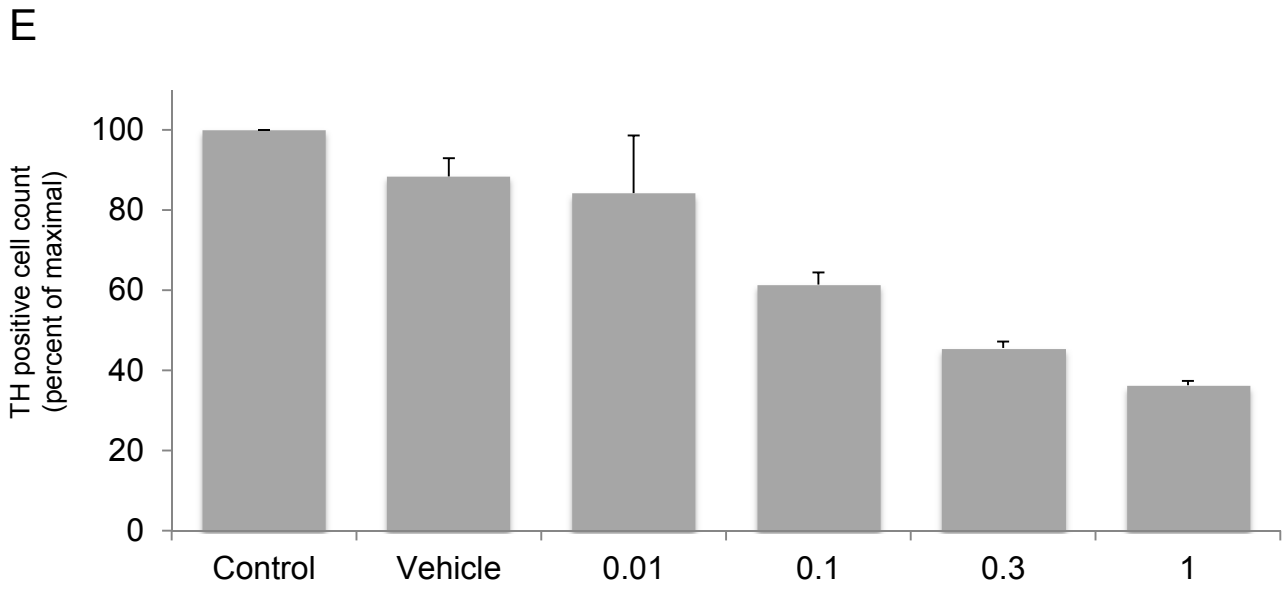
E
TH positive cell count
(percent of maximal)
100
80
60
40
20
0
Control
Vehicle
0.01
0.1
0.3
1

Figure 11

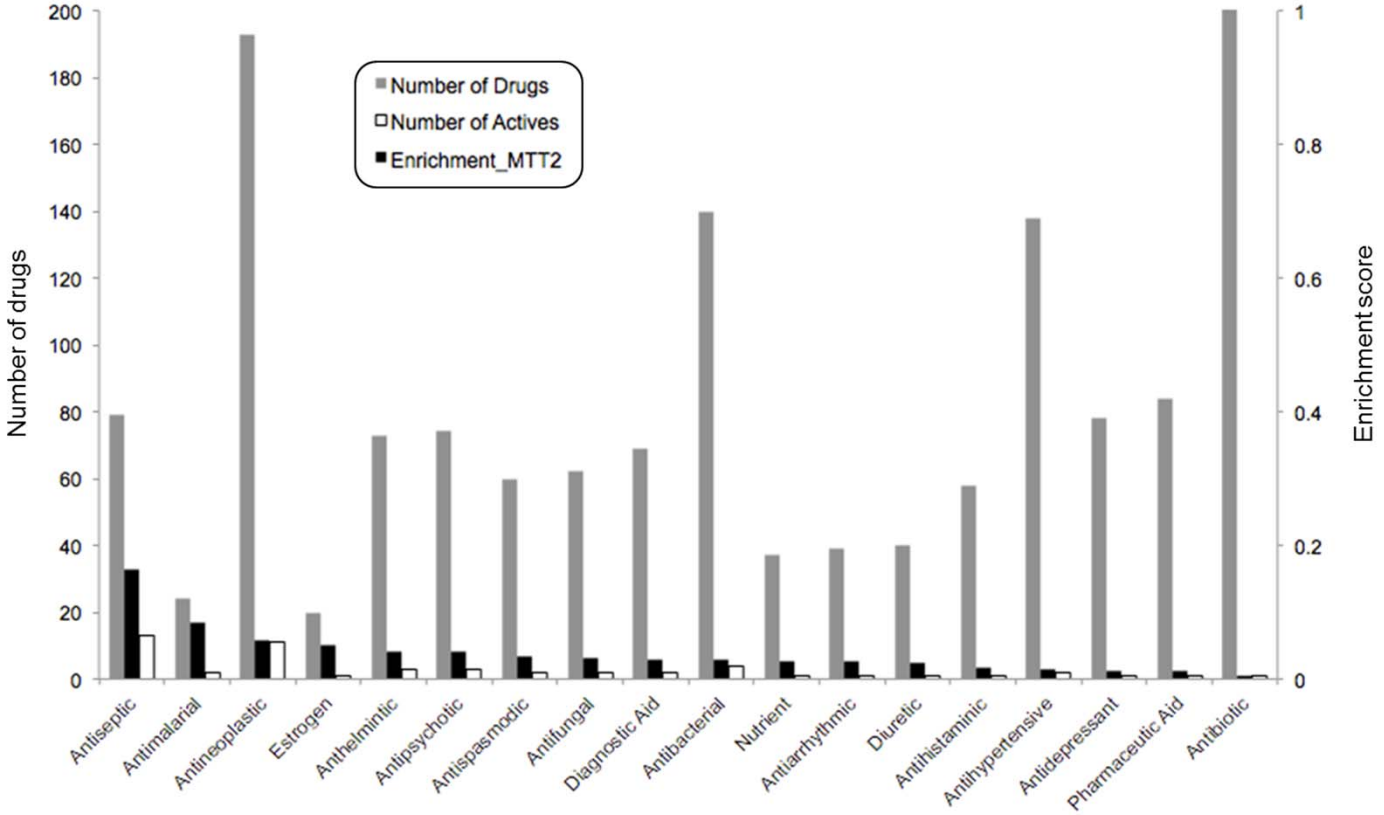
Number of Drugs
Number of Actives
Enrichment_MTT2
Number of drugs
Enrichment score
200
180
160
140
120
100
80
60
40
20
0
1
0.8
0.6
0.4
0.2
0
Antiseptic
Antimalarial
Antineoplastic
Estrogen
Anthelmintic
Antipsychotic
Antispasmodic
Antifungal
Diagnostic Aid
Antibacterial
Nutrient
Antiarrhythmic
Diuretic
Antihistaminic
Antihypertensive
Antidepressant
Pharmaceutic Aid
Antibiotic

Figure 12

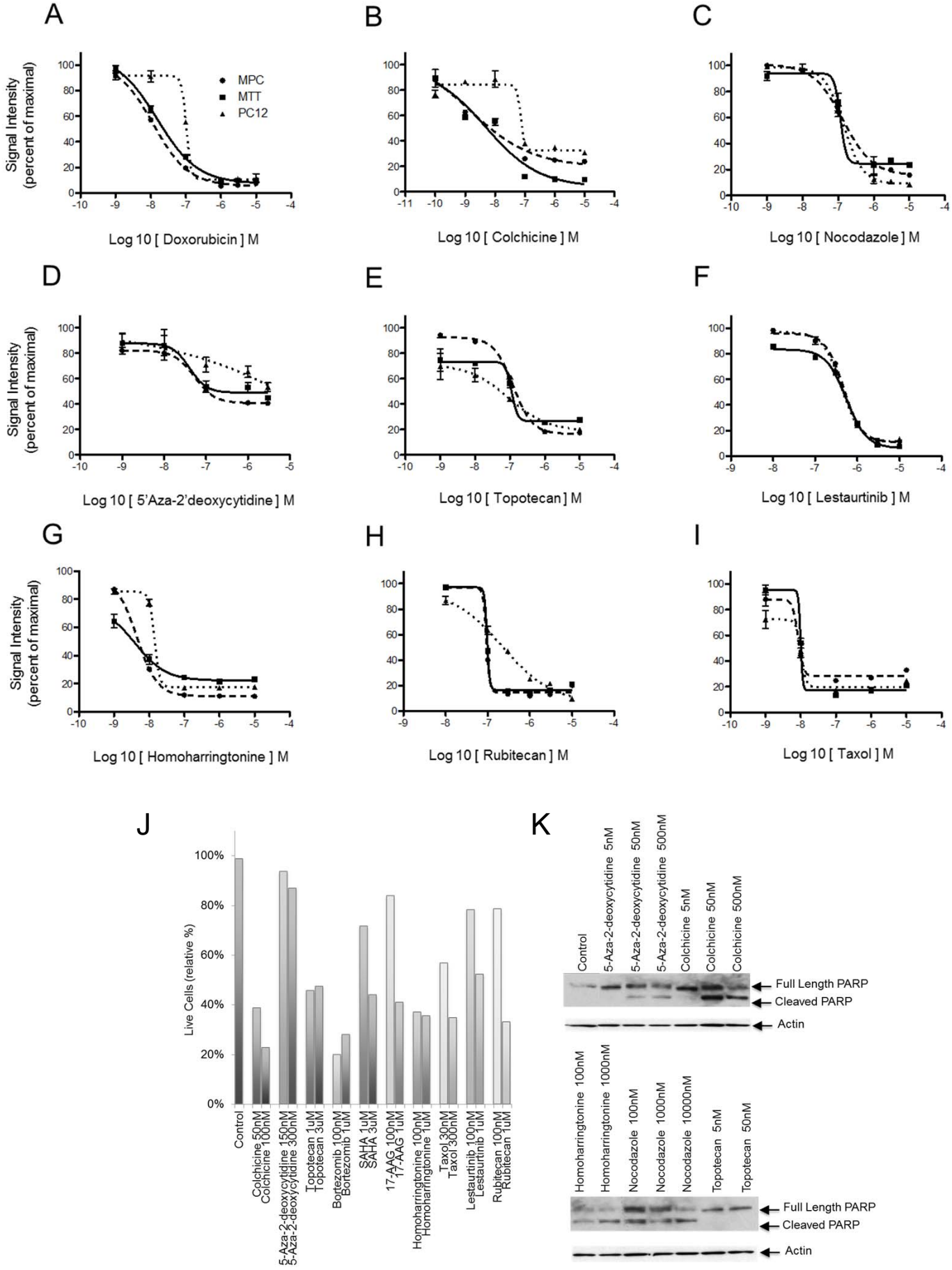
A
B
C
D
E
F
G
H
I
J
K
Signal Intensity (percent of maximal)
MPC
MTT
PC12
Log 10 [Doxorubicin] M
Log 10 [Colchicine] M
Log 10 [Nocodazole] M
Log 10 [5'Aza-2'deoxycytidine] M
Log 10 [Topotecan] M
Log 10 [Lestaurtinib] M
Log 10 [Homoharringtonine] M
Log 10 [Rubitecan] M
Log 10 [Taxol] M
Live Cells (relative %)
Control
Colchicine 50nM
Colchicine 100nM
5-Aza-2-deoxycytidine 150nM
5-Aza-2-deoxycytidine 300nM
Topotecan 1uM
Topotecan 3uM
Bortezomib 100nM
Bortezomib 1uM
SAHA 1uM
SAHA 3uM
17-AAG 100nM
17-AAG 1uM
Homoharringtonine 100nM
Homoharringtonine 1uM
Taxol 30nM
Taxol 300nM
Lestaurtinib 100nM
Lestaurtinib 1uM
Rubitecan 100nM
Rubitecan 1uM
Control
5-Aza-2-deoxycytidine 5nM
5-Aza-2-deoxycytidine 50nM
5-Aza-2-deoxycytidine 500nM
Colchicine 5nM
Colchicine 50nM
Colchicine 500nM
Full Length PARP
Cleaved PARP
Actin
Homoharringtonine 100nM
Homoharringtonine 1000nM
Nocodazole 100nM
Nocodazole 1000nM
Nocodazole 10000nM
Topotecan 5nM
Topotecan 50nM
Full Length PARP
Cleaved PARP
Actin

Figure 13

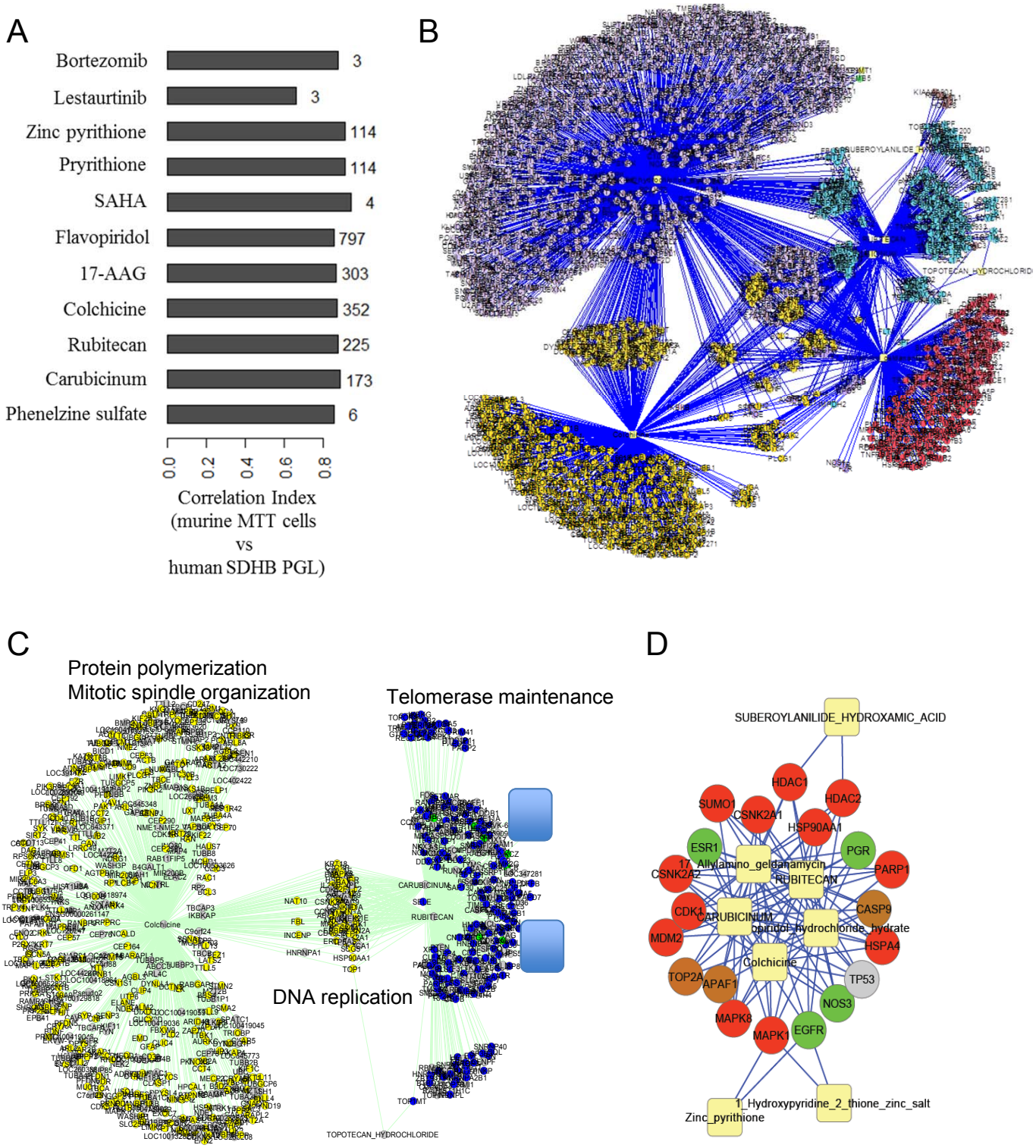
A
Bortezomib 3
Lestaurtinib 3
Zinc pyrithione 114
Pyrithione 114
SAHA 4
Flavopiridol 797
17-AAG 303
Colchicine 352
Rubitecan 225
Carubicinum 173
Phenelzine sulfate 6
0.0 0.2 0.4 0.6 0.8
Correlation Index (murine MTT cells vs human SDHB PGL)
B
C
Protein polymerization
Mitotic spindle organization
Telomerase maintenance
DNA replication
Colchicine
RUBITECAN
CARUBICINUM
TOPOTECAN_HYDROCHLORIDE
D
SUBEROYLANILIDE_HYDROXAMIC_ACID
HDAC1
HDAC2
SUMO1
CSNK2A1
HSP90AA1
ESR1
PGR
17-Allylamino_geldanamycin
PARP1
CSNK2A2
RUBITECAN
CDK1
CARUBICINUM
CASP9
MDM2
Flavopiridol_hydrochloride_hydrate
HSPA4
Colchicine
TOP2A
APAF1
TP53
NOS3
MAPK8
MAPK1
EGFR
1_Hydroxypyridine_2_thione_zinc_salt
Zinc_pyrithione

Figure 14

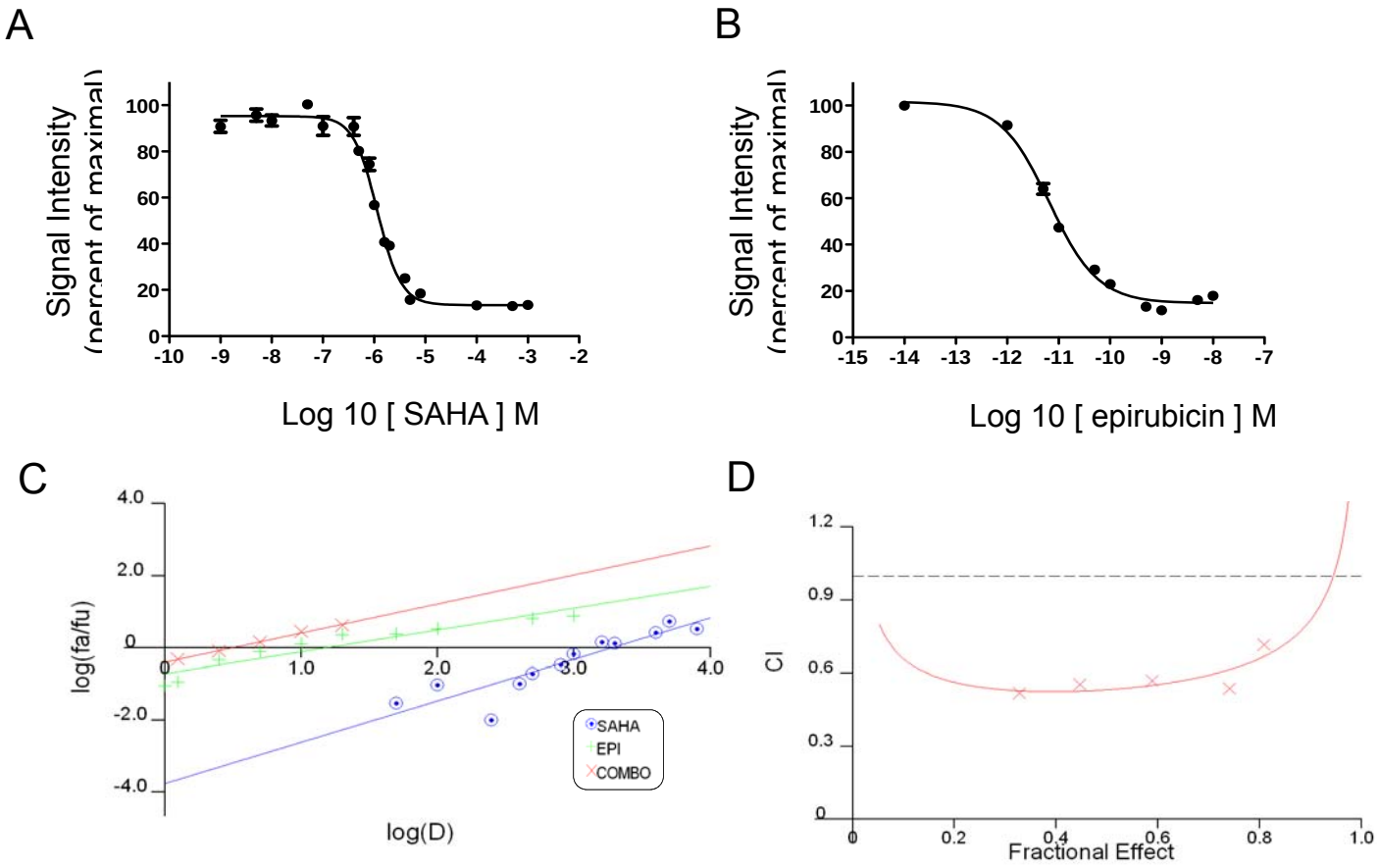
A
Signal Intensity
(percent of maximal)
100
80
60
40
20
0
-10
-9
-8
-7
-6
-5
-4
-3
-2
Log 10 [SAHA] M
B
Signal Intensity
(percent of maximal)
100
80
60
40
20
0
-15
-14
-13
-12
-11
-10
-9
-8
-7
Log 10 [epirubicin] M
C
log(fa/fu)
4.0
2.0
0
-2.0
-4.0
0
1.0
2.0
3.0
4.0
log(D)
SAHA
EPI
COMBO
D
CI
1.2
0.9
0.6
0.3
0
0
0.2
0.4
0.6
0.8
1.0
Fractional Effect